

1 **Title: Five-year flask measurements of long-lived trace gases in India**

2

3 X. Lin<sup>1</sup>, N. K. Indira<sup>2</sup>, M. Ramonet<sup>1</sup>, M. Delmotte<sup>1</sup>, P. Ciais<sup>1</sup>, B. C. Bhatt<sup>3</sup>, M. V. Reddy<sup>4</sup>, D.  
4 Angchuk<sup>3</sup>, S. Balakrishnan<sup>4</sup>, S. Jorphail<sup>3</sup>, T. Dorjai<sup>3</sup>, T. T. Mahey<sup>3</sup>, S. Patnaik<sup>4</sup>, M. Begum<sup>5</sup>,  
5 C. Brenninkmeijer<sup>6</sup>, S. Durairaj<sup>5</sup>, R. Kirubakaran<sup>7</sup>, M. Schmidt<sup>1,8</sup>, P. S. Swathi<sup>2</sup>, N. V.  
6 Vinithkumar<sup>5</sup>, C. Yver Kwok<sup>1</sup>, and V. K. Gaur<sup>2</sup>

7

8 <sup>1</sup> Laboratoire des Sciences du Climat et de l'Environnement (LSCE), UMR CEA-CNRS-  
9 UVSQ, Gif-sur-Yvette 91191, France

10 <sup>2</sup> CSIR Fourth Paradigm Institute (formerly CSIR Centre for Mathematical Modelling and  
11 Computer Simulation), NAL Belur Campus, Bangalore 560 037, India

12 <sup>3</sup> Indian Institute of Astrophysics, Bangalore 560 034, India

13 <sup>4</sup> Department of Earth Sciences, Pondicherry University, Puducherry 605 014, India

14 <sup>5</sup> Andaman and Nicobar Centre for Ocean Science and Technology (ANCOST), ESSO-NIOT,  
15 Port Blair 744103, Andaman and Nicobar Islands, India

16 <sup>6</sup> Max Planck Institute for Chemistry, Hahn-Meitner-Weg 1, D-55128 Mainz, Germany

17 <sup>7</sup> Earth System Sciences Organisation - National Institute of Ocean Technology (ESSO-  
18 NIOT), Ministry of Earth Sciences, Government of India, Tamil Nadu, Chennai 600 100,  
19 India

20 <sup>8</sup> Institut für Umweltphysik, Universität Heidelberg, INF 229, 69120 Heidelberg, Germany

21

22 **Abstract**

23 With a rapid growth in population and economic development, emissions of greenhouse  
24 gases (GHGs) from the Indian subcontinent have sharply increased during recent decades.  
25 However, evaluation of regional fluxes of GHGs and characterization of their spatial and  
26 temporal variations by atmospheric inversions remain uncertain due to a sparse regional  
27 atmospheric observation network. As a result of an Indo-French collaboration, three new  
28 atmospheric stations were established in India at Hanle (HLE), Pondicherry (PON) and Port  
29 Blair (PBL), with the objective of monitoring the atmospheric concentrations of GHGs and  
30 other trace gases. Here we present the results of the five-year measurements (2007–2011) of  
31 CO<sub>2</sub>, CH<sub>4</sub>, N<sub>2</sub>O, SF<sub>6</sub>, CO, and H<sub>2</sub> from regular flask sampling at these three stations. For each  
32 species, annual means, seasonal cycles and gradients between stations were calculated and  
33 related to variations in the natural GHG fluxes, anthropogenic emissions, and the monsoon  
34 circulations. Covariances between species at the synoptic scale were analyzed to investigate  
35 the likely source(s) of emissions. The flask measurements of various trace gases at the three  
36 stations show potential to constrain the inversions of fluxes over Southern and Northeastern  
37 India. However, this network of ground stations needs further extension to other parts of  
38 India to better constrain the GHG budgets at regional and continental scales.

39

## 40 **1 Introduction**

41 Since the pre-industrial times, anthropogenic greenhouse gas (GHG) emissions have  
42 progressively increased the radiative forcing of the atmosphere, leading to impacts on the  
43 climate system and human society (IPCC, 2013, 2014a, b). With rapid socio-economic  
44 development and urbanization during recent decades, a large and growing share of GHG  
45 emissions is contributed by emerging economies like China and India. In 2010, India became  
46 the world's third largest GHG emitter, next to China and the USA (EDGAR v4.2; Le Quéré  
47 et al., 2014). Between 1991 and 2010, anthropogenic GHG emissions in India increased by  
48 ~100% from 1.4 to 2.8 GtCO<sub>2</sub>eq, much faster than rates of most developed countries and  
49 economies like the USA (9%) and EU (-14%) over the same period (EDGAR v4.2). Without  
50 a systematic effort at mitigation, this trend would continue in the coming decades, given that  
51 the per capita emission rate in India is still much below that of the more developed countries.  
52 For comparison, in 2010, the per capita GHG emission rates were 2.2, 10.9, 17.6, and 21.6  
53 tonCO<sub>2</sub>eq/capita for India, the UK, Russia, and the USA, respectively (EDGAR v4.2). In  
54 particular, non-CO<sub>2</sub> GHG emissions are substantial in India, most of which are contributed by  
55 agricultural activities over populous rural areas (Pathak et al., 2010). In 2010, anthropogenic  
56 CH<sub>4</sub> and N<sub>2</sub>O emissions in India amounted to 29.6 TgCH<sub>4</sub> (≈0.62 GtCO<sub>2</sub>eq) and 0.8 TgN<sub>2</sub>O  
57 (≈0.23 GtCO<sub>2</sub>eq), together accounting for 32% of the country's GHG emissions, of which  
58 contributions of the agricultural sector were 60 and 73%, respectively (EDGAR v4.2).  
59 Reducing emissions of these two non-CO<sub>2</sub> GHGs may offer a more cost-effective way to  
60 mitigate future climate change than by attempting to directly reduce CO<sub>2</sub> emissions (Montzka  
61 et al., 2011).

62

63 Effective climate mitigation strategies need accurate reporting of sources and sinks of GHGs.

64 This is also a requirement of the United Nations Framework Convention on Climate Change

65 (UNFCCC). Current estimates of GHG budgets in India, either from the top-down  
66 approaches (based on atmospheric inversions) or bottom-up approaches (based on emission  
67 inventories or biospheric models), have larger uncertainties than for other continents. For  
68 instance, Patra et al. (2013) reported a net biospheric CO<sub>2</sub> sink of  $-104 \pm 150$  TgCyr<sup>-1</sup> over  
69 South Asia during 2007–2008 based on global inversions from 10 TransCom-CO<sub>2</sub> models  
70 (Peylin et al., 2013) and a regional inversion (Patra et al., 2011b), while the bottom-up  
71 approach gave an estimate of  $-191 \pm 193$  TgCyr<sup>-1</sup> over the period of 2000–2009 (Patra et al.,  
72 2013). Notably, these estimates have uncertainties as high as 100–150%, much larger  
73 compared to those of Europe (~30%, see Luysaert et al., 2012) and North America (~60%,  
74 see King et al., 2015), where observational networks are denser and emission inventories are  
75 more accurate. Evaluation of N<sub>2</sub>O emissions from 5 TransCom-N<sub>2</sub>O inversions also exhibited  
76 the largest differences over South Asia (Thompson et al., 2014b). A main source of  
77 uncertainty is the lack of atmospheric observation datasets with sufficient temporal and  
78 spatial coverage (Patra et al., 2013; Thompson et al., 2014b). Networks of atmospheric  
79 stations that were used to constrain estimates of global GHG fluxes show gaps over South  
80 Asia (Patra et al., 2011a; Thompson et al., 2014b, c; Peylin et al., 2013), with Cape Rama  
81 (CRI – 15.08°N, 73.83°E, 60m a.s.l.) on the southwest coast of India being the only Indian  
82 station (Rayner et al., 2008; Patra et al., 2009; Tiwari et al., 2011; Bhattacharya et al., 2009;  
83 Saikawa et al., 2014). Recently a few other ground stations have been established in Western  
84 India and the Himalayas to monitor GHGs and atmospheric pollutants, which are located in  
85 Sinhadgad (SNG – 18.35°N, 73.75°E, 1600m a.s.l.; Tiwari and Kumar, 2012; Tiwari et al.,  
86 2014), Mount Abu (24.60°N, 72.70°E, 1700m a.s.l.; S. Lal, personal communication),  
87 Ahmedabad (23.00°N, 72.50°E, 55m a.s.l.; Lal et al., 2015), Nainital (29.37°N, 79.45°E,  
88 1958m a.s.l.; Kumar et al., 2010) and Darjeeling (27.03°N, 88.15°E, 2194m a.s.l.; Ganesan  
89 et al., 2013). Most of these stations started to measure atmospheric GHG concentrations very

90 recently (e.g. Sinhadgad – since 2009; Ahmedabad – since 2013; Mount Abu – since 2013;  
91 Nainital – since 2006; Darjeeling – since 2011), and datasets are not always available. In  
92 addition, aircraft and satellite observations have also been carried out and provided useful  
93 constraints on estimates of GHG fluxes in this region (Park et al., 2007; Xiong et al., 2009;  
94 Schuck et al., 2010; Patra et al., 2011b; Niwa et al., 2012; Zhang et al., 2014). Although  
95 inclusion of measurements from South Asia significantly reduces uncertainties in top-down  
96 estimates of regional GHG emissions (e.g., Huang et al., 2008; Niwa et al., 2012; Zhang et al.,  
97 2014), a denser atmospheric observational network with sustained measurements is still  
98 needed over this vast and fast-growing region for an improved, more detailed, and necessary  
99 understanding of GHG budgets.

100

101 Besides the lack of a comprehensive observational network, the seasonally reversing Indian  
102 monsoon circulations and orographic effects complicate simulation of regional atmospheric  
103 transport, which contributes to uncertainty of the inverted GHG fluxes (e.g., Thompson et al.,  
104 2014b). The Indian monsoon system is a prominent meteorological phenomenon in South  
105 Asia, which, at lower altitudes, is characterized by strong southwesterlies from the Arabian  
106 Sea to the Indian subcontinent during the boreal summer, and northeasterlies during the  
107 boreal winter (Goswami, 2005). The summer monsoon is associated with deep convection,  
108 which mixes the boundary layer air into the upper troposphere and lower stratosphere  
109 (Schuck et al., 2010; Lawrence and Lelieveld, 2010). On the contrary, little deep convection  
110 occurs over South Asia during the winter monsoon period, which carries less moisture  
111 (Lawrence and Lelieveld, 2010). The Indian monsoon also impacts biogenic activities (e.g.,  
112 vegetation growth, microbial activity) and GHG fluxes through its effects on rainfall  
113 variations (Tiwari et al., 2013; Valsala et al., 2013; Gadgil, 2003). Given that accurate  
114 atmospheric transport is critical for retrieving reliable inversion of GHG fluxes, an

115 observational network that comprises a range of altitudes including monitoring stations in  
116 mountainous regions would be valuable for validating and improving atmospheric transport  
117 models.

118

119 Since the 2000s, three new atmospheric ground stations have been established in India as part  
120 of the Indo-French collaboration, with the objective of monitoring the atmospheric  
121 concentrations of GHGs and other trace gases in flask air samples. Of the three Indian  
122 stations, Hanle (HLE) is a high-altitude station situated in the western Indian Himalayas,  
123 while Pondicherry (PON) and Port Blair (PBL) are tropical surface stations located  
124 respectively on the southeastern coast of South India and on an oceanic island in the  
125 southeastern Bay of Bengal. In this study, we briefly describe the main features of these  
126 stations and present time series of flask air sample measurements of multiple trace gases at  
127 HLE, PON, and PBL over the period 2007–2011. Descriptions of the three stations as well as  
128 methods used to analyze and calibrate the flask measurements are given in Sect. 2. For each  
129 station, four GHG species ( $\text{CO}_2$ ,  $\text{CH}_4$ ,  $\text{N}_2\text{O}$ ,  $\text{SF}_6$ ) and two additional trace gases ( $\text{CO}$ ,  $\text{H}_2$ )  
130 were measured to characterize the annual means and seasonal cycles, with results and  
131 discussions presented in Sect. 3. Gradients between different stations are interpreted in the  
132 context of regional flux patterns and monsoon circulations (Sect. 3.1). We examine synoptic  
133 variations of  $\text{CO}_2$ ,  $\text{CH}_4$  and  $\text{CO}$  by analyzing the co-variances between species, using  
134 deviations from their smoothed fitting curves (Sect. 3.2). Finally, we investigate two  
135 abnormal  $\text{CH}_4$  and  $\text{CO}$  events at PBL and propose likely sources and origins (Sect. 3.3). A  
136 summary of the paper as well as conclusions drawn from these results are given in Sect. 4.

137

## 138 **2 Sampling stations and methods**

## 139 2.1 Sampling stations

140 Figure 1 and S1 in the supplement show the locations of HLE, PON, and PBL. We also  
141 present five-day back-trajectories from each station for all sampling dates in April–June  
142 (AMJ; Fig. 1a), July–September (JAS; Fig. 1b), October–December (OND; Fig. 1c) and  
143 January–March (JFM; Fig. 1d), respectively. Note that this four-period classification scheme  
144 is slightly different from the climatological seasons defined by the India Meteorological  
145 Department (IMD; Attri and Tyagi, 2010), in which months of a year are categorized into the  
146 pre-monsoon season (March–May), SW monsoon season (June–September), post-monsoon  
147 season (October–December) and the winter season (January and February). We adapted the  
148 IMD classification to facilitate better display and further analyses (e.g., Sect. 3.2), making  
149 sure that samples are fairly evenly distributed across all seasons. The back-trajectories were  
150 generated using the Hybrid Single Particle Lagrangian Integrated Trajectory (HYSPLIT4)  
151 model (Draxler and Rolph, 2003), driven by wind fields from the Global Data Assimilation  
152 System (GDAS) archive data based on National Centers for Environmental Prediction (NCEP)  
153 model output (<https://ready.arl.noaa.gov/gdas1.php>).

154

155 The Hanle (HLE) station (32.780 °N, 78.960 °E, 4517 m a.s.l.) is located in the campus of the  
156 Indian Astronomical Observatory (IAO) atop Mt. Saraswati, about 300 m above the  
157 Nilamkhul Plain in the Hanle Valley of southeastern Ladakh in northwestern Himalayas. The  
158 station was established in 2001 as a collaborative project between the Indian Institute of  
159 Astrophysics and LSCE, France. The flask sampling inlet is installed on the top of a 3 m mast  
160 fixed on the roof of a 2m high building, and the ambient air is pumped through a Dekabon  
161 tubing with a diameter of 1/4". The area around the station is a cold mountain desert, with  
162 sparse vegetation and a small population of ~1700 distributed over an area of ~20 km<sup>2</sup>.  
163 Anthropogenic activities are limited to small-scale crop production (e.g., barley and wheat)

164 and livestock farming (e.g., yaks, cows, goats, and sheep). The nearest populated city of Leh  
165 (34.25 °N, 78.00 °E, 3480 m a.s.l.) with ~27 000 inhabitants, lies 270 km to the northwest of  
166 this station. By virtue of its remoteness, high altitude, and negligible biotic and anthropogenic  
167 influences, HLE is representative of the background free tropospheric air masses in the  
168 northern mid-latitudes. Regular flask air sampling at this station has been operational since  
169 February, 2004, and continuous in-situ CO<sub>2</sub> measurements started in September, 2005. Over  
170 the period 2007–2011, a total of 188 flask sample pairs were collected at HLE. Back-  
171 trajectories show that, HLE dominantly samples air masses that pass over northern Africa and  
172 the Middle East throughout the year, and those coming from South and Southeast Asia during  
173 the SW monsoon season (Fig. 1a). More detailed station information of HLE would be found  
174 in several earlier publications (Babu et al., 2011; Moorthy et al., 2011).

175

176 The Pondicherry (PON) station (12.010 °N, 79.860 °E, 20 m a.s.l) is located on the southeast  
177 coast of India, about 8 km north of the city of Pondicherry with a population of ~240,000  
178 (Census India, 2011). The station was established in collaboration with Pondicherry  
179 University in 2006. The flask sampling inlet, initially located on a 10 m mast fixed on the  
180 roof of the University Guest House, was later moved to a 30 m high tower in June, 2011. The  
181 ambient air is pumped from the top of the tower through a Dekabon tubing with a diameter of  
182 1/4". The surrounding village Kalapet, has a population of ~9000 (Sivakumar and Anitha,  
183 2012). A four-lane highway runs nearly 80 m to the west of the station with a low traffic flow  
184 especially during the nighttime, while the Indian Ocean stands about 100 m to the east of the  
185 station. Moreover, the two nearest megalopolises of Chennai and Bangalore, both with  
186 populations of over 6 million (Census India, 2011), are approximately 143 km to the north  
187 and 330 km to the west of the station. In order to minimize the influences of local GHG  
188 sources/sinks, flask air sampling at PON is performed between 12:00 and 18:00 local time



189 (LT), when the sea breeze moves clean air masses towards the land and the boundary layer  
190 air is well mixed. Flask sampling at PON began in September, 2006 and over the period  
191 2007–2011, a total of 185 flask sample pairs were collected at the site. As shown in Fig. 1a,  
192 the air masses received at PON are strongly related to the monsoon circulations. During the  
193 boreal summer when the southwest monsoon prevails, PON is influenced by air masses  
194 originating from the Arabian Sea and South India, whereas during the boreal winter, it  
195 receives air masses from the east and northeast parts of the Indian subcontinent, and the Bay  
196 of Bengal. During the boreal spring and autumn when the monsoon changes its direction, air  
197 masses of both origins are observed.

198

199 The Port Blair (PBL) station (11.650 °N, 92.760 °E, 20 m a.s.l.) is located on the small  
200 Andaman Islands in the southeastern Bay of Bengal, ~1400 km east of Pondicherry, and  
201 roughly 600 km west of Myanmar and Thailand. The station was established in collaboration  
202 with the National Institute of Ocean Technology (NIOT), India, and flask air sampling was  
203 initiated in July, 2009. The flask sampling inlet is located on the top of a 30 m high tower,  
204 and the ambient air is pumped through a Dekabon tubing with a diameter of 1/4". The main  
205 city on the Andaman Islands, Port Blair, is about 8 km to the north of the station, with a  
206 population of ~100,000 (Census India, 2011). Due to its proximity to vegetation and a small  
207 rural community, the station is not completely free from influences of local GHG fluxes.  
208 Therefore, flask samples at PBL are obtained in the afternoon between 13:00 and 15:00 LT,  
209 when the sea breeze moves towards the land, to minimize significant local influences. Over  
210 the period 2009–2011, a total of 63 flask sample pairs were collected at PBL. Back-  
211 trajectories show that the air masses sampled at PBL are also controlled by the seasonally  
212 reversing monsoon circulations (Fig. 1a), with air masses from the Indian Ocean south of the  
213 Equator during the southwest monsoon season, and from the northeast part of the Indian

214 subcontinent, the Bay of Bengal, and Southeast Asia during the northeast monsoon season.  
215 As for PON, air masses of both origins are detected at PBL during the boreal spring and  
216 autumn when the monsoon changes its direction.

217

## 218 **2.2 Flask sampling and analysis**

### 219 **2.2.1 Flask sampling**

220 In principle, flask samples are taken in pairs on a weekly basis at all three stations. However,  
221 in practice air samples are collected less frequently (on average every 10-12 days) due to bad  
222 meteorological conditions or technical problems. Whole air samples are filled into pre-  
223 conditioned 1-L cylindrical borosilicate glass flasks (Normag Labor und Prozesstechnik  
224 GmbH, Germany) with valves sealed by caps made from KEL-F (PTCFE) fitted at both ends.  
225 Besides, a few flasks are equipped with valves sealed by the original Teflon PFA O-ring  
226 (Glass Expansion, Australia), accounting for ~5.0, 1.2 and 1.1% of air samples respectively  
227 for HLE, PON and PBL during the study period. For the air samples stored in flasks sealed  
228 with the original Teflon PFA O-ring, corrections are made for the loss of CO<sub>2</sub> (+0.0027  
229 ppm/day) and of N<sub>2</sub>O (+0.0035 ppb/day) after analyses of the samples. The correction factors  
230 are empirically determined based on laboratory storage tests using flasks filled with  
231 calibrated gases. Drying of the air is performed using 10 g of magnesium perchlorate  
232 (Mg(ClO<sub>4</sub>)<sub>2</sub>) confined at each end with a glass wool plug in a stainless steel cartridge, located  
233 upstream of the pump unit. To prevent entrainment of material inside the sampling unit, a 7  
234 μm filter is attached at the end of the cartridge. The flasks are flushed prior to sampling for  
235 10-20 min at a rate of 4–5 L min<sup>-1</sup>, and the air is compressed in the flasks to about 1 bar over  
236 the ambient pressure (pump: KNF Neuberger diaphragm pump powered by a 12V DC motor,

237 Germany, N86KNDC with EPDM membrane). The pressurizing process lasts for less than a  
238 minute.

239

### 240 **2.2.2 Flask analyses**

241 On average the flasks arrive at LSCE, France about 150 days after the sampling date, and are  
242 analyzed for CO<sub>2</sub>, CH<sub>4</sub>, N<sub>2</sub>O, SF<sub>6</sub>, CO, and H<sub>2</sub> with two coupled gas chromatograph (GC)  
243 systems. The first gas chromatograph (HP6890, Agilent) is equipped with a flame ionization  
244 detector (FID) for CO<sub>2</sub> and CH<sub>4</sub> detection, and an electron capture detector (ECD) for N<sub>2</sub>O  
245 and SF<sub>6</sub> detection. It is coupled with a second GC equipped with a reduced gas detector  
246 (RGD, Peak Laboratories, Inc., California, USA), for analyzing CO and H<sub>2</sub> via reduction of  
247 HgO and subsequent detection of Hg vapor through UV absorption. In the following  
248 paragraph we summarize the major configurations and parameters of the GC systems (also  
249 see Table S1). Further details on the analyzer configuration are described in Lopez (2012)  
250 and Yver et al. (2009).

251

252 Both GC systems are composed of three complementary parts: the injection device, the  
253 separation elements and the detection sensors. As flask samples are already dried during  
254 sampling, they are only passed through a 5 mL glass trap maintained in an ethanol bath kept  
255 at -55°C by a cryocooler (Thermo Neslab CC-65) to remove any remaining water vapor. The  
256 air samples are flushed with flask overpressure through a 15 mL sample loop for CO<sub>2</sub> and  
257 CH<sub>4</sub> analyses, a 15 mL sample loop for N<sub>2</sub>O and SF<sub>6</sub> analyses, and a 1 mL sample loop for  
258 CO and H<sub>2</sub>, at a flow rate of 200 mL min<sup>-1</sup>. After temperature and pressure equilibration, the  
259 air sample is injected into the columns. The CO<sub>2</sub> and CH<sub>4</sub> separation is performed using a  
260 Hayesep-Q (12' × 3/16"OD, mesh 80/100) analytical column placed in an oven at 80°C, with

261 a N<sub>2</sub> 5.0 carrier gas at a flow rate of 50 ml min<sup>-1</sup>. Detection of CH<sub>4</sub> and CO<sub>2</sub> (after conversion  
262 to CH<sub>4</sub> using a Ni catalyst and H<sub>2</sub> gas) is performed in the FID kept at 250°C. The flame is  
263 fed with H<sub>2</sub> (provided by a NM-H<sub>2</sub> generator from F-DBS) at a flow rate of 100 ml min<sup>-1</sup> and  
264 zero air (provided by a 75-82 zero air generator from Parker-Balston) at a flow rate of 300 ml  
265 min<sup>-1</sup>. For N<sub>2</sub>O and SF<sub>6</sub> separation, a Hayesep-Q (4' × 3/16" OD, mesh 80/100) pre-column  
266 and a Hayesep-Q (6' × 3/16" OD, mesh 80/100) analytical column, both placed in an oven at  
267 80°C, are used together with an Ar/CH<sub>4</sub> carrier gas at a flow rate of 40 ml min<sup>-1</sup>. Detection of  
268 N<sub>2</sub>O and SF<sub>6</sub> is performed in the ECD heated at 395°C. For CO and H<sub>2</sub>, we use a Unibeads  
269 1S pre-column (16.5" × 1/8" OD; mesh 60/80) to separate the two gases from the air matrix,  
270 and use a Molecular Sieve 5Å analytical column (80" × 1/8" OD; mesh 60/80) to effectively  
271 separate H<sub>2</sub> from CO. Both columns are placed in an oven kept at 105°C. CO and H<sub>2</sub> are  
272 analyzed in the RGD detector heated to 265°C. A measurement takes ~5 min and calibration  
273 gases are measured at least every 0.45 hour. For CO<sub>2</sub>, CH<sub>4</sub>, N<sub>2</sub>O, and SF<sub>6</sub>, we use two  
274 calibration gases, one with a high concentration and the other with a low concentration. The  
275 calibration and quality control cylinders are filled and spiked in a matrix of synthetic air  
276 containing N<sub>2</sub>, O<sub>2</sub> and Ar prepared by Deuste Steininger (Germany). The concentration of the  
277 sample is calculated using a linear regression between the two calibration gases with a time  
278 interpolation between the two measurements of the same calibration gas (Messenger, 2007;  
279 Lopez, 2012). For CO and H<sub>2</sub>, we use only one standard and apply a correction for the non-  
280 linearity of the analyzer (Yver et al., 2009; Yver, 2010). The nonlinearity is verified regularly  
281 with 5 calibration cylinders for CO and 8 calibration cylinders for H<sub>2</sub>. All the calibration  
282 gases themselves are determined against an international primary scale (CO<sub>2</sub>: WMOX2007;  
283 CH<sub>4</sub>: NOAA2004; N<sub>2</sub>O: NOAA2005A; SF<sub>6</sub>: NOAA2005; CO: WMOX2004; H<sub>2</sub>:  
284 WMOX2009; Hall et al., 2007; Dlugokencky et al., 2005; Jordan and Steinberg, 2011; Zhao  
285 and Tans, 2006). Finally, a "target" gas is measured every two hours after the calibration

286 gases as a quality control of the scales and of the analyzers. The repeatability of the GC  
287 systems estimated from the target cylinder measurements over several days is 0.06 ppm for  
288 CO<sub>2</sub>, 1 ppb for CH<sub>4</sub>, 0.3 ppb for N<sub>2</sub>O, 0.1 ppt for SF<sub>6</sub>, 1 ppb for CO and 2 ppb for H<sub>2</sub>.  
289 Additional quality control is made by checking the values of a flask target (a flask filled with  
290 calibrated gases) placed on each measurement sequence.

291

292 For both of the GC systems, data acquisition, valve shunting, and temperature regulation are  
293 entirely processed by the Chemstation software from Agilent. Concentrations are calculated  
294 with a software developed at LSCE using peak height or area depending on the species.

295

### 296 **2.2.3 Uncertainty of flask measurements**

297 Uncertainties in the measured concentrations stemmed from both the sampling method and  
298 the analysis. Collecting flask samples in pairs and measuring each flask twice allow us to  
299 evaluate these uncertainties. A large discrepancy between two analyses of the same flask  
300 reveals a problem in the analysis system, while a difference between a pair of flasks reflects  
301 both analysis and sampling uncertainties. Flask pairs with differences in mole fractions  
302 beyond a certain threshold are flagged and rejected (see Table S2 in the supplement for the  
303 threshold for each species). The percentages of flask pairs retained for analyses are 65.9-88.3%  
304 for CO<sub>2</sub>, 88.6-94.1% for CH<sub>4</sub>, 74.6-91.5% for N<sub>2</sub>O, 92.0-96.8% for SF<sub>6</sub>, 68.6-88.3% for CO,  
305 and 76.2-95.2% for H<sub>2</sub> (Table S3). For each species, we evaluate the uncertainties by  
306 averaging differences between the two injections of the same flask (analysis uncertainty) and  
307 between the pair of flasks (analysis uncertainty + sampling uncertainty) across all retained  
308 flask pairs from the three Indian stations (Table S4). For all species except SF<sub>6</sub>, the sampling  
309 uncertainty turns out to be the major uncertainty, while the analysis uncertainty is equivalent

310 to the reproducibility of the instrument. For SF<sub>6</sub>, both uncertainties are extremely low due to  
311 the small amplitudes and variations of the signals at the three stations.

312

313 At LSCE, there are regular comparison exercises in which flasks are measured by different  
314 laboratories on the same primary scale (e.g., Inter-Comparison Project (ICP) loop, Integrated  
315 non-CO<sub>2</sub> Greenhouse gas Observing System (InGOS) ‘Cucumber’ intercomparison project).  
316 These comparisons allow us to estimate possible biases in our measurements. In Table S4, the  
317 bias for each species is calculated over the sampling period using the ICP flask exercise that  
318 circulates flasks of low, medium and high concentrations between different laboratories. For  
319 CO<sub>2</sub>, CH<sub>4</sub>, SF<sub>6</sub> and CO, the biases are reported against NOAA (NOAA-LSCE) as it is the  
320 laboratory responsible for the primary scales for these species. The bias of H<sub>2</sub> is calculated  
321 against Max Planck Institute for Biogeochemistry (MPI-BGC) in Jena, Germany, which is  
322 responsible for the primary scale of H<sub>2</sub>. The bias of N<sub>2</sub>O is reported against MPI-BGC instead  
323 of NOAA. Although NOAA is responsible for the primary scale of N<sub>2</sub>O, the instruments they  
324 use for the N<sub>2</sub>O flask analyses and cylinder calibration are not the same as ours. For CH<sub>4</sub>,  
325 N<sub>2</sub>O, SF<sub>6</sub> and H<sub>2</sub>, the estimated biases are within the noise level of the instrument and  
326 negligible. For CO<sub>2</sub> and CO, we observe a bias of  $-0.15 \pm 0.11$  ppm and  $3.5 \pm 2.2$  ppb,  
327 respectively (Table S4), which could be due to the nonlinearity of the instrument and/or an  
328 improper attribution of the secondary scale values.

329

## 330 **2.3 Data analyses**

### 331 **2.3.1 Curve-fitting procedures**

332 For each time series of flask measurements, we calculated annual means and seasonal cycles  
333 using a curve-fitting routine (CCGvu) developed by NOAA/CMDL (Thoning et al., 1989). A

334 smoothed function was fitted to the retained data, consisting of a first-order polynomial for  
335 the growth rate and two harmonics for the annual cycle (Levin et al., 2002; Ramonet et al.,  
336 2002), as well as a low pass filter with 80 and 667 days as short-term and long-term cutoff  
337 values, respectively (Bakwin et al., 1998). Residuals were then calculated as the differences  
338 between the original data and the smoothed fitting curve. Any data lying outside three  
339 standard deviations of the residuals were regarded as outliers and discarded from the time  
340 series (Harris et al., 2000; Zhang et al., 2007). This procedure was repeated until no outliers  
341 remained. These outliers were likely a result of pollution by local emissions and not  
342 representative of regional background concentrations. The data discarded through this  
343 filtering procedure accounts for less than 4% of the retained flask pairs after flagging (Table  
344 S3). The annual means, as well as the amplitude and phases of seasonal cycles, were  
345 determined from the smoothed fitting curve and its harmonic component. We bootstrapped  
346 the curve-fitting procedures 1000 times by randomly sampling the original data with  
347 replacement to further estimate uncertainties of annual means and seasonal cycles. Since the  
348 observation records are relatively short, we used all flask measurements between 2006 and  
349 2011 to fit the smooth curve when available (Fig. S2). For each species, we also compared  
350 results with measurements from stations outside India that belong to networks of  
351 NOAA/ESRL (<http://www.esrl.noaa.gov/gmd/>) and Integrated Carbon Observation System  
352 (ICOS, <https://www.icos-cp.eu/>). Locations and the fitting periods of these stations are also  
353 given in Table S5, Figs. S1 and S2.

354

### 355 **2.3.2 Ratio of species**

356 We analyzed CH<sub>4</sub>-CO, CH<sub>4</sub>-CO<sub>2</sub>, and CO-CO<sub>2</sub> correlations using the residuals from the  
357 smoothed fitting curves that represent synoptic-scale variations (Harris et al., 2000; Ramonet  
358 et al., 2002; Grant et al., 2010). To determine the ratio between each species pair, as in

359 previous studies, we used the slope calculated from the orthogonal distance regression (Press  
360 et al., 2007) to equally account for variances of both species (Harris et al., 2000; Ramonet et  
361 al., 2002; Schuck et al., 2010; Baker et al., 2012). We also bootstrapped the orthogonal  
362 distance regression procedure 1000 times and estimated the 1- $\sigma$  uncertainty for each ratio.  
363 The analyses were performed with R3.1.0 (R Core Team, 2014) following the recipes  
364 described in Teetor (2011).

365

## 366 **3 Results and discussions**

### 367 **3.1 Annual means and seasonal cycles**

#### 368 **3.1.1 CO<sub>2</sub>**

369 Figure 2 shows CO<sub>2</sub> flask measurements and the corresponding smooth curves fitted to the  
370 data at HLE, PON and PBL, as well as two additional NOAA/ESRL stations, namely Plateau  
371 Assy, Kazakhstan (KZM – 43.25 °N, 77.88 °E, 2519 m a.s.l.) and Waliguan, China (WLG –  
372 36.29 °N, 100.90 °E, 3810 m a.s.l.) (Dlugokencky et al., 2014b). HLE observed an increase  
373 in CO<sub>2</sub> mole fractions from 382.3±0.3 to 391.4±0.3 between 2007 and 2011, with annual  
374 mean values being lower (by 0.2–1.9 ppm) than KZM and WLG (Fig. 2c and d, Table 1). At  
375 PON, the annual mean CO<sub>2</sub> mole fractions were generally higher than at HLE, with  
376 differences ranging 1.8–4.3 ppm (Fig. 2a, Table 1). The annual mean CO<sub>2</sub> gradient between  
377 PON and HLE reflects the altitudinal difference of the two stations, and a larger influence of  
378 CO<sub>2</sub> emissions at PON, mostly from South India (Fig. 1a, EDGAR v4.2). Besides this, as  
379 shown in Fig. 2a and Table 1, the CO<sub>2</sub> observations at PON are influenced by synoptic scale  
380 events, with a large variability of individual measurements relative to the fitting curve (see  
381 the relative SDs (RSD) in Table 1). At PBL, the annual mean CO<sub>2</sub> mole fractions were on  
382 average 1.2–1.8 ppm lower than that at HLE (Table 1). The negative gradient between PBL



383 and HLE is particularly large during summer, possibly due to clean air masses transported  
384 from the ocean (Figs. 1a and 2b). Note that caution should be exercised in interpreting the  
385 gradient at PBL because of the data gap and short duration of the time series.

386

387 The different CO<sub>2</sub> seasonal cycles observed at the five stations reflect the seasonality of  
388 carbon exchange in the northern terrestrial biosphere as well as influences of long-range  
389 transport and the monsoon circulations. At HLE, the peak-to-peak amplitude of the mean  
390 seasonal cycle was  $8.2 \pm 0.4$  ppm, with the maximum early May and the minimum mid-  
391 September, respectively (Fig. 3, Table 1). The mean seasonal cycle estimated from flask  
392 measurements at HLE is in good agreement with that derived from vertical profiles of in-situ  
393 aircraft measurements over New Delhi (~500 km southwest of HLE) from the  
394 Comprehensive Observation Network for Trace gases by Airliner (CONTRAIL,  
395 <http://www.cger.nies.go.jp/contrail/>) project at similar altitudes ( $R=0.98-0.99$ ,  $p<0.001$ , Fig.  
396 3a; Machida et al., 2008), and back-trajectories show that they represent air masses with  
397 similar origins as HLE (Fig. S7), confirming that HLE is representative of the regional free  
398 mid-troposphere background concentrations. When comparing with the two other background  
399 stations located further north in central and East Asia, a significant delay of the CO<sub>2</sub> phase is  
400 seen at HLE compared to KZM and WLG (Fig. 3b, Table 1). We also note that the CO<sub>2</sub> mean  
401 seasonal cycle at HLE is in phase with the composite zonal marine boundary layer (MBL)  
402 reference at 32°N, while for KZM and WLG, an advance in the CO<sub>2</sub> phase by about 1 month  
403 is observed compared to the zonal MBL reference (Fig. S3; Dlugokency et al., 2014b). The  
404 phase shifts in the CO<sub>2</sub> seasonal cycles mainly result from differences in the air mass origins  
405 between stations. HLE is influenced by the long-range transport of air masses from mid-  
406 latitudes around 30 °N, as well as air masses passing over the Indian subcontinent in the  
407 boreal summer (Fig. 1a), therefore its CO<sub>2</sub> seasonal cycle is related to the seasonality of

408 vegetation activity over the entire latitude band. KZM and WLG receive air masses passing  
409 over the Middle East and western Asia as HLE does, but they are also influenced by air  
410 masses of more northern origins with signals of strong CO<sub>2</sub> uptake over Siberia during JAS  
411 (Fig. S4). At WLG, negative CO<sub>2</sub> synoptic events, indicative of large-scale transport of air  
412 masses exposed to carbon sinks in Siberia in summer, were also detected by in-situ  
413 measurements during 2009-2011 (Fang et al., 2014). Moreover, the back trajectories indicate  
414 that WLG and KZM are more influenced than HLE by air masses that have exchanged with  
415 the boundary layer air being affected by vegetation CO<sub>2</sub> uptake (Fig. S5a,d,e). This could  
416 additionally account for the earlier CO<sub>2</sub> phase observed at KZM and WLG compared to HLE.

417

418 At PON and PBL, the peak-to-peak amplitudes of the CO<sub>2</sub> mean seasonal cycles were  
419  $7.6\pm 1.4$  and  $11.1\pm 1.3$  ppm, with their maxima observed in April. The CO<sub>2</sub> mean seasonal  
420 cycle is controlled by changes in the monsoon circulations, in combination with the  
421 seasonality of CO<sub>2</sub> biotic exchange and anthropogenic emissions in India. During the boreal  
422 winter when the NE monsoon prevails, PON and PBL receive air masses enriched in CO<sub>2</sub>  
423 from the East and Northeast Indian subcontinent as well as from Southeast Asia, with large  
424 anthropogenic CO<sub>2</sub> emissions (EDGAR v4.2; Wang et al., 2013; Kurokawa et al., 2013).  
425 During April when the SW monsoon begins to develop, the two stations record a decrease in  
426 CO<sub>2</sub> because of the arrival of air masses depleted in CO<sub>2</sub> originating from the Indian Ocean  
427 south of the Equator (Fig. 1a, Fig. 3c). Compared to PBL, the CO<sub>2</sub> decrease at PON is less  
428 pronounced and longer, probably because of the influence of anthropogenic emissions in  
429 South India. The CO<sub>2</sub> mean seasonal cycle at PON is also similar to that observed at CRI  
430 ( $15.08^{\circ}\text{N}$ ,  $73.83^{\circ}\text{E}$ , 60m a.s.l.), another station on the southwest coast of India, yet the  
431 seasonal maximum at CRI is reached slightly earlier than at PON in March (Bhattacharya et  
432 al., 2009; Tiwari et al., 2011, 2014). The SNG station ( $18.35^{\circ}\text{N}$ ,  $73.75^{\circ}\text{E}$ , 1600m a.s.l.),

433 located over the Western Ghats, observes a larger CO<sub>2</sub> seasonal cycle with a peak-to-peak  
434 amplitude of ~20 ppm (Tiwari et al., 2014).

435

### 436 **3.1.2 CH<sub>4</sub>**

437 Figure 4 presents the time series of CH<sub>4</sub> flask measurements at the three Indian stations and  
438 the two NOAA/ESRL stations (Dlugokencky et al., 2014a), with their corresponding  
439 smoothed curves for 2007–2011. At HLE, the annual mean CH<sub>4</sub> concentration increased from  
440 1814.8±2.9 to 1849.5±5.2 ppb between 2007 and 2011 (Fig. 4, Table 1). The multiyear mean  
441 CH<sub>4</sub> value at HLE was lower than at KZM and WLG by on average 25.7±3.1 and 19.6±7.8  
442 ppb (Fig. 4c and d, Table 1), respectively, reflecting the latitudinal and altitudinal CH<sub>4</sub>  
443 gradients. Indeed, KZM and WLG receive air masses transported from Siberia with large  
444 wetland CH<sub>4</sub> emissions in summer, as well as those from regional sources closer to the  
445 stations (Fang et al., 2013; Fig. S4), which may further contribute to the positive gradients  
446 between these two stations and HLE. At PON and PBL, the annual mean CH<sub>4</sub> mole fractions  
447 were higher than those at HLE by as much as 37.4±10.7 and 19.8±24.5 ppb respectively (Fig.  
448 4a and b, Table 1). The positive gradients indicate significant regional CH<sub>4</sub> emissions,  
449 especially during winter when the NE monsoon transports air masses from East and  
450 Northeast India and Southeast Asia, where emissions from livestock, rice paddies and a  
451 variety of waterlogged anaerobic sources and residential biofuel burning are high (EDGAR  
452 v4.2; Baker et al., 2012; Kurokawa et al., 2013). The in-situ measurements at Darjeeling,  
453 India (27.03°N, 88.25°E, 2194 m a.s.l.), another station located in the eastern Himalayas, also  
454 showed large variability and frequent pollution events in CH<sub>4</sub> mole fractions, which largely  
455 result from the transport of CH<sub>4</sub>-polluted air masses from the densely populated Indo-  
456 Gangetic Plains to the station (Ganesan et al., 2013).

457

458 The CH<sub>4</sub> seasonal cycles exhibit contrasting patterns across stations. As shown in Fig. 5, a  
459 distinct characteristic of the mean seasonal cycle at HLE is a CH<sub>4</sub> maximum from June to  
460 September. Even KZM and WLG do not show a minimum in summer that would be  
461 characteristic for the enhanced CH<sub>4</sub> removal rate by reaction with OH. The pronounced HLE  
462 feature is consistent with the result from the aircraft flask measurements over India at flight  
463 altitudes of 8–12.5 km by the Civil Aircraft for the Regular Investigation of the atmosphere  
464 Based on an Instrument Container (CARIBIC, <http://www.caribic-atmospheric.com/>) project  
465 (Schuck et al., 2010, 2012; Baker et al., 2012), although a larger seasonal cycle amplitude is  
466 found in the CARIBIC composite data due to vertical mixing between the mid- and upper  
467 troposphere (Fig. 5a). CARIBIC sampled the mid- to upper tropospheric air masses that were  
468 earlier and more strongly enriched in CH<sub>4</sub> due to the rapid uplift in regions of strong  
469 convection. Xiong et al. (2009) also reported enhancements of CH<sub>4</sub> during the summer  
470 monsoon season over South Asia based on satellite retrievals of CH<sub>4</sub> using the Atmospheric  
471 Infrared Sounder (AIRS) on the EOS/Aqua platform as well as model simulations. Moreover,  
472 the mean CH<sub>4</sub> seasonal cycle at HLE agrees well with the seasonal variations of CH<sub>4</sub>  
473 emissions from wetlands and rice paddies and convective precipitation over the Indian  
474 subcontinent (Fig. 5b), suggesting that the summer maximum at HLE are likely related to the  
475 enhanced biogenic CH<sub>4</sub> emissions from wetlands and rice paddies and deep convection that  
476 mixes surface emissions into the mid-to-upper troposphere. During the SW monsoon period  
477 (June–September), convection over the Indian subcontinent and the Bay of Bengal rapidly  
478 mixes surface polluted air with the upper troposphere, therefore concentrations of trace gases  
479 would be enhanced at higher altitudes rather than at the surface (Schuck et al., 2010;  
480 Lawrence and Lelieveld, 2010). Further analyses of carbon isotopic measurements and/or  
481 chemical transport model are needed to disentangle and quantify the contributions of

482 meteorology and biogenic emissions to the CH<sub>4</sub> summer maximum at HLE. As stated above,  
483 KZM and WLG also record CH<sub>4</sub> increases during summertime, but with smaller magnitudes  
484 (Fig. 5a), possibly because they are not directly influenced by deep convection from the  
485 Indian monsoon system.

486

487 In contrast to HLE, the CH<sub>4</sub> mean seasonal cycles at PON and PBL have distinct phases and  
488 much larger amplitudes, with minimum CH<sub>4</sub> values during July (Fig. 5c). These not only  
489 reflect higher rates of removal by OH, but rather the influence of southern hemispheric air  
490 transported at low altitudes from the southwest as well as the dilution effect by increased  
491 local planetary boundary layer height. In boreal winter, the maxima at PON and PBL are  
492 associated with CH<sub>4</sub>-enriched air masses transported from East and Northeast India, and  
493 Southeast Asia, mostly polluted by agricultural-related sources (e.g., livestock, rice paddies,  
494 agricultural waste burning). As PON and PBL, the flask measurements at CRI also showed  
495 the seasonal maximum CH<sub>4</sub> values during the NE monsoon season, reflecting influences of  
496 air masses with elevated CH<sub>4</sub> from the Indian subcontinent (Bhattacharya et al., 2009; Tiwari  
497 et al., 2013).

498

### 499 **3.1.3 N<sub>2</sub>O**

500 Nitrous oxide (N<sub>2</sub>O) is a potent greenhouse gas that has the third largest contribution to  
501 anthropogenic radiative forcing after CO<sub>2</sub> and CH<sub>4</sub> (IPCC, 2013). It also becomes the  
502 dominant ozone depleting substance (ODS) emitted in the 21<sup>st</sup> century with the decline of  
503 chlorofluorocarbons (CFCs) under the Montreal Protocol (Ravishankara et al., 2009). Since  
504 the pre-industrial era, the atmospheric N<sub>2</sub>O increased rapidly from ~270 ppb to ~325 ppb in  
505 2011 (IPCC, 2013), largely as the result of human activities. Of the several known N<sub>2</sub>O

506 sources, agricultural activities (mainly through nitrogen fertilizer use) contribute to ~58% of  
507 the global anthropogenic N<sub>2</sub>O emissions, with a higher share in a predominantly agrarian  
508 country like India (~75%; Garg et al., 2012).

509

510 The time series of N<sub>2</sub>O flask measurements over the period of 2007–2011 and their smoothed  
511 curves are presented in Fig. 6. At HLE, the annual mean N<sub>2</sub>O concentration rose from  
512 322.2±0.1 to 325.2±0.1 ppb during 2007–2011 (Table 1), with a mean annual growth rate of  
513 0.8±0.0 ppb yr<sup>-1</sup> (r<sup>2</sup> = 0.97, p = 0.001), smaller than that at MLO (1.0±0.0 ppb yr<sup>-1</sup>, Table 1).  
514 At PON and PBL, the annual mean N<sub>2</sub>O mole fractions are higher than at HLE by 3.1±0.3  
515 and 3.8±1.7 ppb (Fig. 6, Table 1), respectively. The N<sub>2</sub>O gradients between PON, PBL and  
516 HLE are larger than typical N<sub>2</sub>O gradients observed between stations scattered in Europe or  
517 in North America. For example, Haszpra et al. (2008) presented N<sub>2</sub>O flask measurements at a  
518 continental station – Hegyhátsál, Hungary (HUN – 46.95 °N, 16.65 °W, 248 m a.s.l.) from  
519 1997 to 2007. The annual mean N<sub>2</sub>O mole fraction at HUN was higher than at Mace Head  
520 (MHD) by only 1.3 ppb. We also analyzed N<sub>2</sub>O time series of flask measurements during  
521 2007–2011 at several European coastal stations – BGU in Spain, FIK in Greece, and LPO in  
522 France (Table S5), and the N<sub>2</sub>O gradients between these stations and MHD were 1.1±0.2,  
523 0.4±0.1, and 2.1±0.6 ppb, respectively (Fig. S9, Table S6). In the United States, N<sub>2</sub>O flask  
524 measurements from the NOAA/ESRL stations at Park Falls, Wisconsin (LEF – 45.95 °N,  
525 90.27 °W, 472 m a.s.l.), Harvard Forest, Massachusetts (HFM – 42.54 °N, 72.17 °W, 340 m  
526 a.s.l.) and a continental, high-altitude station at Niwot Ridge, Colorado (NWR – 40.05 °N,  
527 105.58 °W, 3523 m a.s.l.) also show that, the annual mean N<sub>2</sub>O concentrations at HFM and  
528 LEF were higher than that at NWR by only 0.5±0.1 and 0.3±0.1 ppb, respectively (Fig. S9,  
529 Table S6). Besides, the N<sub>2</sub>O concentrations measured at PON and PBL have a notably higher  
530 variability (around the smoothed fitting curve) than that at European and US stations (see

531 relative SDs (RSD) in Table 1 and Table S6). The larger N<sub>2</sub>O gradient between PON, PBL  
532 and HLE, as well as higher variability at PON and PBL, demonstrate the presence of  
533 substantial N<sub>2</sub>O sources in South Asia and over the Indian Ocean during the observation  
534 period. The in-situ measurements at Darjeeling also exhibited N<sub>2</sub>O enhancements to be above  
535 the background level, suggesting significant N<sub>2</sub>O sources in this region (Ganesan et al., 2013).  
536 These sources may be related to emissions from natural and cultivated soils probably  
537 enhanced by extensive use of nitrogen fertilizers, as well as emissions from regions of coastal  
538 upwelling in the Arabian Sea (Bange et al., 2001; Garg et al., 2012; Saikawa et al., 2014).

539

540 Compared to CO<sub>2</sub> and CH<sub>4</sub>, the seasonal cycle of N<sub>2</sub>O is very small due to the long lifetime  
541 of ~120 years (Minschwaner et al., 1993; Volk et al., 1997), and has a larger uncertainty  
542 probably because synoptic events are more likely to mask the seasonal signal. At HLE, PON  
543 and PBL, the peak-to-peak amplitudes of the N<sub>2</sub>O seasonal cycle are 0.6±0.1, 1.2±0.5, and  
544 2.2±0.6 ppb, respectively (Table 1). HLE displays a N<sub>2</sub>O maximum in mid-August (Student's  
545 t-test, t=1.78, p=0.06), and a secondary maximum is in January/February but not significant  
546 (Student's t-test, t=-0.84, p=0.79) (Table 1, Fig. 7, Table S7 for detailed t-test statistics). The  
547 N<sub>2</sub>O seasonal cycle at HLE is out of phase with that at other northern background stations  
548 such as MHD (Fig. S10, Table S6), where an N<sub>2</sub>O summer minimum is always observed,  
549 likely due to the downward transport of N<sub>2</sub>O-depleted air from the stratosphere to the  
550 troposphere during spring and summer (Liao et al., 2004; Morgan et al., 2004; Jiang et al.,  
551 2007b). The timing of the summer N<sub>2</sub>O maximum at HLE is consistent with that of CH<sub>4</sub>  
552 (Table 1; Figs. 5 and 7), giving evidence that the N<sub>2</sub>O seasonal cycle may probably be  
553 influenced by the convective mixing of surface air, rather than by the influx of stratospheric  
554 air into the troposphere. Given that the populous Indo-Gangetic plains have high N<sub>2</sub>O  
555 emission rates due to the intensive use of nitrogen fertilizers (Garg et al., 2012; Thompson et

556 al., 2014a), during summer, the surface air enriched in N<sub>2</sub>O is vertically transported by deep  
557 convection and enhances N<sub>2</sub>O mole fractions in the mid-to-upper troposphere. Like CH<sub>4</sub>, the  
558 N<sub>2</sub>O enhancement at HLE during the summer monsoon period (June–September) is consistent  
559 with the aircraft flask measurements at flight altitudes 8–12.5 km from the CARIBIC project  
560 in 2008 (Schuck et al., 2010).

561

562 At PON, N<sub>2</sub>O also decreases during February–April and reaches a minimum at the end of  
563 May. However, the decrease of N<sub>2</sub>O does not persist during June–September, which is in  
564 contrast with CH<sub>4</sub> (Table 1, Fig. 7a). One reason may be that the air masses arriving at the  
565 site during the southwest monsoon period is relatively enriched in N<sub>2</sub>O compared to CH<sub>4</sub>,  
566 reflecting differences in their relative emissions along the air mass route. The increase of N<sub>2</sub>O  
567 at PON during June–August and the maximum during September–October are likely related  
568 to N<sub>2</sub>O emissions from coastal upwelling along the southern Indian continental shelf, which  
569 peak during the SW monsoon season (Patra et al., 1999; Bange et al., 2001). According to  
570 Bange et al. (2001), the annual N<sub>2</sub>O emission for the Arabian Sea is 0.33–0.70 Tg/yr, of  
571 which N<sub>2</sub>O emissions during the SW monsoon account for about 64–70%. This coastal  
572 upwelling N<sub>2</sub>O flux is significantly larger than the annual anthropogenic N<sub>2</sub>O emissions in  
573 South India south of 15 °N, which is estimated to be on average 0.07–0.08 Tg/yr during  
574 2000–2010 (EDGAR v4.2). At PBL, the maximum and minimum N<sub>2</sub>O occur in November  
575 and February/March, respectively (Table 1, Fig. 7b). The late N<sub>2</sub>O peak at PBL in November  
576 may be associated with the N<sub>2</sub>O-enriched air masses transported from South and Southeast  
577 Asia, which could be attributed to natural and agricultural N<sub>2</sub>O emissions from this region  
578 (Saikawa et al., 2014). It should be noted that, the mean seasonal cycles of N<sub>2</sub>O at PON and  
579 PBL are subject to high uncertainties because of the short observation periods and data gaps  
580 (shaded area in Fig. 7). The N<sub>2</sub>O maximum and/or minimum obtained from the mean



581 seasonal cycle are marginally significant for PON and PBL (Table S7 for detailed t-test  
582 statistics). Therefore, caution should be exercised in interpreting mean seasonal cycles at  
583 these stations. Sustained, long-term measurements are needed in order to generate more  
584 reliable estimates of the seasonal cycles for the two stations.

585

### 586 **3.1.4 SF<sub>6</sub>**

587 Sulfur hexafluoride (SF<sub>6</sub>) is an extremely stable greenhouse gas, with an atmospheric lifetime  
588 as long as 800–3200 year and a global warming potential (GWP) of ~23,900 over a 100-year  
589 time horizon (Ravishankara et al., 1993; Morris et al., 1995; IPCC, 2013). The main sources  
590 of atmospheric SF<sub>6</sub> emissions are electricity distribution systems, magnesium production, and  
591 semi-conductor manufacturing (Olivier et al., 2005), while its natural sources are negligible  
592 (Busenberg and Plummer, 2000). As its sources are almost purely anthropogenic (Maiss et al.,  
593 1996), SF<sub>6</sub> is widely considered as a good tracer for population density, energy consumption  
594 and anthropogenic GHG emissions (Haszpra et al., 2008).

595

596 Figure 8 presents the time series of SF<sub>6</sub> flask measurements and corresponding fitting curves  
597 at HLE, PON, and PBL. At HLE, the annual mean SF<sub>6</sub> mole fractions increased from  
598  $6.26 \pm 0.03$  to  $7.38 \pm 0.01$  ppt between 2007 and 2011, which is in good agreement with the SF<sub>6</sub>  
599 trend observed at MLO during the same period (HLE:  $0.29 \pm 0.05$  ppt/yr,  $r^2=0.99$ ,  $p<0.001$ ;  
600 MLO:  $0.29 \pm 0.03$  ppt/yr,  $r^2=0.99$ ,  $p<0.001$ ; Figs. 8 and S11a, Table 1, Table S8). The annual  
601 mean SF<sub>6</sub> gradient between PON and HLE is  $-0.060 \pm 0.030$  ppt, whereas the gradient between  
602 PBL and HLE is statistically insignificant ( $-0.002 \pm 0.097$  ppt). The slight negative gradient  
603 between PON and HLE is a reversed signal compared with the SF<sub>6</sub> observations at stations  
604 influenced by continental emissions in Europe and United States. For example, the SF<sub>6</sub> mole

605 fractions at HUN over the years of 1997–2007 are higher than those at MHD by on average  
606 0.19 ppt (Haszpra et al., 2008). We also analyzed the SF<sub>6</sub> gradients between two coastal  
607 European stations – BGU (41.97 °N, 3.3 °E, 30 m a.s.l.) and LPO (48.80 °N, 3.57 °W, 30 m  
608 a.s.l.) – and MHD, which are 0.10±0.03 and 0.05±0.02 ppt averaged over the period of 2007–  
609 2011, respectively. At HFM, the SF<sub>6</sub> mole fractions are higher than those of the NWR on  
610 average by 0.15±0.06 ppt during 2007–2011 (Table S8). Given the long atmospheric lifetime  
611 of SF<sub>6</sub>, the positive gradients between continental European and US stations and background  
612 reference stations suggest significant sources in Europe and the US. On the contrary, the  
613 slight negative gradient between PON and HLE implies weak SF<sub>6</sub> emissions over the Indian  
614 subcontinent, which is also indicated by recent high-frequency in-situ SF<sub>6</sub> measurements at  
615 Darjeeling (Ganesan et al., 2013). It is also worthwhile to note that high SF<sub>6</sub> values occur  
616 repeatedly at HLE and PBL in winter, which is likely related to episodic SF<sub>6</sub> pollution events  
617 from the Middle East, South/Southeast Asia and China (Figs. 8b and S6d).

618

619 The annual mean SF<sub>6</sub> seasonal cycles for HLE, PON, and PBL are presented in Fig. 9. The  
620 peak-to-peak amplitudes at the three stations are 0.15±0.03, 0.24±0.02, and 0.48±0.07 ppt,  
621 respectively (Table 1). At HLE, the SF<sub>6</sub> seasonal cycle is bimodal as for N<sub>2</sub>O, with an  
622 absolute maximum occurring in November (Student's t-test, t=2.425, p=0.014) and a  
623 secondary maximum in May (Student's t-test, t=2.443, p=0.016) (Table S9 for detailed t-test  
624 statistics). Given that SF<sub>6</sub> increases monotonously and that its sources are purely  
625 anthropogenic and not subject to seasonally variations (Maiss et al., 1996), the seasonal cycle  
626 of SF<sub>6</sub> should be driven by changes in atmospheric circulations, e.g., the SW monsoon  
627 convection and stratosphere-atmosphere exchange (Levin et al., 2002). We note that, at HLE,  
628 no enhancement of SF<sub>6</sub> during the SW monsoon season is recorded, unlike what is observed  
629 for CH<sub>4</sub> and N<sub>2</sub>O (Figs. 5 and 7). Although the CARIBIC aircraft flask measurements over

630 the Indian region demonstrated SF<sub>6</sub> enhancements in the upper troposphere at ~30 °N  
631 (approximately where HLE is located) in August, 2008, back-trajectories from the CARIBIC  
632 flights showed that the summer enhancements in SF<sub>6</sub> were more related to the influences of  
633 westerly jet transport in the upper troposphere, rather than the SW monsoon and sources from  
634 India that contributed to the summer maxima in CH<sub>4</sub> and N<sub>2</sub>O (Schuck et al., 2010, Fig. S8).  
635 The absence of SF<sub>6</sub> enhancement in summer at HLE confirms weak SF<sub>6</sub> emissions in India.  
636 At PBL, the SF<sub>6</sub> seasonal cycle is related to the monsoon circulation and convection (Figs. 9b  
637 and S6d). The maximum during November–December (Student's t-test, t=5.138, p<0.001;  
638 Table S9) is likely due to frequent episodic SF<sub>6</sub> polluted air masses transported from  
639 Southeast Asia and China (Fig. S6d).

640

### 641 **3.1.5 CO**

642 Carbon monoxide (CO) plays important roles in atmospheric chemistry, as the dominant sink  
643 for the hydroxyl radical (OH, the main tropospheric oxidant) and a precursor of tropospheric  
644 ozone under high NO<sub>x</sub> (NO+NO<sub>2</sub>) concentrations (Logan et al., 1981; Novelli et al., 1998;  
645 Seinfeld and Pandis, 2006). Although CO does not act as a greenhouse gas, it modulates the  
646 atmospheric concentrations of CH<sub>4</sub> (the second anthropogenic greenhouse gas after CO<sub>2</sub>)  
647 through competition for the OH radicals. At the global scale, it contributes to an indirect  
648 positive radiative forcing of  $0.23 \pm 0.07 \text{ W m}^{-2}$  (IPCC, 2013). Besides, CO is an excellent tracer  
649 for combustion processes, with emission sources mainly contributed by incomplete  
650 combustion of fossil fuel and biofuels, and by biomass burning (Granier et al., 2011). In India,  
651 biofuel and agricultural waste burning account for 70–80% of the total anthropogenic CO  
652 emissions (EDGAR v4.2; Streets et al., 2003b; Yevich and Logan, 2003).

653

654 The time series of CO flask measurements and corresponding smoothed curves are shown in  
655 Fig. 10. Over the period of 2007–2011, HLE recorded a slight decrease in CO mole fractions  
656 from  $104.7 \pm 1.4$  to  $99.4 \pm 2.2$  ppb, with an annual rate of  $-2.2 \pm 0.0$  ppb yr<sup>-1</sup> ( $r^2 = 0.65$ ,  $p = 0.06$ ).  
657 The CO mole fractions at HLE are lower than those at KZM and WLG (Novelli et al., 2014b),  
658 by on average  $18.8 \pm 2.5$  and  $30.2 \pm 7.4$  ppb, respectively (Table 1, Fig. 10c and d). The  
659 positive gradient between KZM, WLG and HLE does not only reflect decreasing CO with  
660 altitude and the N-S global gradient, but also suggests differences in regional emission  
661 sources. For example, compared to HLE, the CO signals at WLG are more influenced by  
662 transport of polluted air, especially during summer when about 30% air masses pass over  
663 industrialized and urbanized areas southeast of the station (Zhang et al., 2011). Besides, the  
664 positive CO gradient between KZM, WLG and HLE may be further contributed by air  
665 masses of northern Siberia origin in summer (Fig. S4), with higher CO emissions from  
666 biomass burning and secondary CO from the oxidation of CH<sub>4</sub> and non-CH<sub>4</sub> hydrocarbons  
667 (Konovalov et al., 2014). At PON and PBL, the annual mean CO mole fractions are higher  
668 than that at HLE by on average  $82.4 \pm 10.7$  and  $52.5 \pm 8.5$  ppb, respectively (Table 1, Fig. 10a  
669 and b). The PON and PBL stations are influenced by CO regional emissions, mainly due to  
670 biofuel and agricultural burning over South and Southeast Asia (Lelieveld et al., 2001; Streets  
671 et al., 2003a, b; Yevich and Logan, 2003). We also note that, for all the five stations, the CO  
672 time series show larger variability with respect to their corresponding smoothed curves than  
673 other species do (see the residual SD (RSD) in Table 1, Fig. 10), as a result of the unevenly  
674 distributed CO sources and short atmospheric lifetime (Novelli et al., 1992).

675

676 As shown in Fig. 11, the CO seasonal cycle at HLE reaches a maximum in mid-March and a  
677 minimum by the end of October, with a peak-to-peak amplitude of  $28.4 \pm 2.3$  ppb (Table 1,  
678 Fig. 11). The phase of the mean CO seasonal cycle at HLE generally agrees with the ones

679 observed at KZM and WLG, with a lag of up to 1 month in the timing of seasonal minimum  
680 at the two stations (Table 1, Fig. 11c and d). In contrast with the three stations representative  
681 of large-scale free tropospheric air masses, the stations at the maritime boundary layer in the  
682 mid-to-high Northern Hemisphere observe the lowest CO values in July or August (Novelli et  
683 al., 1992, 1998), when the concentration of OH – the major sink of CO – is highest (Logan et  
684 al., 1981). The delay in timing of the seasonal CO minimum at the three free troposphere  
685 stations in Central and South Asia compared to those boundary layer stations is probably due  
686 to the mixing time of regional surface CO emissions and the relatively short lifetime of CO  
687 (1-2 months on average). During summer, KZM and WLG sample air masses from Siberia  
688 impacted by CO fire emissions (Duncan et al., 2003; Kasischke et al., 2005), as well as CO-  
689 polluted air from urbanized and industrialized area (Zhang et al., 2011), while HLE is  
690 influenced by convective mixing of CO emissions from India, either from anthropogenic  
691 sources or oxidation of VOCs. It is interesting to note that the CO seasonal cycle at HLE does  
692 not show an enhancement during JAS as CH<sub>4</sub> and N<sub>2</sub>O do (Figs. 5 and 7), possibly as a result  
693 of OH oxidation that reduces CO and acts oppositely to vertical transport, and/or differences  
694 in seasonal emission patterns between CO and the other two species (Baker et al., 2012).  
695 However, the CO enhancement during summer was observed in the upper troposphere over  
696 South Asia from the CARIBIC aircraft measurements at flight altitudes 8-12.5 km and  
697 Microwave Limb Sounder observations at 100–200 hPa (Li et al., 2005; Jiang et al., 2007a;  
698 Schuck et al., 2010). The differences in the CO seasonal cycles at different altitudes suggest  
699 faster transport (and younger air masses) at 10 km than at 5 km due to convection, controlling  
700 the vertical profile of CO, which makes it difficult to directly compare aircraft measurements  
701 in the upper troposphere and column remote sensing observations with surface data.

702

703 At PON and PBL, the mean CO seasonal cycles show maxima in the boreal winter and  
704 minima in the boreal summer, with peak-to-peak amplitudes of  $78.2 \pm 11.6$  and  $144.1 \pm 16.0$   
705 ppb, respectively (Fig. 11a and b). A strong and positive correlation is found between  
706 detrended CO and CH<sub>4</sub> at PON ( $r=0.70$ ,  $p<0.001$ ) and PBL ( $r=0.84$ ,  $p<0.001$ ), suggesting that  
707 the seasonal cycles of both species are dominated by the seasonally varying atmospheric  
708 transport. During summer when the southwest monsoon prevails, the surface CO  
709 concentrations at PON and PBL are low due to rapid convective uplifting and advection of  
710 clean air masses from the ocean. During winter, the two stations are influenced by  
711 northeasterly air masses enriched in CO from Northeast India, Southeast Asia and China  
712 (back-trajectories in Fig. S6e), probably influenced by biofuel and agricultural waste burning  
713 in these regions (Yevich and Logan, 2003; Lelieveld et al., 2001).

714

### 715 **3.1.6 H<sub>2</sub>**

716 Hydrogen (H<sub>2</sub>) is the second most abundant reduced trace gas in the troposphere after CH<sub>4</sub>,  
717 with an average mole fraction of ~530 ppb (Novelli et al., 1999). It plays important roles in  
718 tropospheric and stratospheric chemistry and indirectly impacts budgets of CH<sub>4</sub>, CO and non-  
719 methane hydrocarbons (NMHCs) through reaction with the OH radicals (Novelli et al., 1999;  
720 Ehhalt and Rohrer, 2009). Like CO, H<sub>2</sub> is also a good tracer for incomplete combustion  
721 emissions from fossil fuel and biomass/biofuel burning, which is quite extensive in India  
722 (Streets et al., 2003b; Yevich and Logan, 2003).

723

724 Figure 12 shows the time series of H<sub>2</sub> flask measurements with smoothed curves at HLE,  
725 PON, and PBL, respectively. No significant trend was observed at any of the three stations  
726 (Table 1, Fig. 12), consistent with the long-term H<sub>2</sub> measurements at other background

727 stations during the last three decades (Novelli et al., 1999; Ehhalt and Rohrer, 2009; Grant et  
728 al., 2010). For the year 2008, comparing to KZM and WLG (Novelli et al., 2014a), HLE  
729 recorded higher H<sub>2</sub> mole fractions by ~40 ppb, reflecting the latitudinal gradient of H<sub>2</sub> with  
730 lower concentrations towards northern high latitudes, due to land uptake by soils (Novelli et  
731 al., 1999; Price et al., 2007; Hauglustaine and Ehhalt, 2002; Ehhalt and Rohrer, 2009). Note  
732 that these results based on only one-year comparison need to be confirmed by extended data  
733 more up-to-date, which are not available yet. At PON and PBL, the annual mean H<sub>2</sub> mole  
734 fractions were higher than at HLE by 29.8±4.1 and 21.8±4.6 ppb, respectively (Table 1; Fig.  
735 12). Comparisons with H<sub>2</sub> measurements at Mariana Island, Guam (GMI – 13.39 °N,  
736 144.66 °E, 0.00 m a.s.l.) (Novelli et al., 2014a), another maritime station in the western  
737 Pacific at a similar latitude as PON and PBL, also showed positive gradients of ~40 ppb (Fig.  
738 S12c and d; Table S10), suggesting substantial regional H<sub>2</sub> sources over the footprint area of  
739 PBL and PON. During October–March when the NE monsoon prevails, both PON and PBL  
740 receive H<sub>2</sub>-enriched air masses from South and Southeast Asia, mainly influenced by fossil  
741 fuel combustion and biomass burning (Fig. S6f; GFED v3.1; Hauglustaine and Ehhalt, 2002;  
742 Price et al., 2007; Ehhalt and Rohrer, 2009; van der Werf et al., 2010). During April–  
743 September, with the northward movement of Intertropical Convergence Zone (ITCZ), the two  
744 stations are influenced by advection of air from south of the Equator. For PON, H<sub>2</sub>-polluted  
745 air masses are occasionally sampled during JAS when the SW monsoon moves over the  
746 continent of South India with high population and heavy industry (Fig. S6f; Census India,  
747 2011).

748

749 The mean H<sub>2</sub> seasonal cycles for HLE, PON, and PBL are presented in Fig. 13. At HLE, the  
750 peak-to-peak H<sub>2</sub> seasonal amplitude is 15.8±2.2 ppb, less than half of the seasonal amplitudes  
751 at BMW (39.6±2.6 ppb) and MID (38.0±2.4 ppb) of similar latitudes (Novelli et al., 2014a),

752 and that at WLG ( $22.8\pm 3.0$  ppb) (Figs. 13d and S13a, Tables 1 and S10). The maximum and  
753 minimum of H<sub>2</sub> occur in April and September, respectively. The dampening of the H<sub>2</sub>  
754 seasonal amplitude with increasing altitude was previously found for another high-altitude  
755 continental station at Jungfrauoch, Switzerland (JUN – 46.53 °N, 7.98 °E, 3580.00 m a.s.l.)  
756 (Bond et al., 2011), and was also captured by the GEOS-Chem global chemical transport  
757 model (Price et al., 2007). Since the soil sink dominates much of the surface H<sub>2</sub> seasonal  
758 cycle in the mid-to-high Northern Hemisphere (Hauglustaine and Ehhalt, 2002; Price et al.,  
759 2007; Bousquet et al., 2011; Yver et al., 2011; Yashiro et al., 2011), the smaller amplitude in  
760 the H<sub>2</sub> seasonal cycle at HLE may be attributed to the weakened soil sink with increasing  
761 altitude due to vertical mixing (Price et al., 2007; Bond et al., 2011).

762

763 At PON and PBL, the mean H<sub>2</sub> seasonal cycles are characterized by the peak-to-peak  
764 amplitudes of  $21.6\pm 3.4$  and  $21.3\pm 5.0$  ppb respectively, comparable to that at GMI ( $21.5\pm 1.2$   
765 ppb) (Tables 1 and S10, Figs. 13a and b and S13b). At PBL, the H<sub>2</sub> maximum in March–  
766 April and a secondary increase during September–October coincide with the double biomass  
767 burning peaks in each hemisphere – in March for northern tropics, in August/September for  
768 southern tropics (van der Werf et al., 2006; Price et al., 2007; Bousquet et al., 2011; Yver et  
769 al., 2011). Given that the seasonal variation of soil H<sub>2</sub> uptake is probably small in the tropics  
770 (Price et al., 2007; Bousquet et al., 2011; Yver et al., 2011; Yashiro et al., 2011), this bimodal  
771 H<sub>2</sub> seasonal cycle at PBL could be related to biomass burning.

772

### 773 **3.2 Synoptic variations**

774 In this section we analyze synoptic variations of CO<sub>2</sub>, CH<sub>4</sub>, and CO by examining  
775 correlations between species, after subtracting the smoothed curve from the original data.



776 Ratios of trace gas mole fractions or their enhancements have been widely used in previous  
777 studies to partition contributions from different source types and origins (Langenfelds et al.,  
778 2002; Paris et al., 2008, Lopez et al., 2012), to estimate emissions of one species given  
779 emissions of another one that is better-known (Gamnitzer et al., 2006; Rivier et al., 2006;  
780 Turnbull et al., 2006; Schuck et al., 2010), and to provide valuable constraints on inversion of  
781 sources and sinks of trace gases (Xiao et al., 2004; Pison et al., 2009).

782

### 783 **3.2.1 $\Delta\text{CH}_4/\Delta\text{CO}$**

784 Figure 14 shows scatterplots of  $\text{CH}_4$  and  $\text{CO}$  residuals with the orthogonal distance regression  
785 lines at HLE, PON, and PBL for different seasons. A significant and positive correlation  
786 between  $\text{CH}_4$  and  $\text{CO}$  residuals (hereafter  $\Delta\text{CH}_4/\Delta\text{CO}$ , unit  $\text{ppb ppb}^{-1}$ ) is found for all three  
787 stations throughout the year. Furthermore, the  $\Delta\text{CH}_4/\Delta\text{CO}$  ratio also shows seasonal variation  
788 at each of the three stations. The most prominent feature is the occurrence of maximum  
789 slopes in July–September (also October–December at PON), especially at HLE and the  
790 generally higher ratios at this station. Wada et al. (2011) and Niwa et al. (2014) also reported  
791 increased summer  $\Delta\text{CH}_4/\Delta\text{CO}$  over the western North Pacific, according to the in-situ  
792 measurements at several surface stations and aircraft flask measurements in the mid-  
793 troposphere. The main process for this seasonal variation of  $\Delta\text{CH}_4/\Delta\text{CO}$  might be the  
794 enhanced emissions of biogenic  $\text{CH}_4$  in summer (e.g., wetland and rice paddy emissions;  
795 Streets et al., 2003a; Yan et al., 2003) combined with concurrent lower anthropogenic  $\text{CO}$   
796 emissions in summer than in winter (due to less residential fuel use for heating, see Streets et  
797 al., 2003a). The faster photochemical destruction of  $\text{CO}$  by increased  $\text{OH}$  during summer  
798 cannot explain such large changes (less than 15% according to Wada et al. (2011)).

799

800 At HLE, the  $\Delta\text{CH}_4/\Delta\text{CO}$  ratio varies from  $1.2\pm 0.3$  to  $4.0\pm 1.2$  ppb ppb<sup>-1</sup> throughout the year,  
801 with a maximum in JAS, corresponding to the summer monsoon season (Fig. 14a-d). Based  
802 on the CARIBIC flights between 10 and 12 km from Frankfurt, Germany to Chennai, India,  
803 Baker et al. (2012) derived a  $\Delta\text{CH}_4/\Delta\text{CO}$  ratio in the range  $1.88(\pm 0.22)$  to  $4.43(\pm 0.56)$  in JAS  
804 over South Asia. The maximum  $\Delta\text{CH}_4/\Delta\text{CO}$  observed during summer in the mid-to-upper  
805 troposphere may be the result of higher biogenic CH<sub>4</sub> emission over the Indian subcontinent,  
806 lower CO emissions, combined with frequent widespread convective uplift of surface air  
807 during the SW monsoon (Schuck et al., 2010; Baker et al., 2012). The CARIBIC flights  
808 recorded similar  $\Delta\text{CH}_4/\Delta\text{CO}$  values to HLE, confirming that convection plays a dominant  
809 role compared to advection during the SW monsoon season. Outside the SW monsoon season,  
810 both the CARIBIC flights and HLE do generally not record strong effects of surface  
811 emissions due to the weakened vertical transport. With respect to the  $\Delta\text{CH}_4/\Delta\text{CO}$  ratios for  
812 January–March, April–June and October–December, our estimates are 1.5 to 4 times that of  
813 the ratios determined for air masses with signatures of fossil fuel combustion, according to  
814 several aircraft and ground observations in East and Southeast Asia (Table S11; Sawa et al.,  
815 2004; Lai et al., 2010; Wada et al., 2011; Niwa et al., 2014), which rules out fossil fuel  
816 combustion as an explanation for the higher ratios. Our ratios are comparable to the  
817  $\Delta\text{CH}_4/\Delta\text{CO}$  values inferred for air masses of Siberian origin during winter (Table S11; Harris  
818 et al., 2000; Chi et al., 2013), and we also obtain similar estimates of  $\Delta\text{CH}_4/\Delta\text{CO}$  from the  
819 flask measurements at KZM over the study period (The  $\Delta\text{CH}_4/\Delta\text{CO}$  ratios for KZM are  
820  $0.8\pm 0.2$ ,  $1.7\pm 0.2$  and  $1.5\pm 0.3$  ppb ppb<sup>-1</sup> for AMJ, OND and JFM, respectively), which are  
821 influenced by air masses originating from North Africa, the Middle East, and Central Asia as  
822 seen at HLE (see back-trajectories in Fig. S4). Given that oil and gas production accounts for  
823 50–70% of CH<sub>4</sub> emissions in these regions (EDGAR v4.2) and that over dry areas the  
824 daytime boundary layer is higher which favors injection of surface emissions into the

825 troposphere, the preferential enrichment in CH<sub>4</sub> relative to CO at HLE may tentatively be  
826 attributed to fossil CH<sub>4</sub> emissions over gas extraction regions and transported eastwards by  
827 westerlies (Harris et al., 2000; Tohjima et al., 1996).

828

829 At PON and PBL, the  $\Delta\text{CH}_4/\Delta\text{CO}$  ratios are in general considerably higher than 0.3 for all  
830 seasons, putting them in the range of ratios indicative of urban/industrial sources (Table S11;  
831 Harriss et al., 1994; Sawa et al., 2004; Xiao et al., 2004; Bakwin et al., 1995; Lai et al., 2010;  
832 Wada et al., 2011; Niwa et al., 2014). However, this does not rule out contributions from  
833 biomass/biofuel burning with emissions having a typical  $\Delta\text{CH}_4/\Delta\text{CO}$  ratio less than 0.3  
834 (Mauzerall et al., 1998; Andreae and Merlet, 2001; Mühle et al., 2002). Considering that  
835 biofuel and agriculture waste burning are the primary energy sources in rural India (Streets et  
836 al., 2003a; Yevich and Logan, 2003; Venkataraman et al., 2005), CO emissions from biofuel  
837 burning must be substantial (Lelieveld et al., 2001). This is the case for NE India located  
838 upwind of PON and PBL when the NE monsoon prevails during December–March.  
839 Nevertheless, the relatively low  $\Delta\text{CH}_4/\Delta\text{CO}$  derived from biomass/biofuel burning could be  
840 increased by CH<sub>4</sub> emissions from livestock with similarly distributed sources (EDGAR v4.2).  
841 Emissions of both trace gases from livestock and biomass/biofuel burning in the Indian  
842 subcontinent compiled by EDGAR v4.2 also indicate a CH<sub>4</sub> to CO ratio of 0.64–0.69 over the  
843 period of 2000–2008, close to the atmospheric measurements of  $\Delta\text{CH}_4/\Delta\text{CO}$  at PON and PBL  
844 during JFM (Fig. 14h and l).

845

### 846 **3.2.2 $\Delta\text{CH}_4/\Delta\text{CO}_2$**

847 The  $\Delta\text{CH}_4/\Delta\text{CO}_2$  ratios are strongly influenced by the high variability of CO<sub>2</sub> and the  
848 interpretation is complex. Unlike the positive correlation between CH<sub>4</sub> and CO consistently

849 observed at all three stations, the relationships between CH<sub>4</sub> and CO<sub>2</sub> residuals exhibit  
850 scattered and differences in the residual slopes for different stations and seasons (Fig. 15). At  
851 HLE, no significant correlations are found during AMJ, JAS, and OND (Fig. 15a–c), because  
852 CH<sub>4</sub> and CO<sub>2</sub> have distinct biogenic and/or photochemical sources and sinks over the  
853 northern mid-latitudes. During JFM when biogenic CO<sub>2</sub> fluxes and anthropogenic emissions  
854 are positive to the atmosphere, there is a significant and positive relationship between CH<sub>4</sub>  
855 and CO<sub>2</sub>, with a  $\Delta\text{CH}_4/\Delta\text{CO}_2$  ratio of  $45.6 \pm 1846.8$  ppb ppm<sup>-1</sup> ( $r=0.37$ ,  $p=0.03$ ; Fig. 15d). This  
856 value is close to the ratio of CH<sub>4</sub> and CO<sub>2</sub> anthropogenic emissions over North Africa (39.1–  
857 46.2 mmol mol<sup>-1</sup>), Central Asia (44.4–49.5 mmol mol<sup>-1</sup>) and to a lesser degree the Middle  
858 East (25.8–28.4 mmol mol<sup>-1</sup>) during the period of 2000–2010 (EDGAR v4.2), corresponding  
859 to the back-trajectories reaching HLE (Fig. 1a). It should be noted that this estimate of  
860  $\Delta\text{CH}_4/\Delta\text{CO}_2$  is subject to large uncertainty according to the standard deviation calculated  
861 with 1000 bootstrap replications (Fig. 15d), implying that CH<sub>4</sub> and CO<sub>2</sub> sources of various  
862 types and origins influence the HLE records.

863

864 At PON, in contrast to HLE, positive correlations occur between CH<sub>4</sub> and CO<sub>2</sub> residuals for  
865 all seasons except OND, with a  $\Delta\text{CH}_4/\Delta\text{CO}_2$  ratio of  $6.7 \pm 2.4$  ppb ppm<sup>-1</sup> ( $r=0.72$ ,  $p<0.001$ ) in  
866 AMJ and  $8.5 \pm 0.9$  ppb ppm<sup>-1</sup> in JAS ( $r=0.74$ ,  $p<0.001$ ), respectively (Fig. 15e and f). The  
867 relatively narrow ranges of slopes compared to that for HLE and PBL likely suggest co-  
868 located urban and industrial sources in South India upwind of PON during April–September  
869 (see back-trajectories in Fig. 1a). Emissions from biofuel burning could be a common source  
870 for both CH<sub>4</sub> and CO<sub>2</sub>, given the substantial biofuel use in South India (Yevich and Logan,  
871 2003) and the biofuel burning emission ratio of CH<sub>4</sub> and CO<sub>2</sub> derived from previous studies  
872 (5–10 mmol mol<sup>-1</sup>; Andreae and Merlet, 2001). Note that the CARIBIC flask measurements  
873 over India south of 20°N indicate a negative correlation between CH<sub>4</sub> and CO<sub>2</sub> at the altitudes

874 of 10-12 km during July–September, 2008 ( $r=-0.80$ ,  $p=0.002$ ; Fig. S14a), interpreted as the  
875 concurrent strong uptake of  $\text{CO}_2$  with enhanced emissions of  $\text{CH}_4$  during the SW monsoon.  
876 During JFM when the NE monsoon predominates,  $\text{CH}_4$  is positively correlated with  $\text{CO}_2$  with  
877 a  $\Delta\text{CH}_4/\Delta\text{CO}_2$  ratio of  $31.9\pm 1635.7$  ppb  $\text{ppm}^{-1}$  ( $r=0.45$ ,  $p=0.02$ ; Fig. 15h). Like at HLE, this  
878 ratio is subject to large uncertainty due to variability in  $\text{CH}_4$  and  $\text{CO}_2$  sources. The ratio based  
879 on the CARIBIC observations in the upper troposphere (10-12 km) is  $23.5\pm 41.4$  ppb  $\text{ppm}^{-1}$   
880 ( $r=0.67$ ,  $p=0.004$ ; Fig. S14b). The inconsistency of the  $\Delta\text{CH}_4/\Delta\text{CO}_2$  ratios estimated from the  
881 two datasets suggest that the flask measurements at the surface station PON do provide  
882 information more specific for constraining estimates of regional  $\text{CH}_4$  and  $\text{CO}_2$  fluxes.

883

884 Finally, at PBL, the prominent feature of the  $\text{CH}_4$ – $\text{CO}_2$  relationship is the significant and  
885 negative correlation observed during JAS, with a  $\Delta\text{CH}_4/\Delta\text{CO}_2$  ratio of  $-14.6\pm 16.4$  ppb  $\text{ppm}^{-1}$   
886 ( $r=-0.73$ ,  $p=0.007$ ; Fig. 15j). Since the time series of flask measurements at PBL is relatively  
887 short and has large data gaps (Fig. S2), correlations between trace gases could be influenced  
888 by abnormal pollution events. For example, excluding the event with  $\text{CH}_4$  residuals  $> +20$   
889 ppb (corresponding to the observation at PBL on 16 September 2009, the point marked with  
890 black circle in Fig. 15j) would substantially decrease the strength of negative correlation  
891 between  $\text{CH}_4$  and  $\text{CO}_2$  ( $r=-0.54$ ,  $p=0.09$ ). We will investigate the  $\text{CH}_4$  enriched event further  
892 in Sect. 3.3.

893

### 894 **3.2.3 $\Delta\text{CO}/\Delta\text{CO}_2$**

895 As shown in Fig. 16, at HLE, CO is positively correlated with  $\text{CO}_2$  during AMJ, with a  
896  $\Delta\text{CO}/\Delta\text{CO}_2$  ratio of  $35.8\pm 12.1$  ppb  $\text{ppm}^{-1}$  ( $r=0.53$ ,  $p=0.001$ ; Fig. 16a). During JFM, there is  
897 no significant relationship between CO and  $\text{CO}_2$  ( $r=0.15$ ,  $p=0.39$ ; Fig. 16d). However,

898 excluding an abnormal event with  $\Delta\text{CO}_2 = -1.8$  ppm on 8 January 2007 (the point marked  
899 with black circle in Fig. 16d) would give a significant and positive correlation between CO  
900 and  $\text{CO}_2$ , with a  $\Delta\text{CO}/\Delta\text{CO}_2$  ratio of  $55.7 \pm 259.1$  ppb  $\text{ppm}^{-1}$  ( $r=0.40$ ,  $p=0.02$ ; the red solid line  
901 in Fig. 16d). This ratio is less than half the emission ratio of CO to  $\text{CO}_2$  from forest/grassland  
902 biomass burning (Mauzerall et al., 1998; Andreae and Merlet, 2001), but higher than ratios of  
903 anthropogenic combustion sources in developed countries that are typically in the range of  
904 10–15 ppb  $\text{ppm}^{-1}$  (e.g., Suntharalingam et al., 2004; Wada et al., 2011; Takegawa et al., 2004).  
905 This could be attributed not only to the lower combustion efficiency of fuels in North Africa,  
906 the Middle East, and Central Asia where air masses at HLE originate from, but also to  
907 additional contribution from biofuel burning with relatively high CO to  $\text{CO}_2$  emission ratios  
908 (e.g., fuelwood, charcoal, agricultural residuals; Andreae and Merlet, 2001). Besides, the  
909 relatively high  $\Delta\text{CO}/\Delta\text{CO}_2$  in JFM compared to AMJ may further indicate a contribution of  
910 CO emissions from residential biofuel burning in winter (Wada et al., 2011), especially in  
911 developing countries within the footprint area.

912

913 At PON, a positive and significant correlation between CO and  $\text{CO}_2$  is found during AMJ,  
914 with a  $\Delta\text{CO}/\Delta\text{CO}_2$  ratio of  $13.4 \pm 76.8$  ppb  $\text{ppm}^{-1}$  ( $r=0.46$ ,  $p=0.03$ ; Fig. 16e). This ratio is  
915 similar to the ratios determined for air masses influenced by both fossil fuel emissions and  
916 biomass/biofuel burning during the same seasons. For example, based on the in-situ  
917 measurements in the upper troposphere during the CARIBIC flights between South China  
918 and Philippines in April 2007, Lai et al. (2010) reported the  $\Delta\text{CO}/\Delta\text{CO}_2$  ratios of 15.6–29.3  
919 ppb  $\text{ppm}^{-1}$  during pollution events influenced by both biomass/biofuel burning and fossil fuel  
920 combustion in Indochinese Peninsula. At PBL, CO is significantly and negatively correlated  
921 with  $\text{CO}_2$  during JAS ( $r=-0.68$ ,  $p=0.01$ ; Fig. 16j). However, we note that the  $\text{CH}_4$  abnormal  
922 event discussed in Sect. 3.2.2 is enriched in CO as well, and the negative relationship

923 between CO and CO<sub>2</sub> would no longer exist if we removed the event ( $r=-0.45$ ,  $p=0.16$ ). The  
924 simultaneous enhancement of CO and CH<sub>4</sub> may suggest possible influences of biomass  
925 burning episodes, which we will explore in detail in Sect. 3.3. During JFM, no significant  
926 relationship is found between CO and CO<sub>2</sub> for PON or PBL (Fig. 16h and l).

927

### 928 **3.3 Elevated CH<sub>4</sub> and CO events at PBL**

929 In this section, we discuss two elevated CH<sub>4</sub> and CO events at PBL during the SW monsoon  
930 season. Significant enhancements of CH<sub>4</sub> and CO were observed on September 16, 2009  
931 (July 29, 2011), with residuals from smoothed curves as high as 34.2 (29.2) ppb and 36.2  
932 (17.9) ppb for CH<sub>4</sub> and CO, respectively. We further analyzed CH<sub>4</sub> and CO measurements at  
933 Bukit Kototabang (BKT – 0.20 °S, 100.32 °E, 845.00 m a.s.l.), Indonesia, located upwind of  
934 PBL when the southwest monsoon prevails. The flask measurements at BKT detected  
935 enhanced CH<sub>4</sub> and CO with a magnitude of 38.0 and 66.1 ppb on September 8, 2009, about  
936 one week before the occurrence of the first CH<sub>4</sub> and CO event at PBL (Fig. 17a). The in-situ  
937 measurements at BKT also showed CH<sub>4</sub> and CO enhancements about one week before the  
938 second event at PBL, lasting over the period of 17 July–21 July 2011 (Fig. 17b). The  
939 coincidence of the two abnormal CH<sub>4</sub> and CO events at PBL and BKT possibly suggests  
940 influences of polluted air masses with common sources and origins. Moreover, the fire  
941 radiative power (FRP, mWm<sup>-2</sup>) during the sampling dates implies that the two abnormal CH<sub>4</sub>  
942 and CO events could be related to fire emissions in Indonesia (GFAS product version 1.0;  
943 Kaiser et al. 2012; Fig. S15). Note that the mechanisms we propose for the abnormal CH<sub>4</sub> and  
944 CO events and the possible linkage between PBL and BKT during the SW monsoon season  
945 are still speculative. Model experiments are needed to further confirm these hypotheses.

946

#### 947 **4 Conclusions**

948 In this paper we present the results of flask measurements of CO<sub>2</sub>, CH<sub>4</sub>, N<sub>2</sub>O, SF<sub>6</sub>, CO, and  
949 H<sub>2</sub> at three stations in India: Hanle (HLE), Pondicherry (PON) and Port-Blair (PBL), over the  
950 period of 2007–2011. Of these three stations, HLE is located at a high altitude and regarded  
951 as a continental background station in the mid-latitude of the Northern Hemisphere; PON is a  
952 tropical surface station located on the southwest coast of India, while PBL is an oceanic  
953 station located on the Andaman Islands, of similar latitude to PON. With a total of 188, 185,  
954 and 63 flask pair samples collected respectively from HLE, PON and PBL between 2007 and  
955 2011 (for PBL between 2009 and 2011), and analyzed at LSCE, the program represents an  
956 important logistical and analytical effort to produce a unique dataset of atmospheric trace gas  
957 observations over the Indian subcontinent. The observed records will serve as an important  
958 source of information to infer regional patterns of trace gas fluxes and atmospheric transport  
959 in this under-documented region. Several conclusions and implications are drawn from the  
960 first analyses of the datasets.

961

962 The annual gradients of the atmospheric mole fractions observed at PON and PBL, with  
963 respect to HLE as a reference, suggest significant emission sources of CO<sub>2</sub>, CH<sub>4</sub>, N<sub>2</sub>O, CO,  
964 and H<sub>2</sub> over the footprints of those stations, whereas SF<sub>6</sub> emission sources are weak. In  
965 particular, the annual mean N<sub>2</sub>O mole fractions at PON and PBL are higher than at HLE by  
966  $3.1 \pm 0.3$  and  $3.8 \pm 1.7$  ppb, notably larger than the typical N<sub>2</sub>O gradients observed between  
967 stations in Europe or North America, indicating substantial N<sub>2</sub>O emissions. The analyses of  
968 the atmospheric mole fractions with back-trajectories at the three stations further confirmed  
969 emission sources from South and NE India, and SE Asia, all of which are populous with high  
970 demand for food and energy, and thus high emissions from industrial, residential, and/or  
971 agricultural sectors.



972

973 The seasonal cycles for each trace gas reflect not only the seasonal variations of natural  
974 sources/sinks and anthropogenic emissions over the Indian subcontinent, but also the  
975 seasonally varying atmospheric transport, especially the monsoon circulations (including  
976 convection). Strong influences of the monsoon circulations are well depicted by the  
977 contrasting phases of CH<sub>4</sub> seasonal cycles between HLE and PON/PBL. At HLE, the distinct  
978 CH<sub>4</sub> maximum during June-September is likely related to the enhanced biogenic CH<sub>4</sub>  
979 emissions from wetlands and rice paddies in summer, combined with deep convection  
980 associated with the SW monsoon that mixes surface emissions into the mid-to-upper  
981 troposphere. By contrast, the CH<sub>4</sub> seasonal cycles at PON and PBL have seasonal minima  
982 during the SW monsoon season, reflecting influences of southern hemispheric air depleted in  
983 CH<sub>4</sub> transported at low altitudes, as well as high rates of OH oxidation. Covariance between  
984 species variations at the synoptic scale further helps identification and attribution of different  
985 sources and sinks, like fossil fuel combustion, biofuel burning and biogenic emissions.  
986 Besides, measurements of  $\delta^{13}\text{C-CO}_2$  have been recently started for HLE, and the 4-D  
987 distributions of CO<sub>2</sub> and CH<sub>4</sub> have been realistically simulated using a chemical transport  
988 model (LMDz-OR-INCA, Hauglustaine et al., 2004; Folberth et al., 2006) with zoom over  
989 South and East Asia (manuscript in preparation). Both of them may serve as valuable tools to  
990 disentangle and quantify contributions of different sources and meteorology to trace gas  
991 signals.

992

993 Apart from the flask measurements of trace gases presented in this study for the three stations,  
994 in-situ continuous measurements of CO<sub>2</sub> and CH<sub>4</sub> have also been deployed at HLE, PON and  
995 PBL in parallel, which would considerably contribute to the value of the stations through  
996 high-frequency air sampling. While the three stations have the potential to provide useful

997 constraints on estimates of trace gas fluxes over South and NE India (for example, Swathi et  
998 al. (2013) reported considerable reduction in the uncertainty of inverted CO<sub>2</sub> fluxes over  
999 temperate Eurasia by the inclusion of measurements at HLE), the monitoring network  
1000 requires further expansion to sample air masses from other parts of the Indian subcontinent.  
1001 Recently a few other atmospheric ground stations have been established in western India  
1002 (Bhattacharya et al., 2009; Tiwari et al., 2011; Tiwari et al., 2014; Tiwari and Kumar, 2012)  
1003 and the Himalayas (Kumar et al., 2010; Ganesan et al., 2013), with their concentration  
1004 footprints covering Central India (e.g., the Sinhadgad station; Tiwari et al., 2014; Tiwari and  
1005 Kumar, 2012), the Indo-Gangetic Plains and a large extent of the Himalayas (e.g., the  
1006 Dajeeling station; Ganesan et al., 2013). More efforts are needed to develop a comprehensive  
1007 observation network with adequate spatial and temporal coverage in this region.

1008

## 1009 **Acknowledgement**

1010 This study has been initiated within the framework of CaFICA-CEFIPRA project (2809-1). X.  
1011 Lin acknowledges PhD funding support from AIRBUS D&S and ESF T Torch Short Visiting  
1012 Grant for the 1<sup>st</sup> ICOS Science Conference (No. 6849). P. Ciais acknowledges support of the  
1013 Synergy grant ERC-2013-SyG-610028 IMBALANCE-P of the European Research Council.  
1014 The authors thank the engineers and staff from Indian Astronomical Observatory, Hanle, who  
1015 have been helpful at the station in Hanle, and Mr. Manil Kumar, Mr. Shambhulinga and Mr.  
1016 Prabhath Prabhu, who helped in flask sampling at Pondicherry University, Mr. B.  
1017 Parmeshwar from National Institute of Ocean Technology for operating and maintaining the  
1018 facilities in the stations. We also acknowledge the LSCE staff (L. Klenov, A. Crevier, B. Gal,  
1019 C. Peureux, M. Grand, L. Hogrel, V. Bazantay and A. Orgun) taking in charge the RAMCES  
1020 network logistics, measurements, and data processing.

1021

1022 **References**

- 1023 Attri, S. D., and Tyagi, A.: Climate Profile of India: Contribution to the Indian Network of Climate  
 1024 Change Assessment (NATIONAL COMMUNICATION-II) Ministry of Environment and Forests,  
 1025 Met Monograph No. Environment Meteorology-01/2010, India Meteorological Department,  
 1026 Ministry of Earth Sciences, New Delhi, 2010.
- 1027 Andreae, M. O., and Merlet, P.: Emission of trace gases and aerosols from biomass burning, *Global*  
 1028 *Biogeochem. Cy.*, 15, 955-966, 10.1029/2000gb001382, 2001.
- 1029 Babu, S. S., Chaubey, J. P., Krishna Moorthy, K., Gogoi, M. M., Kompalli, S. K., Sreekanth, V., Bagare, S.  
 1030 P., Bhatt, B. C., Gaur, V. K., Prabhu, T. P., and Singh, N. S.: High altitude (4520 m amsl)  
 1031 measurements of black carbon aerosols over western trans-Himalayas: Seasonal  
 1032 heterogeneity and source apportionment, *J. Geophys. Res.-Atmos.*, 116, D24201,  
 1033 10.1029/2011jd016722, 2011.
- 1034 Baker, A. K., Schuck, T. J., Brenninkmeijer, C. A. M., Rauthe-Schöch, A., Slemr, F., van Velthoven, P. F.  
 1035 J., and Lelieveld, J.: Estimating the contribution of monsoon-related biogenic production to  
 1036 methane emissions from South Asia using CARIBIC observations, *Geophys. Res. Lett.*, 39,  
 1037 L10813, 10.1029/2012gl051756, 2012.
- 1038 Bakwin, P. S., Tans, P. P., Zhao, C., Ussler, W., and Quesnell, E.: Measurements of carbon dioxide on a  
 1039 very tall tower, *Tellus B*, 47, 535-549, 10.1034/j.1600-0889.47.issue5.2.x, 1995.
- 1040 Bakwin, P. S., Tans, P. P., Hurst, D. F., and Zhao, C.: Measurements of carbon dioxide on very tall  
 1041 towers: results of the NOAA/CMDL program, *Tellus B*, 50B, 401-415, 1998.
- 1042 Bange, H. W., Andreae, M. O., Lal, S., Law, C. S., Naqvi, S. W. A., Patra, P. K., Rixen, T., and Upstill-  
 1043 Goddard, R. C.: Nitrous oxide emissions from the Arabian Sea: A synthesis, *Atmos. Chem.*  
 1044 *Phys.*, 1, 61-71, 10.5194/acp-1-61-2001, 2001.
- 1045 Bhattacharya, S. K., Borole, D. V., Francey, R. J., Allison, C. E., Steele, L. P., Krummel, P. B.,  
 1046 Langenfelds, R., Masarie, K. A., Tiwari, Y. K., and Patra, P. K.: Trace gases and CO<sub>2</sub> isotope  
 1047 records from Cabo de Rama, India, *Curr. Sci.*, 97, 1336-1344, 2009.
- 1048 Bond, S. W., Vollmer, M. K., Steinbacher, M., Henne, S., and Reimann, S.: Atmospheric molecular  
 1049 hydrogen (H<sub>2</sub>): observations at the high-altitude site Jungfraujoch, Switzerland, *Tellus B*, 63,  
 1050 64-76, 10.1111/j.1600-0889.2010.00509.x, 2011.
- 1051 Bousquet, P., Yver, C., Pison, I., Li, Y. S., Fortems, A., Hauglustaine, D., Szopa, S., Rayner, P. J., Novelli,  
 1052 P., Langenfelds, R., Steele, P., Ramonet, M., Schmidt, M., Foster, P., Morfopoulos, C., and  
 1053 Ciais, P.: A three-dimensional synthesis inversion of the molecular hydrogen cycle: Sources  
 1054 and sinks budget and implications for the soil uptake, *J. Geophys. Res.-Atmos.*, 116, D01302,  
 1055 10.1029/2010jd014599, 2011.
- 1056 Busenberg, E. and Plummer, L. N.: Dating young groundwater with sulfur hexafluoride: Natural and  
 1057 anthropogenic sources of sulfur hexafluoride, *Water Resour. Res.*, 36(10), 3011-3030,  
 1058 doi:10.1029/2000WR900151, 2000.
- 1059 Chi, X., Winderlich, J., Mayer, J. C., Panov, A. V., Heimann, M., Birmili, W., Heintzenberg, J., Cheng, Y.,  
 1060 and Andreae, M. O.: Long-term measurements of aerosol and carbon monoxide at the  
 1061 ZOTTO tall tower to characterize polluted and pristine air in the Siberian taiga, *Atmos. Chem.*  
 1062 *Phys.*, 13, 12271-12298, 10.5194/acp-13-12271-2013, 2013.
- 1063 Dlugokencky, E. J., Myers, R. C., Lang, P. M., Masarie, K. A., Crotwell, A. M., Thoning, K. W., Hall, B. D.,  
 1064 Elkins, J. W., and Steele, L. P.: Conversion of NOAA atmospheric dry air CH<sub>4</sub> mole fractions to  
 1065 a gravimetrically prepared standard scale, *J. Geophys. Res.-Atmos.*, 110, D18306,  
 1066 10.1029/2005jd006035, 2005.
- 1067 Dlugokencky, E.J., P.M. Lang, A.M. Crotwell, K.A. Masarie, and Crotwell, M. J.: Atmospheric Methane  
 1068 Dry Air Mole Fractions from the NOAA ESRL Carbon Cycle Cooperative Global Air Sampling  
 1069 Network, 1983-2013, Version: 2014-06-24, Path:  
 1070 [ftp://aftp.cmdl.noaa.gov/data/trace\\_gases/ch4/flask/surface/](ftp://aftp.cmdl.noaa.gov/data/trace_gases/ch4/flask/surface/) (last access: 11 December  
 1071 2014), 2014a.

1072 Dlugokencky, E.J., P.M. Lang, K.A. Masarie, A.M. Crotwell, and Crotwell, M.J.: Atmospheric Carbon  
1073 Dioxide Dry Air Mole Fractions from the NOAA ESRL Carbon Cycle Cooperative Global Air  
1074 Sampling Network, 1968-2013, Version: 2014-06-27, Path:  
1075 [ftp://aftp.cmdl.noaa.gov/data/trace\\_gases/co2/flask/surface/](ftp://aftp.cmdl.noaa.gov/data/trace_gases/co2/flask/surface/) (last access: 11 December  
1076 2014), 2014b.

1077 Draxler, R. R., and Rolph, G. D.: HYSPLIT (HYbrid Single-Particle Lagrangian Integrated Trajectory),  
1078 Model access via NOAA ARL READY website <http://www.arl.noaa.gov/ready/hysplit4.html>  
1079 (last access: 9 January 2014), NOAA Air Resources Laboratory, Silver Spring, MD, 2003.

1080 Duncan, B. N., Martin, R. V., Staudt, A. C., Yevich, R., and Logan, J. A.: Interannual and seasonal  
1081 variability of biomass burning emissions constrained by satellite observations, , J. Geophys.  
1082 Res.-Atmos., 108, 4100, 10.1029/2002jd002378, 2003.

1083 EC-JRC/PBL (European Commission, Joint Research Centre/Netherlands Environmental Assessment  
1084 Agency): Emission Database for Global Atmospheric Research (EDGAR), release version 4.2:  
1085 available at: <http://edgar.jrc.ec.europa.eu> (last access: 16 August 2014), 2011

1086 Ehhalt, D. H., and Rohrer, F.: The tropospheric cycle of H<sub>2</sub>: a critical review, Tellus B, 61, 500-535,  
1087 10.1111/j.1600-0889.2009.00416.x, 2009.

1088 Fang, S.-X., Zhou, L.-X., Masarie, K. A., Xu, L. and Rella, C. W.: Study of atmospheric CH<sub>4</sub> mole  
1089 fractions at three WMO/GAW stations in China, J. Geophys. Res.-Atmos., 118(10), 4874–  
1090 4886, doi:10.1002/jgrd.50284, 2013.

1091 Fang, S. X., Zhou, L. X., Tans, P. P., Ciais, P., Steinbacher, M., Xu, L., and Luan, T.: In situ measurement  
1092 of atmospheric CO<sub>2</sub> at the four WMO/GAW stations in China, Atmos. Chem. Phys., 14, 2541-  
1093 2554, 10.5194/acp-14-2541-2014, 2014.

1094 Folberth, G. A., Hauglustaine, D. A., Lathière, J. and Brocheton, F.: Interactive chemistry in the  
1095 Laboratoire de Météorologie Dynamique general circulation model: model description and  
1096 impact analysis of biogenic hydrocarbons on tropospheric chemistry, Atmos. Chem. Phys.,  
1097 6(8), 2273–2319, doi:10.5194/acp-6-2273-2006, 2006.

1098 Gadgil, S.: The Indian Monsoon and its variability, Annu. Rev. Earth Planet Sci., 31, 429-467,  
1099 10.1146/annurev.earth.31.100901.141251, 2003.

1100 Gamnitzer, U., Karstens, U., Kromer, B., Neubert, R. E. M., Meijer, H. A. J., Schroeder, H., and Levin, I.:  
1101 Carbon monoxide: A quantitative tracer for fossil fuel CO<sub>2</sub>?, J. Geophys. Res.-Atmos., 111,  
1102 D22302, 10.1029/2005jd006966, 2006.

1103 Ganesan, A. L., Chatterjee, A., Prinn, R. G., Harth, C. M., Salameh, P. K., Manning, A. J., Hall, B. D.,  
1104 Mühle, J., Meredith, L. K., Weiss, R. F., O'Doherty, S., and Young, D.: The variability of  
1105 methane, nitrous oxide and sulfur hexafluoride in Northeast India, Atmos. Chem. Phys., 13,  
1106 10633-10644, 10.5194/acp-13-10633-2013, 2013.

1107 Garg, A., Shukla, P. R., Kapshe, M., and Menon, D.: Indian methane and nitrous oxide emissions and  
1108 mitigation flexibility, Atmos. Environ., 38, 1965-1977, [http://dx.doi.org/10.1016/](http://dx.doi.org/10.1016/j.atmosenv.2003.12.032)  
1109 [j.atmosenv.2003.12.032](http://dx.doi.org/10.1016/j.atmosenv.2003.12.032), 2004.

1110 Garg, A., Shukla, P. R., and Upadhyay, J.: N<sub>2</sub>O emissions of India: an assessment of temporal, regional  
1111 and sector trends, Clim. Change, 110, 755-782, 10.1007/s10584-011-0094-9, 2012.

1112 Goswami, B. N.: South Asian Monsoon, in: Intraseasonal variability in the Atmosphere-Ocean Climate  
1113 System, edited by: Lau, W. K. M., and Waliser, D. E., Springer & Praxis Publishing, Chichester,  
1114 UK, 2005.

1115 Granier, C., Bessagnet, B., Bond, T., D'Angiola, A., Denier van der Gon, H., Frost, G., Heil, A., Kaiser, J.,  
1116 Kinne, S., Klimont, Z., Kloster, S., Lamarque, J.-F., Lioussé, C., Masui, T., Meleux, F., Mieville,  
1117 A., Ohara, T., Raut, J.-C., Riahi, K., Schultz, M., Smith, S., Thompson, A., van Aardenne, J., van  
1118 der Werf, G. and van Vuuren, D.: Evolution of anthropogenic and biomass burning emissions  
1119 of air pollutants at global and regional scales during the 1980–2010 period, Clim. Change,  
1120 109(1-2), 163–190, doi:10.1007/s10584-011-0154-1, 2011.

1121 Grant, A., Witham, C. S., Simmonds, P. G., Manning, A. J., and O'Doherty, S.: A 15 year record of high-  
1122 frequency, in situ measurements of hydrogen at Mace Head, Ireland, *Atmos. Chem. Phys.*, 10,  
1123 1203-1214, 10.5194/acp-10-1203-2010, 2010.

1124 Hall, B. D., Dutton, G. S., and Elkins, J. W.: The NOAA nitrous oxide standard scale for atmospheric  
1125 observations, *J. Geophys. Res.-Atmos.*, 112, D09305, 10.1029/2006jd007954, 2007.

1126 Harris, J. M., Dlugokencky, E. J., Oltmans, S. J., Tans, P. P., Conway, T. J., Novelli, P. C., Thoning, K. W.,  
1127 and Kahl, J. D. W.: An interpretation of trace gas correlations during Barrow, Alaska, winter  
1128 dark periods, 1986–1997, *J. Geophys. Res.-Atmos.*, 105, 17267-17278,  
1129 10.1029/2000jd900167, 2000.

1130 Harriss, R. C., Sachse, G. W., Collins, J. E., Wade, L., Bartlett, K. B., Talbot, R. W., Browell, E. V., Barrie,  
1131 L. A., Hill, G. F., and Burney, L. G.: Carbon monoxide and methane over Canada: July–August  
1132 1990, *J. Geophys. Res.-Atmos.*, 99, 1659-1669, 10.1029/93jd01906, 1994.

1133 Haszpra, L., Barcza, Z., Hidy, D., Szilágyi, I., Dlugokencky, E., and Tans, P.: Trends and temporal  
1134 variations of major greenhouse gases at a rural site in Central Europe, *Atmos. Environ.*, 42,  
1135 8707-8716, <http://dx.doi.org/10.1016/j.atmosenv.2008.09.012>, 2008.

1136 Hauglustaine, D. A., and Ehhalt, D. H.: A three-dimensional model of molecular hydrogen in the  
1137 troposphere, *J. Geophys. Res.- Atmos.*, 107, 4330, 10.1029/2001jd001156, 2002.

1138 Hauglustaine, D. A., Hourdin, F., Jourdain, L., Filiberti, M. A., Walters, S., Lamarque, J. F., and Holland,  
1139 E. A.: Interactive chemistry in the Laboratoire de Météorologie Dynamique general  
1140 circulation model: Description and background tropospheric chemistry evaluation, *J.*  
1141 *Geophys. Res.-Atmos.*, 109, D04314, 10.1029/2003jd003957, 2004.

1142 Huang, J., Golombek, A., Prinn, R., Weiss, R., Fraser, P., Simmonds, P., Dlugokencky, E. J., Hall, B.,  
1143 Elkins, J., Steele, P., Langenfelds, R., Krummel, P., Dutton, G. and Porter, L.: Estimation of  
1144 regional emissions of nitrous oxide from 1997 to 2005 using multinet network measurements, a  
1145 chemical transport model, and an inverse method, *J. Geophys. Res.-Atmos.*, 113(D17),  
1146 D17313, doi:10.1029/2007JD009381, 2008.

1147 IPCC: Climate Change 2013: The Physical Science Basis. Contribution of Working Group I to the Fifth  
1148 Assessment Report of the Intergovernmental Panel on Climate Change, Cambridge  
1149 University Press, Cambridge, 2013.

1150 IPCC: Climate Change 2014: Impacts, Adaptation, and Vulnerability. Part A: Global and Sectoral  
1151 Aspects. Contribution of Working Group II to the Fifth Assessment Report of the  
1152 Intergovernmental Panel on Climate Change [Field, C.B., V.R. Barros, D.J. Dokken, K.J. Mach,  
1153 M.D. Mastrandrea, T.E. Bilir, M. Chatterjee, K.L. Ebi, Y.O. Estrada, R.C. Genova, B. Girma, E.S.  
1154 Kissel, A.N. Levy, S. MacCracken, P.R. Mastrandrea, and L.L. White (eds.)], Cambridge  
1155 University Press, Cambridge, United Kingdom and New York, NY, USA, 2014a.

1156 IPCC: Climate Change 2014: Impacts, Adaptation, and Vulnerability. Part B: Regional Aspects.  
1157 Contribution of Working Group II to the Fifth Assessment Report of the Intergovernmental  
1158 Panel on Climate Change [Barros, V.R., C.B. Field, D.J. Dokken, M.D. Mastrandrea, K.J. Mach,  
1159 T.E. Bilir, M. Chatterjee, K.L. Ebi, Y.O. Estrada, R.C. Genova, B. Girma, E.S. Kissel, A.N. Levy, S.  
1160 MacCracken, P.R. Mastrandrea, and L.L. White (eds.)], Cambridge University Press,  
1161 Cambridge, United Kingdom and New York, NY, USA, 2014b.

1162 Jiang, J. H., Livesey, N. J., Su, H., Neary, L., McConnell, J. C., and Richards, N. A. D.: Connecting surface  
1163 emissions, convective uplifting, and long-range transport of carbon monoxide in the upper  
1164 troposphere: New observations from the Aura Microwave Limb Sounder, *Geophys. Res. Lett.*,  
1165 34, L18812, 10.1029/2007gl030638, 2007a.

1166 Jiang, X., Ku, W. L., Shia, R.-L., Li, Q., Elkins, J. W., Prinn, R. G., and Yung, Y. L.: Seasonal cycle of N<sub>2</sub>O:  
1167 Analysis of data, *Global Biogeochemical Cycles*, 21, GB1006, 10.1029/2006gb002691, 2007b.

1168 Jordan, A., and Steinberg, B.: Calibration of atmospheric hydrogen measurements, *Atmos. Meas.*  
1169 *Tech.*, 4, 509-521, 10.5194/amt-4-509-2011, 2011.

1170 Kaiser, J. W., Heil, A., Andreae, M. O., Benedetti, A., Chubarova, N., Jones, L., Morcrette, J. J.,  
1171 Razingerg, M., Schultz, M. G., Suttie, M., and van der Werf, G. R.: Biomass burning emissions

1172 estimated with a global fire assimilation system based on observed fire radiative power,  
1173 Biogeosciences, 9, 527-554, 10.5194/bg-9-527-2012, 2012.

1174 Kaplan, J. O., Folberth, G. and Hauglustaine, D. A.: Role of methane and biogenic volatile organic  
1175 compound sources in late glacial and Holocene fluctuations of atmospheric methane  
1176 concentrations, Global Biogeochem. Cycles, 20(2), GB2016, doi:10.1029/2005GB002590,  
1177 2006.

1178 Kasischke, E. S., Hyer, E. J., Novelli, P. C., Bruhwiler, L. P., French, N. H. F., Sukhinin, A. I., Hewson, J.  
1179 H., and Stocks, B. J.: Influences of boreal fire emissions on Northern Hemisphere  
1180 atmospheric carbon and carbon monoxide, Global Biogeochem. Cy., 19, GB1012,  
1181 10.1029/2004gb002300, 2005.

1182 King, A. W., Andres, R. J., Davis, K. J., Hafer, M., Hayes, D. J., Huntzinger, D. N., de Jong, B., Kurz, W.  
1183 A., McGuire, A. D., Vargas, R., Wei, Y., West, T. O. and Woodall, C. W.: North America's net  
1184 terrestrial CO<sub>2</sub> exchange with the atmosphere 1990–2009, Biogeosciences, 12(2), 399–414,  
1185 doi:10.5194/bg-12-399-2015, 2015.

1186 Konovalov, I. B., Berezin, E. V., Ciais, P., Broquet, G., Beekmann, M., Hadji-Lazaro, J., Clerbaux, C.,  
1187 Andreae, M. O., Kaiser, J. W., and Schulze, E. D.: Constraining CO<sub>2</sub> emissions from open  
1188 biomass burning by satellite observations of co-emitted species: a method and its  
1189 application to wildfires in Siberia, Atmos. Chem. Phys., 14, 10383-10410, 10.5194/acp-14-  
1190 10383-2014, 2014.

1191 Kumar, R., Naja, M., Venkataramani, S., and Wild, O.: Variations in surface ozone at Nainital: A high-  
1192 altitude site in the central Himalayas, J. Geophys. Res.-Atmos., 115, D16302,  
1193 10.1029/2009jd013715, 2010.

1194 Kurokawa, J., Ohara, T., Morikawa, T., Hanayama, S., Janssens-Maenhout, G., Fukui, T., Kawashima,  
1195 K., and Akimoto, H.: Emissions of air pollutants and greenhouse gases over Asian regions  
1196 during 2000–2008: Regional Emission inventory in ASia (REAS) version 2, Atmos. Chem. Phys.,  
1197 13, 11019-11058, 10.5194/acp-13-11019-2013, 2013.

1198 Lai, S. C., Baker, A. K., Schuck, T. J., van Velthoven, P., Oram, D. E., Zahn, A., Hermann, M., Weigelt, A.,  
1199 Slemr, F., Brenninkmeijer, C. A. M., and Ziereis, H.: Pollution events observed during CARIBIC  
1200 flights in the upper troposphere between South China and the Philippines, Atmos. Chem.  
1201 Phys., 10, 1649-1660, 10.5194/acp-10-1649-2010, 2010.

1202 Lal, S., Chandra, N., Venkataramani, S.: A study of CO<sub>2</sub> and related trace gases using a laser based  
1203 technique at an urban site in western India. Submitted to Curr. Sci., 2015.

1204 Langenfelds, R. L., Francey, R. J., Pak, B. C., Steele, L. P., Lloyd, J., Trudinger, C. M., and Allison, C. E.:  
1205 Interannual growth rate variations of atmospheric CO<sub>2</sub> and its  $\delta^{13}\text{C}$ , H<sub>2</sub>, CH<sub>4</sub>, and CO between  
1206 1992 and 1999 linked to biomass burning, Global Biogeochem. Cy., 16, 1048,  
1207 10.1029/2001gb001466, 2002.

1208 Lawrence, M. G., and Lelieveld, J.: Atmospheric pollutant outflow from southern Asia: a review,  
1209 Atmos. Chem. Phys., 10, 11017-11096, 10.5194/acp-10-11017-2010, 2010.

1210 Lelieveld, J., Crutzen, P. J., Ramanathan, V., Andreae, M. O., Brenninkmeijer, C. A. M., Campos, T.,  
1211 Cass, G. R., Dickerson, R. R., Fischer, H., de Gouw, J. A., Hansel, A., Jefferson, A., Kley, D., de  
1212 Laat, A. T. J., Lal, S., Lawrence, M. G., Lobert, J. M., Mayol-Bracero, O. L., Mitra, A. P.,  
1213 Novakov, T., Oltmans, S. J., Prather, K. A., Reiner, T., Rodhe, H., Scheeren, H. A., Sikka, D., and  
1214 Williams, J.: The Indian Ocean Experiment: Widespread Air Pollution from South and  
1215 Southeast Asia, Science, 291, 1031-1036, 2001.

1216 Le Quéré, C., Moriarty, R., Andrew, R. M., Peters, G. P., Ciais, P., Friedlingstein, P., Jones, S. D., Sitch,  
1217 S., Tans, P., Arneeth, A., Boden, T. A., Bopp, L., Bozec, Y., Canadell, J. G., Chevallier, F., Cosca, C.  
1218 E., Harris, I., Hoppema, M., Houghton, R. A., House, J. I., Jain, A. K., Johannessen, T., Kato, E.,  
1219 Keeling, R. F., Kitidis, V., Klein Goldewijk, K., Koven, C., Landa, C. S., Landschützer, P., Lenton,  
1220 A., Lima, I. D., Marland, G. H., Mathis, J. T., Metz, N., Nojiri, Y., Olsen, A., Ono, T., Peters, W.,  
1221 Pfeil, B., Poulter, B., Raupach, M. R., Regnier, P., Rödenbeck, C., Saito, S., Sailsbury, J. E.,  
1222 Schuster, U., Schwinger, J., Séférian, R., Segsneider, J., Steinhoff, T., Stocker, B. D., Sutton,

1223 A. J., Takahashi, T., Tilbrook, B., van der Werf, G. R., Viovy, N., Wang, Y.-P., Wanninkhof, R.,  
1224 Wiltshire, A., and Zeng, N.: Global Carbon Budget 2014. *Earth Syst. Sci. Data Discuss.*,  
1225 doi:10.5194/essdd-7-521-2014, 2014

1226 Levin, I., Ciais, P., Langenfelds, R., Schmidt, M., Ramonet, M., Sidorov, K., Tchebakova, N., Gloor, M.,  
1227 Heimann, M., Schulze, E. D., Vygodskaya, N. N., Shibistova, O., and Lloyd, J.: Three years of  
1228 trace gas observations over the EuroSiberian domain derived from aircraft sampling — a  
1229 concerted action, *Tellus B*, 54, 696-712, 10.1034/j.1600-0889.2002.01352.x, 2002.

1230 Li, Q., Jiang, J. H., Wu, D. L., Read, W. G., Livesey, N. J., Waters, J. W., Zhang, Y., Wang, B., Filipiak, M.  
1231 J., Davis, C. P., Turquety, S., Wu, S., Park, R. J., Yantosca, R. M., and Jacob, D. J.: Convective  
1232 outflow of South Asian pollution: A global CTM simulation compared with EOS MLS  
1233 observations, *Geophys. Res. Lett.*, 32, L14826, 10.1029/2005gl022762, 2005.

1234 Liao, T., Camp, C. D., and Yung, Y. L.: The seasonal cycle of N<sub>2</sub>O, *Geophys. Res. Lett.*, 31, L17108,  
1235 10.1029/2004gl020345, 2004.

1236 Logan, J. A., Prather, M. J., Wofsy, S. C., and McElroy, M. B.: Tropospheric chemistry: A global  
1237 perspective, *J. Geophys. Res.-Oceans*, 86, 7210-7254, 10.1029/JC086iC08p07210, 1981.

1238 Lopez, M.: Estimation des émissions de gaz à effet de serre à différentes échelles en France à l'aide  
1239 d'observations de haute précision, Ph.D, Université Paris-Sud, 2012.

1240 Lopez, M., Schmidt, M., Ramonet, M., Bonne, J.-L., Colomb, A., Kazan, V., Laj, P., and Pichon, J.-M.: A  
1241 gas chromatograph system for semi-continuous greenhouse gas measurements at Puy de  
1242 Dôme station, Central France, *Atmos. Meas. Tech. Discuss.*, 8(3), 3121–3170,  
1243 doi:10.5194/amtd-8-3121-2015, 2015.

1244 Luyssaert, S., Abril, G., Andres, R., Bastviken, D., Bellassen, V., Bergamaschi, P., Bousquet, P.,  
1245 Chevallier, F., Ciais, P., Corazza, M., Dechow, R., Erb, K.-H., Etiope, G., Fortems-Cheiney, A.,  
1246 Grassi, G., Hartmann, J., Jung, M., Lathière, J., Lohila, A., Mayorga, E., Moosdorf, N., Njakou,  
1247 D. S., Otto, J., Papale, D., Peters, W., Peylin, P., Raymond, P., Rödenbeck, C., Saarnio, S.,  
1248 Schulze, E.-D., Szopa, S., Thompson, R., Verkerk, P. J., Vuichard, N., Wang, R., Wattenbach, M.  
1249 and Zaehle, S.: The European land and inland water CO<sub>2</sub>, CO, CH<sub>4</sub> and N<sub>2</sub>O balance between  
1250 2001 and 2005, *Biogeosciences*, 9(8), 3357–3380, doi:10.5194/bg-9-3357-2012, 2012.

1251 Machida, T., Matsueda, H., Sawa, Y., Nakagawa, Y., Hirokuni, K., Kondo, N., Goto, K., Nakazawa, T.,  
1252 Ishikawa, K., and Ogawa, T.: Worldwide Measurements of Atmospheric CO<sub>2</sub> and Other Trace  
1253 Gas Species Using Commercial Airlines, *J. Atmos. Ocean. Tech.*, 25, 1744-1754,  
1254 10.1175/2008jtecha1082.1, 2008.

1255 Maiss, M., Steele, L. P., Francey, R. J., Fraser, P. J., Langenfelds, R. L., Trivett, N. B. A., and Levin, I.:  
1256 Sulfur hexafluoride—A powerful new atmospheric tracer, *Atmos. Environ.*, 30, 1621-1629,  
1257 [http://dx.doi.org/10.1016/1352-2310\(95\)00425-4](http://dx.doi.org/10.1016/1352-2310(95)00425-4), 1996.

1258 Matthews, E., Fung, I. and Lerner, J.: Methane emission from rice cultivation: Geographic and  
1259 seasonal distribution of cultivated areas and emissions, *Global Biogeochem. Cycles*, 5(1), 3–  
1260 24, doi:10.1029/90GB02311, 1991.

1261 Mauzerall, D. L., Logan, J. A., Jacob, D. J., Anderson, B. E., Blake, D. R., Bradshaw, J. D., Heikes, B.,  
1262 Sachse, G. W., Singh, H., and Talbot, B.: Photochemistry in biomass burning plumes and  
1263 implications for tropospheric ozone over the tropical South Atlantic, *J. Geophys. Res.-Atmos.*,  
1264 103, 8401-8423, 10.1029/97jd02612, 1998.

1265 Messenger, C.: Estimation des flux de gaz à effet de serre à l'échelle régionale à partir de mesures  
1266 atmosphériques, Université Paris 7 - Denis Diderot, 2007.

1267 Minschwaner, K., Salawitch, R. J., and McElroy, M. B.: Absorption of solar radiation by O<sub>2</sub>:  
1268 Implications for O<sub>3</sub> and lifetimes of N<sub>2</sub>O, CFC<sub>3</sub>, and CF<sub>2</sub>Cl<sub>2</sub>, *J. Geophys. Res.-Atmos.*, 98,  
1269 10543-10561, 10.1029/93jd00223, 1993.

1270 Montzka, S. A., Dlugokencky, E. J., and Butler, J. H.: Non-CO<sub>2</sub> greenhouse gases and climate change,  
1271 *Nature*, 476, 43-50, 2011.

1272 Moorthy, K. K., Sreekanth, V., Chaubey, J. P., Gogoi, M. M., Babu, S. S., Kompalli, S. K., Bagare, S. P.,  
1273 Bhatt, B. C., Gaur, V. K., Prabhu, T. P., Singh, N. S.: Fine and ultrafine particles at near-free

1274 tropospheric environment over the high-altitude station Hanle in the Trans-Himalaya: New  
1275 particle formation and size distribution, *J. Geophys. Res.-Atmos.*, 116, D20212, doi: 10.1029/  
1276 2011JD016343, 2011

1277 Morgan, C. G., Allen, M., Liang, M. C., Shia, R. L., Blake, G. A., and Yung, Y. L.: Isotopic fractionation of  
1278 nitrous oxide in the stratosphere: Comparison between model and observations, *J. Geophys.*  
1279 *Res.-Atmos.*, 109, D04305, 10.1029/2003jd003402, 2004.

1280 Morris, R. A., Miller, T. M., Viggiano, A. A., Paulson, J. F., Solomon, S., and Reid, G.: Effects of electron  
1281 and ion reactions on atmospheric lifetimes of fully fluorinated compounds, *J. Geophys. Res.-*  
1282 *Atmos.*, 100, 1287-1294, 10.1029/94jd02399, 1995.

1283 Mühle, J., Brenninkmeijer, C. A. M., Rhee, T. S., Slemr, F., Oram, D. E., Penkett, S. A., and Zahn, A.:  
1284 Biomass burning and fossil fuel signatures in the upper troposphere observed during a  
1285 CARIBIC flight from Namibia to Germany, *Geophys. Res. Lett.*, 29, 1910,  
1286 10.1029/2002gl015764, 2002.

1287 Niwa, Y., Machida, T., Sawa, Y., Matsueda, H., Schuck, T. J., Brenninkmeijer, C. A. M., Imasu, R., and  
1288 Satoh, M.: Imposing strong constraints on tropical terrestrial CO<sub>2</sub> fluxes using passenger  
1289 aircraft based measurements, *J. Geophys. Res.-Atmos.*, 117, D11303, 10.1029/  
1290 2012jd017474, 2012.

1291 Niwa, Y., Tsuboi, K., Matsueda, H., Sawa, Y., Machida, T., Nakamura, M., Kawasato, T., Saito, K.,  
1292 Takatsuji, S., Tsuji, K., Nishi, H., Dehara, K., Baba, Y., Kuboike, D., Iwatsubo, S., Ohmori, H.,  
1293 and Hanamiya, Y.: Seasonal Variations of CO<sub>2</sub>, CH<sub>4</sub>, N<sub>2</sub>O and CO in the Mid-Troposphere over  
1294 the Western North Pacific Observed Using a C-130H Cargo Aircraft, *J. Meteor. Soc. Japan. Ser.*  
1295 *II*, 92, 55-70, 10.2151/jmsj.2014-104, 2014.

1296 Novelli, P. C., Steele, L. P., and Tans, P. P.: Mixing ratios of carbon monoxide in the troposphere, *J.*  
1297 *Geophys. Res.-Atmos.*, 97, 20731-20750, 10.1029/92jd02010, 1992.

1298 Novelli, P. C., Masarie, K. A., and Lang, P. M.: Distributions and recent changes of carbon monoxide  
1299 in the lower troposphere, *J. Geophys. Res.-Atmos.*, 103, 19015-19033, 10.1029/98jd01366,  
1300 1998.

1301 Novelli, P. C., Lang, P. M., Masarie, K. A., Hurst, D. F., Myers, R., and Elkins, J. W.: Molecular hydrogen  
1302 in the troposphere: Global distribution and budget, *J. Geophys. Res.-Atmos.*, 104, 30427-  
1303 30444, 10.1029/1999jd900788, 1999.

1304 Novelli, P. C., Lang, P. M., and Masarie, K. A.: Atmospheric Hydrogen Dry Air Mole Fractions from the  
1305 NOAA ESRL Carbon Cycle Cooperative Global Air Sampling Network, 1988-2009, Version:  
1306 2014-08-27, Path: [ftp://aftp.cmdl.noaa.gov/data/trace\\_gases/h2/flask/surface/](ftp://aftp.cmdl.noaa.gov/data/trace_gases/h2/flask/surface/) (last access:  
1307 11 December 2014), 2014a.

1308 Novelli, P.C. and Masarie, K.A.: Atmospheric Carbon Monoxide Dry Air Mole Fractions from the  
1309 NOAA ESRL Carbon Cycle Cooperative Global Air Sampling Network, 1988-2013, Version:  
1310 2014-07-02, Path: [ftp://aftp.cmdl.noaa.gov/data/trace\\_gases/co/flask/surface/](ftp://aftp.cmdl.noaa.gov/data/trace_gases/co/flask/surface/) (last access:  
1311 11 December 2014), 2014b.

1312 Olivier, J. G. J., Van Aardenne, J. A., Dentener, F., Ganzeveld, L. and Peters, J. A. H. W.: Recent trends  
1313 in global greenhouse gas emissions: regional trends and spatial distribution of key sources, in  
1314 *Non-CO<sub>2</sub> Greenhouse Gases (NCGG-4)*, edited by A. Van Amstel, pp. 325–330, Millpress,  
1315 Rotterdam, The Netherlands., 2005.

1316 Paris, J. D., Ciais, P., NÉDÉLec, P., Ramonet, M., Belan, B. D., Arshinov, M. Y., Golitsyn, G. S., Granberg,  
1317 I., Stohl, A., Cayez, G., Athier, G., Boumard, F., and Cousin, J. M.: The YAK-AEROSIB  
1318 transcontinental aircraft campaigns: new insights on the transport of CO<sub>2</sub>, CO and O<sub>3</sub> across  
1319 Siberia, *Tellus B*, 60, 551-568, 10.1111/j.1600-0889.2008.00369.x, 2008.

1320 Park, M., Randel, W. J., Gettelman, A., Massie, S. T., and Jiang, J. H.: Transport above the Asian  
1321 summer monsoon anticyclone inferred from Aura Microwave Limb Sounder tracers, *J.*  
1322 *Geophys. Res.-Atmos.*, 112, D16309, 10.1029/2006jd008294, 2007.



1323 Pathak, H., Bhatia, A., Jain, N., and Aggarwal, P. K.: Greenhouse Gas Emission and Mitigation in  
1324 Indian Agriculture - A Review, in: ING Bulletins on Regional Assessment of Reactive Nitrogen,  
1325 Bulletin No. 19, edited by: Singh, B., SCON-ING, New Delhi, i-iv & 1-34, 2010.

1326 Patra, P., Takigawa, M., Ishijima, K., Choi, B.-C., Cunnold, D., J. Dlugokencky, E., Fraser, P., J. Gomez-  
1327 Pelaez, A., Goo, T.-Y., Kim, J.-S., Krummel, P., Langenfelds, R., Meinhardt, F., Mukai, H.,  
1328 O'Doherty, S., Prinn, R. G., Simmonds, P., Steele, P., Tohjima, Y., Tsuboi, K., Uhse, K., Weiss,  
1329 R., Worthy, D., and Nakazawa, T.: Growth Rate, Seasonal, Synoptic, Diurnal Variations and  
1330 Budget of Methane in the Lower Atmosphere, *J. Meteor. Soc. Japan. Ser. II*, 87, 635-663,  
1331 2009.

1332 Patra, P. K., Lal, S., Venkataramani, S., de Sousa, S. N., Sarma, V. V. S. S., and Sardesai, S.: Seasonal  
1333 and spatial variability in N<sub>2</sub>O distribution in the Arabian Sea, *Deep Sea Res. Part I: Oceanogr*  
1334 *Res. Pap.*, 46, 529-543, [http://dx.doi.org/10.1016/S0967-0637\(98\)00071-5](http://dx.doi.org/10.1016/S0967-0637(98)00071-5), 1999.

1335 Patra, P. K., Houweling, S., Krol, M., Bousquet, P., Belikov, D., Bergmann, D., Bian, H., Cameron-Smith,  
1336 P., Chipperfield, M. P., Corbin, K., Fortems-Cheiney, A., Fraser, A., Gloor, E., Hess, P., Ito, A.,  
1337 Kawa, S. R., Law, R. M., Loh, Z., Maksyutov, S., Meng, L., Palmer, P. I., Prinn, R. G., Rigby, M.,  
1338 Saito, R., and Wilson, C.: TransCom model simulations of CH<sub>4</sub> and related species: linking  
1339 transport, surface flux and chemical loss with CH<sub>4</sub> variability in the troposphere and lower  
1340 stratosphere, *Atmos. Chem. Phys.*, 11, 12813-12837, 10.5194/acp-11-12813-2011, 2011a.

1341 Patra, P. K., Niwa, Y., Schuck, T. J., Brenninkmeijer, C. A. M., Machida, T., Matsueda, H., and Sawa, Y.:  
1342 Carbon balance of South Asia constrained by passenger aircraft CO<sub>2</sub> measurements, *Atmos.*  
1343 *Chem. Phys.*, 11, 4163-4175, 10.5194/acp-11-4163-2011, 2011b.

1344 Patra, P. K., Canadell, J. G., Houghton, R. A., Piao, S. L., Oh, N. H., Ciais, P., Manjunath, K. R., Chhabra,  
1345 A., Wang, T., Bhattacharya, T., Bousquet, P., Hartman, J., Ito, A., Mayorga, E., Niwa, Y.,  
1346 Raymond, P. A., Sarma, V. V. S. S., and Lasco, R.: The carbon budget of South Asia,  
1347 *Biogeosciences*, 10, 513-527, 10.5194/bg-10-513-2013, 2013.

1348 Peylin, P., Law, R. M., Gurney, K. R., Chevallier, F., Jacobson, A. R., Maki, T., Niwa, Y., Patra, P. K.,  
1349 Peters, W., Rayner, P. J., Rödenbeck, C., and Zhang, X.: Global atmospheric carbon budget:  
1350 results from an ensemble of atmospheric CO<sub>2</sub> inversions, *Biogeosciences Discuss.*, 10, 5301-  
1351 5360, 10.5194/bgd-10-5301-2013, 2013.

1352 Pison, I., Bousquet, P., Chevallier, F., Szopa, S., and Hauglustaine, D.: Multi-species inversion of CH<sub>4</sub>,  
1353 CO and H<sub>2</sub> emissions from surface measurements, *Atmos. Chem. Phys.*, 9, 5281-5297,  
1354 10.5194/acp-9-5281-2009, 2009.

1355 Press, W.H., Teukolsky, S.A., Vetterling, W.T., Flannery, B.P., 2007. Straight-Line Data with Errors in  
1356 Both Coordinates, in: *Numerical Recipes: The Art of Scientific Computing*. Cambridge  
1357 University Press, New York, pp. 785–788.

1358 Price, H., Jaeglé, L., Rice, A., Quay, P., Novelli, P. C., and Gammon, R.: Global budget of molecular  
1359 hydrogen and its deuterium content: Constraints from ground station, cruise, and aircraft  
1360 observations, *J. Geophys. Res.-Atmos.*, 112, D22108, 10.1029/2006jd008152, 2007.

1361 R Core Team: R: A language and environment for statistical computing. R Foundation for Statistical  
1362 computing, Vienna, Austria. Available from: <http://www.r-project.org/>, 2014.

1363 Ramonet, M., Ciais, P., Nepomniachii, I., Sidorov, K., Neubert, R. E. M., Langendörfer, U., Picard, D.,  
1364 Kazan, V., Biraud, S., Gusti, M., Kolle, O., Schulze, E. D., and Lloyd, J.: Three years of aircraft-  
1365 based trace gas measurements over the Fyodorovskoye southern taiga forest, 300 km north-  
1366 west of Moscow, *Tellus B*, 54, 713-734, 10.1034/j.1600-0889.2002.01358.x, 2002.

1367 Ravishankara, A. R., Daniel, J. S. and Portmann, R. W.: Nitrous oxide (N<sub>2</sub>O): The dominant ozone-  
1368 depleting substance emitted in the 21<sup>st</sup> century, *Science*, 326(5949), 123–125,  
1369 doi:10.1126/science.1176985, 2009.

1370 Ravishankara, A. R., Solomon, S., Turnipseed, A. A., and Warren, R. F.: Atmospheric lifetimes of long-  
1371 lived halogenated species, *Science*, 259, 194-199, 1993.

1372 Rayner, P. J., Law, R. M., Allison, C. E., Francey, R. J., Trudinger, C. M., and Pickett-Heaps, C.:  
1373 Interannual variability of the global carbon cycle (1992–2005) inferred by inversion of

1374 atmospheric CO<sub>2</sub> and δ<sup>13</sup>CO<sub>2</sub> measurements, *Global Biogeochem. Cy.*, 22, GB3008,  
1375 10.1029/2007gb003068, 2008.

1376 Rivier, L., Ciais, P., Hauglustaine, D. A., Bakwin, P., Bousquet, P., Peylin, P., and Klonecki, A.:  
1377 Evaluation of SF<sub>6</sub>, C<sub>2</sub>Cl<sub>4</sub>, and CO to approximate fossil fuel CO<sub>2</sub> in the Northern Hemisphere  
1378 using a chemistry transport model, *J. Geophys. Res.-Atmos.*, 111, D16311,  
1379 10.1029/2005jd006725, 2006.

1380 Saikawa, E., Prinn, R. G., Dlugokencky, E., Ishijima, K., Dutton, G. S., Hall, B. D., Langenfelds, R.,  
1381 Tohjima, Y., Machida, T., Manizza, M., Rigby, M., O'Doherty, S., Patra, P. K., Harth, C. M.,  
1382 Weiss, R. F., Krummel, P. B., van der Schoot, M., Fraser, P. J., Steele, L. P., Aoki, S., Nakazawa,  
1383 T., and Elkins, J. W.: Global and regional emissions estimates for N<sub>2</sub>O, *Atmos. Chem. Phys.*,  
1384 14, 4617-4641, 10.5194/acp-14-4617-2014, 2014.

1385 Sawa, Y., Matsueda, H., Makino, Y., Inoue, H. Y., Murayama, S., Hirota, M., Tsutsumi, Y., Zaizen, Y.,  
1386 Ikegami, M., and Okada, K.: Aircraft Observation of CO<sub>2</sub>, CO, O<sub>3</sub> and H<sub>2</sub> over the North Pacific  
1387 during the PACE-7 Campaign, *Tellus B*, 56, 2-20, 10.1111/j.1600-0889.2004.00088.x, 2004.

1388 Schuck, T. J., Brenninkmeijer, C. A. M., Baker, A. K., Slemr, F., von Velthoven, P. F. J., and Zahn, A.:  
1389 Greenhouse gas relationships in the Indian summer monsoon plume measured by the  
1390 CARIBIC passenger aircraft, *Atmos. Chem. Phys.*, 10, 3965-3984, 10.5194/acp-10-3965-2010,  
1391 2010.

1392 Schuck, T. J., Ishijima, K., Patra, P. K., Baker, A. K., Machida, T., Matsueda, H., Sawa, Y., Umezawa, T.,  
1393 Brenninkmeijer, C. A. M., and Lelieveld, J.: Distribution of methane in the tropical upper  
1394 troposphere measured by CARIBIC and CONTRAIL aircraft, *J. Geophys. Res.-Atmos.*, 117,  
1395 D19304, 10.1029/2012jd018199, 2012.

1396 Seinfeld, J. H. and Pandis, S. N.: *Atmospheric Chemistry and Physics: From Air Pollution to Climate*  
1397 *Change*, John Wiley and Sons, Hoboken, New Jersey, USA., 2006.

1398 Sivakumar, I., and Anitha, M.: Education and girl children in Puducherry region: Problems and  
1399 perspective, *Int. J. Soc. Sci. Interdiscipl. Res.*, 1, 175-184, 2012.

1400 Streets, D. G., Bond, T. C., Carmichael, G. R., Fernandes, S. D., Fu, Q., He, D., Klimont, Z., Nelson, S. M.,  
1401 Tsai, N. Y., Wang, M. Q., Woo, J. H., and Yarber, K. F.: An inventory of gaseous and primary  
1402 aerosol emissions in Asia in the year 2000, *J. Geophys. Res.-Atmos.*, 108, 8809,  
1403 10.1029/2002jd003093, 2003a.

1404 Streets, D. G., Yarber, K. F., Woo, J. H., and Carmichael, G. R.: Biomass burning in Asia: Annual and  
1405 seasonal estimates and atmospheric emissions, *Global Biogeochem. Cy.*, 17, 1099,  
1406 10.1029/2003gb002040, 2003b.

1407 Suntharalingam, P., Jacob, D. J., Palmer, P. I., Logan, J. A., Yantosca, R. M., Xiao, Y., Evans, M. J.,  
1408 Streets, D. G., Vay, S. L., and Sachse, G. W.: Improved quantification of Chinese carbon fluxes  
1409 using CO<sub>2</sub>/CO correlations in Asian outflow, *J. Geophys. Res.-Atmos.*, 109, D18S18,  
1410 10.1029/2003jd004362, 2004.

1411 Swathi, P. S., Indira, N. K., Rayner, P. J., Ramonet, M., Jagadheesha, D., Bhatt, B. C., Gaur, V. K.:  
1412 Robust inversion of carbon dioxide fluxes over temperate Eurasia in 2006-2008, *Curr. Sci.*,  
1413 105, 201-208, 2013.

1414 Takegawa, N., Kondo, Y., Koike, M., Chen, G., Machida, T., Watai, T., Blake, D. R., Streets, D. G., Woo,  
1415 J. H., Carmichael, G. R., Kita, K., Miyazaki, Y., Shirai, T., Liley, J. B., and Ogawa, T.: Removal of  
1416 NO<sub>x</sub> and NO<sub>y</sub> in Asian outflow plumes: Aircraft measurements over the western Pacific in  
1417 January 2002, *J. Geophys. Res.-Atmos.*, 109, D23S04, 10.1029/2004jd004866, 2004.

1418 Teetor, P., 2011. *Performing Simple Orthogonal Regression*, in: Loukides, M. (Ed.), *R Cookbook*.  
1419 O'Reilly Media, Sebastopol, pp. 340–341.

1420 Thompson, R. L., Chevallier, F., Crotwell, A. M., Dutton, G., Langenfelds, R. L., Prinn, R. G., Weiss, R. F.,  
1421 Tohjima, Y., Nakazawa, T., Krummel, P. B., Steele, L. P., Fraser, P., O'Doherty, S., Ishijima, K.,  
1422 and Aoki, S.: Nitrous oxide emissions 1999 to 2009 from a global atmospheric inversion,  
1423 *Atmos. Chem. Phys.*, 14, 1801-1817, 10.5194/acp-14-1801-2014, 2014a.

1424 Thompson, R. L., Ishijima, K., Saikawa, E., Corazza, M., Karstens, U., Patra, P. K., Bergamaschi, P.,  
1425 Chevallier, F., Dlugokencky, E., Prinn, R. G., Weiss, R. F., O'Doherty, S., Fraser, P. J., Steele, L.  
1426 P., Krummel, P. B., Vermeulen, A., Tohjima, Y., Jordan, A., Haszpra, L., Steinbacher, M., Van  
1427 der Laan, S., Aalto, T., Meinhardt, F., Popa, M. E., Moncrieff, J., and Bousquet, P.: TransCom  
1428 N<sub>2</sub>O model inter-comparison – Part 2: Atmospheric inversion estimates of N<sub>2</sub>O emissions,  
1429 Atmos. Chem. Phys., 14, 6177-6194, 10.5194/acp-14-6177-2014, 2014b.

1430 Thompson, R. L., Patra, P. K., Ishijima, K., Saikawa, E., Corazza, M., Karstens, U., Wilson, C.,  
1431 Bergamaschi, P., Dlugokencky, E., Sweeney, C., Prinn, R. G., Weiss, R. F., O'Doherty, S., Fraser,  
1432 P. J., Steele, L. P., Krummel, P. B., Saunio, M., Chipperfield, M., and Bousquet, P.: TransCom  
1433 N<sub>2</sub>O model inter-comparison – Part 1: Assessing the influence of transport and surface fluxes  
1434 on tropospheric N<sub>2</sub>O variability, Atmos. Chem. Phys., 14, 4349-4368, 10.5194/acp-14-4349-  
1435 2014, 2014c.

1436 Thoning, K. W., Tans, P. P., and Komhyr, W. D.: Atmospheric carbon dioxide at Mauna Loa  
1437 Observatory: 2. Analysis of the NOAA GMCC data, 1974–1985, J. Geophys. Res.-Atmos., 94,  
1438 8549-8565, 10.1029/JD094iD06p08549, 1989.

1439 Tiwari, Y. K., Patra, P. K., Chevallier, F., Francey, R. J., Krummel, P. B., Allison, C. E., Revadekar, J. V.,  
1440 Chakraborty, S., Langenfelds, R. L., Bhattacharya, S. K., Borole, D. V., Kumar, K. R., and Steele,  
1441 L. P.: Carbon dioxide observations at Cape Rama, India for the period 1993-2002:  
1442 implications for constraining Indian emissions, Curr. Sci., 101, 1562-1568, 2011.

1443 Tiwari, Y. K., and Kumar, K. R.: GHG observation programs in India, in: Asian GAW greenhouse gases  
1444 Newsletter, Volume No. 3, Korea Meteorological Administration, Chungnam, South Korea,  
1445 2012.

1446 Tiwari, Y. K., Revadekar, J. V., and Ravi Kumar, K.: Variations in atmospheric Carbon Dioxide and its  
1447 association with rainfall and vegetation over India, Atmos. Environ., 68, 45-51,  
1448 <http://dx.doi.org/10.1016/j.atmosenv.2012.11.040>, 2013.

1449 Tiwari, Y. K., Vellore, R. K., Ravi Kumar, K., van der Schoot, M., and Cho, C.-H.: Influence of monsoons  
1450 on atmospheric CO<sub>2</sub> spatial variability and ground-based monitoring over India, Sci. Total  
1451 Environ., 490, 570-578, <http://dx.doi.org/10.1016/j.scitotenv.2014.05.045>, 2014.

1452 Tohjima, Y., Maksyutov, S., Machida, T., and Inoue, G.: Airborne measurements of atmospheric  
1453 methane over oil fields in western Siberia, Geophys. Res. Lett., 23, 1621-1624,  
1454 10.1029/96gl01027, 1996.

1455 Turnbull, J. C., Miller, J. B., Lehman, S. J., Tans, P. P., Sparks, R. J., and Southon, J.: Comparison of  
1456 14CO<sub>2</sub>, CO, and SF<sub>6</sub> as tracers for recently added fossil fuel CO<sub>2</sub> in the atmosphere and  
1457 implications for biological CO<sub>2</sub> exchange, Geophys. Res. Lett., 33, L01817,  
1458 10.1029/2005gl024213, 2006.

1459 Valsala, V., Tiwari, Y. K., Pillai, P., Roxy, M., Maksyutov, S., and Murtugudde, R.: Intraseasonal  
1460 variability of terrestrial biospheric CO<sub>2</sub> fluxes over India during summer monsoons, J.  
1461 Geophys. Res.-Biogeo., 118, 752-769, 10.1002/jgrg.20037, 2013.

1462 van der Werf, G. R., Randerson, J. T., Giglio, L., Collatz, G. J., Kasibhatla, P. S., and Arellano Jr, A. F.:  
1463 Interannual variability in global biomass burning emissions from 1997 to 2004, Atmos. Chem.  
1464 Phys., 6, 3423-3441, 10.5194/acp-6-3423-2006, 2006.

1465 van der Werf, G. R., Randerson, J. T., Giglio, L., Collatz, G. J., Mu, M., Kasibhatla, P. S., Morton, D. C.,  
1466 DeFries, R. S., Jin, Y., and van Leeuwen, T. T.: Global fire emissions and the contribution of  
1467 deforestation, savanna, forest, agricultural, and peat fires (1997–2009), Atmos. Chem. Phys.,  
1468 10, 11707-11735, 10.5194/acp-10-11707-2010, 2010.

1469 Venkataraman, C., Habib, G., Eiguren-Fernandez, A., Miguel, A. H., and Friedlander, S. K.: Residential  
1470 Biofuels in South Asia: Carbonaceous Aerosol Emissions and Climate Impacts, Science, 307,  
1471 1454-1456, 2005.

1472 Volk, C. M., Elkins, J. W., Fahey, D. W., Dutton, G. S., Gilligan, J. M., Loewenstein, M., Podolske, J. R.,  
1473 Chan, K. R., and Gunson, M. R.: Evaluation of source gas lifetimes from stratospheric  
1474 observations, J. Geophys. Res.-Atmos., 102, 25543-25564, 10.1029/97jd02215, 1997.

1475 Wada, A., Matsueda, H., Sawa, Y., Tsuboi, K., and Okubo, S.: Seasonal variation of enhancement  
1476 ratios of trace gases observed over 10 years in the western North Pacific, *Atmos. Environ.*, 45,  
1477 2129-2137, <http://dx.doi.org/10.1016/j.atmosenv.2011.01.043>, 2011.

1478 Wang, R., Tao, S., Ciais, P., Shen, H. Z., Huang, Y., Chen, H., Shen, G. F., Wang, B., Li, W., Zhang, Y. Y.,  
1479 Lu, Y., Zhu, D., Chen, Y. C., Liu, X. P., Wang, W. T., Wang, X. L., Liu, W. X., Li, B. G., and Piao, S.  
1480 L.: High-resolution mapping of combustion processes and implications for CO<sub>2</sub> emissions,  
1481 *Atmos. Chem. Phys.*, 13, 5189-5203, 10.5194/acp-13-5189-2013, 2013.

1482 Xiao, Y., Jacob, D. J., Wang, J. S., Logan, J. A., Palmer, P. I., Suntharalingam, P., Yantosca, R. M.,  
1483 Sachse, G. W., Blake, D. R., and Streets, D. G.: Constraints on Asian and European sources of  
1484 methane from CH<sub>4</sub>-C<sub>2</sub>H<sub>6</sub>-CO correlations in Asian outflow, *J. Geophys. Res.-Atmos.*, 109,  
1485 D15S16, 10.1029/2003jd004475, 2004.

1486 Xiong, X., Houweling, S., Wei, J., Maddy, E., Sun, F., and Barnet, C.: Methane plume over south Asia  
1487 during the monsoon season: satellite observation and model simulation, *Atmos. Chem. Phys.*,  
1488 9, 783-794, 10.5194/acp-9-783-2009, 2009.

1489 Yan, X., Cai, Z., Ohara, T., and Akimoto, H.: Methane emission from rice fields in mainland China:  
1490 Amount and seasonal and spatial distribution, *J. Geophys. Res.-Atmos.*, 108, 4505,  
1491 10.1029/2002jd003182, 2003.

1492 Yashiro, H., Sudo, K., Yonemura, S., and Takigawa, M.: The impact of soil uptake on the global  
1493 distribution of molecular hydrogen: chemical transport model simulation, *Atmos. Chem.*  
1494 *Phys.*, 11, 6701-6719, 10.5194/acp-11-6701-2011, 2011.

1495 Yevich, R., and Logan, J. A.: An assessment of biofuel use and burning of agricultural waste in the  
1496 developing world, *Global Biogeochem. Cy.*, 17, 1095, 10.1029/2002gb001952, 2003.

1497 Yver, C., Schmidt, M., Bousquet, P., Zahorowski, W., and Ramonet, M.: Estimation of the molecular  
1498 hydrogen soil uptake and traffic emissions at a suburban site near Paris through hydrogen,  
1499 carbon monoxide, and radon-222 semicontinuous measurements, *J. Geophys. Res.-Atmos.*,  
1500 114, D18304, 10.1029/2009jd012122, 2009.

1501 Yver, C.: Estimation des sources et puits du dihydrogène troposphérique - développements  
1502 instrumentaux, mesures atmosphériques et assimilation variationnelle, Ph.D dissertation,  
1503 Université de Versailles - Saint Quentin, 2010.

1504 Yver, C. E., Pison, I. C., Fortems-Cheiney, A., Schmidt, M., Chevallier, F., Ramonet, M., Jordan, A.,  
1505 Søvde, O. A., Engel, A., Fisher, R. E., Lowry, D., Nisbet, E. G., Levin, I., Hammer, S., Necki, J.,  
1506 Bartyzel, J., Reimann, S., Vollmer, M. K., Steinbacher, M., Aalto, T., Maione, M., Arduini, J.,  
1507 O'Doherty, S., Grant, A., Sturges, W. T., Forster, G. L., Lunder, C. R., Privalov, V., Paramonova,  
1508 N., Werner, A., and Bousquet, P.: A new estimation of the recent tropospheric molecular  
1509 hydrogen budget using atmospheric observations and variational inversion, *Atmos. Chem.*  
1510 *Phys.*, 11, 3375-3392, 10.5194/acp-11-3375-2011, 2011.

1511 Zhang, F., Zhou, L. X., Novelli, P. C., Worthy, D. E. J., Zellweger, C., Klausen, J., Ernst, M., Steinbacher,  
1512 M., Cai, Y. X., Xu, L., Fang, S. X., and Yao, B.: Evaluation of in situ measurements of  
1513 atmospheric carbon monoxide at Mount Waliguan, China, *Atmos. Chem. Phys.*, 11, 5195-  
1514 5206, 10.5194/acp-11-5195-2011, 2011.

1515 Zhang, H. F., Chen, B. Z., Machida, T., Matsueda, H., Sawa, Y., Fukuyama, Y., Langenfelds, R., van der  
1516 Schoot, M., Xu, G., Yan, J. W., Cheng, M. L., Zhou, L. X., Tans, P., and Peters, W.: Estimating  
1517 Asian terrestrial carbon fluxes from CONTRAIL aircraft and surface CO<sub>2</sub> observations for the  
1518 period 2006-2010, *Atmos. Chem. Phys.*, 14, 5807-5824, 10.5194/acp-14-5807-2014, 2014.

1519 Zhang, X. I. A., Nakazawa, T., Ishizawa, M., Aoki, S., Nakaoka, S.-I., Sugawara, S., Maksyutov, S., Saeki,  
1520 T., and Hayasaka, T.: Temporal variations of atmospheric carbon dioxide in the southernmost  
1521 part of Japan, *Tellus B*, 59, 654-663, 10.1111/j.1600-0889.2007.00288.x, 2007.

1522 Zhao, C. L., and Tans, P. P.: Estimating uncertainty of the WMO mole fraction scale for carbon  
1523 dioxide in air, *J. Geophys. Res.-Atmos.*, 111, D08S09, 10.1029/2005jd006003, 2006.

1524

1525 **Table**

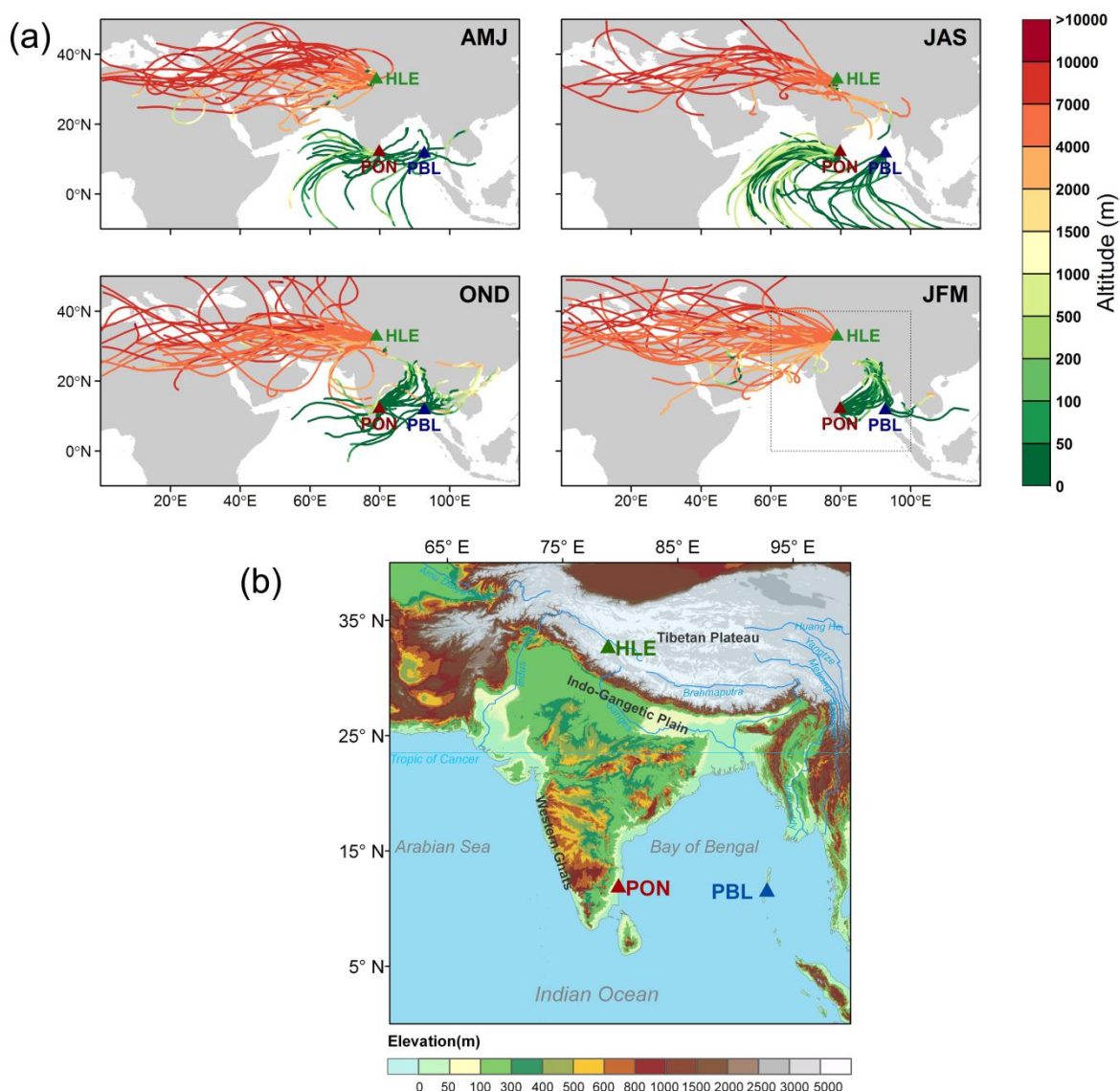
1526 **Table 1** Annual mean values, trend, and average peak-to-peak amplitudes of trace gases at  
 1527 HLE, PON, PBL and the two additional NOAA/ESRL stations – KZM and WLG. For each  
 1528 species at each station, the annual mean values and average peak-to-peak amplitude are  
 1529 calculated from the smoothed curve and mean seasonal cycle, respectively. The residual  
 1530 standard deviation (RSD) around the smoothed curve and the Julian days corresponding to  
 1531 the maximum ( $D_{\max}$ ) and minimum ( $D_{\min}$ ) of the mean seasonal cycle are given as well.  
 1532 Uncertainty of each estimate is calculated from 1 s.d. of 1000 bootstrap replicates.

	HLE	PON	PBL	KZM	WLG
<b>CO<sub>2</sub> (ppm)</b>					
Annual mean 2007	382.3±0.3	386.6±0.9	–	382.7±0.2	384.2±0.2
Annual mean 2008	384.6±0.5	388.1±0.9	–	385.7±0.2	386.0±0.2
Annual mean 2009	387.2±0.2	389.0±0.6	–	–	387.4±0.2
Annual mean 2010	389.4±0.1	391.3±1.5	387.6±0.7	–	390.1±0.2
Annual mean 2011	391.4±0.3	–	390.2±0.6	–	392.2±0.2
Trend (yr <sup>-1</sup> )	2.1±0.0	1.7±0.1	–	–	2.0±0.0
(Trend at MLO: 2.0±0.0)					
RSD	0.7	4.0	1.5	1.5	1.4
Amplitude	8.2±0.4	7.6±1.4	11.1±1.3	13.8±0.5	11.1±0.4
$D_{\max}$	122.0±2.9	111.0±13.4	97.0±26.0	75.0±2.6	100.0±1.5
$D_{\min}$	261.0±3.0	327.0±54.3	242.0±7.7	205.0±2.1	222.0±1.6
<b>CH<sub>4</sub> (ppb)</b>					
Annual mean 2007	1814.8±2.9	1859.2±6.7	–	1842.6±2.4	1841.0±1.8
Annual mean 2008	1833.1±5.4	1856.1±10.4	–	1856.6±2.3	1845.6±1.5
Annual mean 2009	1830.2±1.7	1865.7±5.1	–	–	1851.8±1.9
Annual mean 2010	1830.5±2.1	1876.9±9.1	1867.5±15.4	–	1857.6±1.4
Annual mean 2011	1849.5±5.2	–	1852.0±7.6	–	1859.9±1.2
Trend (yr <sup>-1</sup> )	4.9±0.0	9.4±0.1	–	–	5.3±0.0
(Trend at MLO: 6.2±0.0)					
RSD	9.1	34.4	22.4	14.6	12.3
Amplitude	28.9±4.2	124.1±10.2	143.9±12.4	22.7±4.7	17.5±2.2
$D_{\max}$	219.0±4.6	337.0±6.1	345.0±87.6	236.0±43.2	222.0±6.2
$D_{\min}$	97.0±58.9	189.0±10.7	193.0±13.5	338.0±39.0	340.0±96.6
<b>N<sub>2</sub>O (ppb)</b>					
Annual mean 2007	322.2±0.1	324.8±0.3	–		
Annual mean 2008	322.9±0.1	326.3±0.3	–		
Annual mean 2009	323.5±0.1	326.7±0.3	–		
Annual mean 2010	324.0±0.1	327.1±0.5	329.0±0.5		
Annual mean 2011	325.2±0.1	–	327.9±0.3		

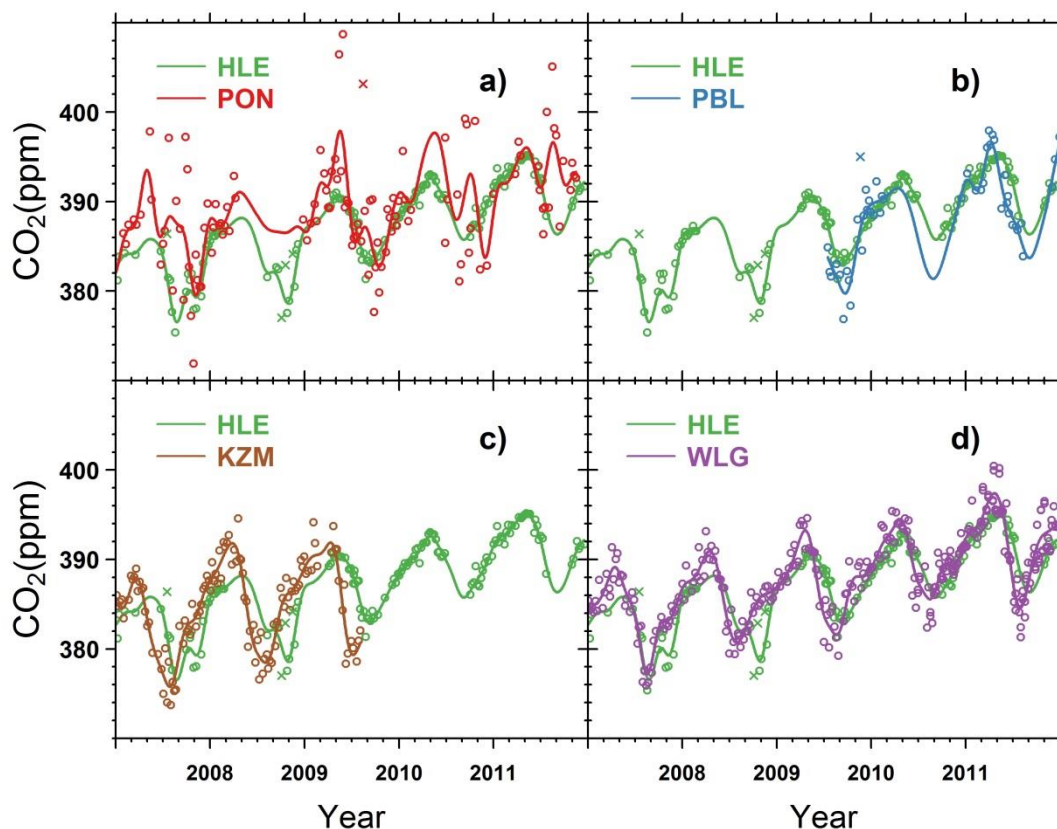
Trend (yr <sup>-1</sup> )	0.8±0.0	0.8±0.1	–		
(Trend at MLO: 1.0±0.0)					
RSD	0.3	1.4	1.1		
Amplitude	0.6±0.1	1.2±0.5	2.2±0.6		
D <sub>max</sub>	227.0±11.8	262.0±83.2	313.0±42.6		
D <sub>min</sub>	115.0±16.4	141.0±48.2	65.0±33.4		
<b>SF<sub>6</sub> (ppt)</b>					
Annual mean 2007	6.26±0.03	6.19±0.01	–		
Annual mean 2008	6.54±0.03	6.49±0.02	–		
Annual mean 2009	6.79±0.01	6.77±0.01	–		
Annual mean 2010	7.17±0.01	7.08±0.02	7.10±0.07		
Annual mean 2011	7.38±0.01	–	7.45±0.03		
Trend (yr <sup>-1</sup> )	0.29±0.05	0.31±0.05	–		
(Trend at MLO: 0.29±0.03)					
RSD	0.07	0.05	0.12		
Amplitude	0.15±0.03	0.24±0.02	0.48±0.07		
D <sub>max</sub>	320.0±8.3	327.0±12.1	342.0±59.9		
D <sub>min</sub>	211.0±65.1	204.0±3.3	210.0±18.1		
<b>CO (ppb)</b>					
Annual mean 2007	104.7±1.4	200.5±7.8	–	121.7±1.7	141.0±4.3
Annual mean 2008	103.1±2.1	175.3±13.1	–	123.7±1.7	129.0±2.9
Annual mean 2009	98.9±1.9	174.3±4.8	–	–	131.9±3.7
Annual mean 2010	99.0±1.2	185.1±8.7	157.6±20.4	–	130.2±3.9
Annual mean 2011	99.4±2.2	–	145.9±9.9	–	124.0±2.3
Trend (yr <sup>-1</sup> )	-2.2±0.0	0.4±0.1	–	–	-1.9±0.0
(Trend at MLO: -1.6±0.0)					
RSD	6.5	32.0	30.8	11.8	22.5
Amplitude	28.4±2.3	78.2±11.6	144.1±16.0	37.1±4.4	38.6±5.1
D <sub>max</sub>	79.0±11.4	4.0±160.2	12.0±117.9	72.0±5.0	94.0±38.2
D <sub>min</sub>	297.0±5.3	238.0±46.1	213.0±23.0	318.0±6.1	331.0±6.2
<b>H<sub>2</sub> (ppb)</b>					
Annual mean 2007	539.6±2.1	574.5±2.4	–	502.4±2.0	500.9±1.5
Annual mean 2008	533.2±3.2	558.2±5.3	–	–	–
Annual mean 2009	533.3±1.6	562.4±1.6	–	–	–
Annual mean 2010	533.5±1.8	563.9±2.3	558.6±2.4	–	–
Annual mean 2011	536.9±1.5	–	555.4±1.6	–	–
Trend (yr <sup>-1</sup> )	-0.5±0.0	-1.3±0.1	–	–	–
RSD	6.6	8.4	7.0	13.3	9.5
Amplitude	15.8±2.2	21.6±3.4	21.3±5.0	16.7±4.0	22.8±3.0
D <sub>max</sub>	120.0±8.7	96.0±9.6	99.0±8.8	120.0±34.2	51.0±13.4
D <sub>min</sub>	266.0±39.6	219.0±10.3	353.0±87.8	341.0±78.3	298.0±6.5

1534 **Figures**

1535 **Figure 1 (a)** Five-day back-trajectories calculated for all sampling dates over the period  
 1536 2007–2011 at Hanle (HLE), Pondicherry (PON), and Port Blair (PBL) during April–June  
 1537 (AMJ), July–September (JAS), October–December (OND) and January–March (JFM),  
 1538 respectively. Back-trajectories are colored by the elevation of air masses at hourly time step.  
 1539 **(b)** Map of terrain over the zoomed box in **(a)**, showing locations of HLE, PON and PBL.  
 1540 The digital elevation data are obtained from NASA Shuttle Radar Topographic Mission  
 1541 (SRTM) product at 1km resolution (<http://srtm.csi.cgiar.org>)

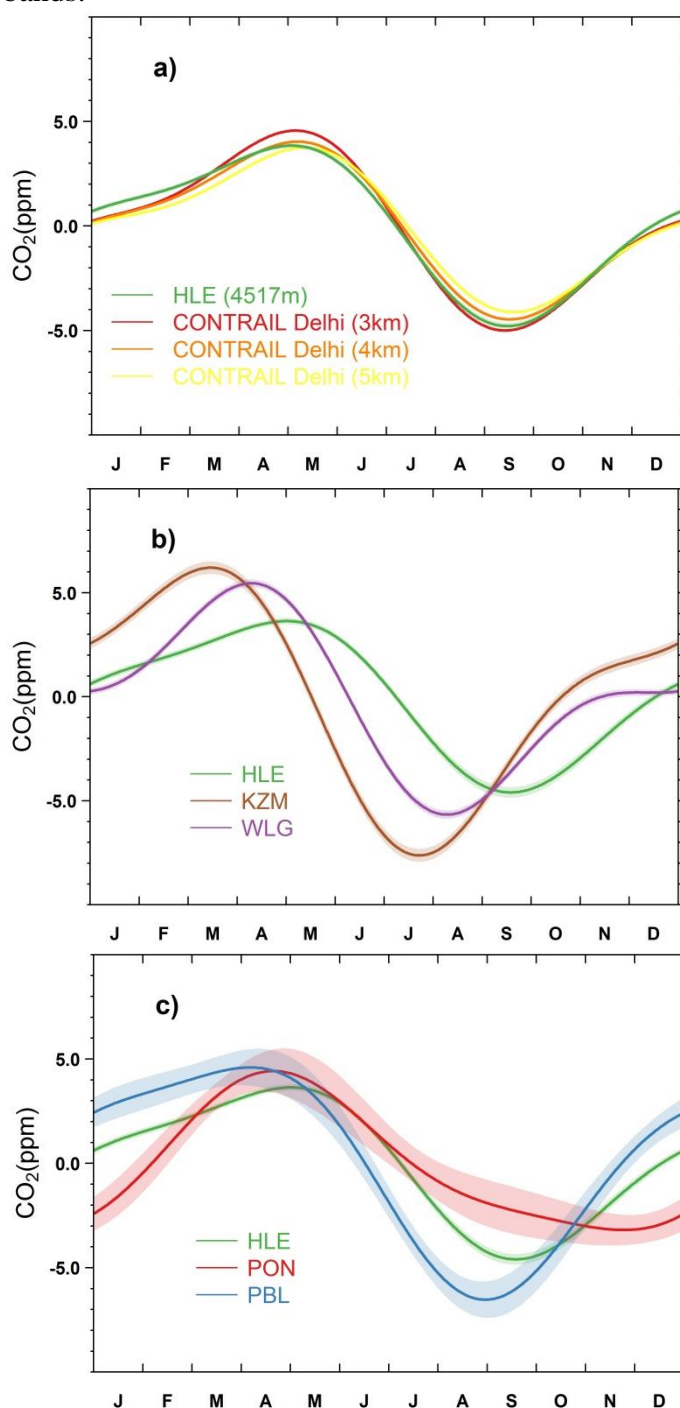


1543 **Figure 2** Time series of CO<sub>2</sub> flask measurements at **(a)** HLE and PON, **(b)** HLE and PBL, **(c)**  
1544 HLE and KZM, and **(d)** HLE and WLG. The open circles denote flask data used to fit the  
1545 smoothed curves, while the crosses denote discarded flask data lying outside 3 times the  
1546 residual standard deviations from the smoothed curve fits. For each station, the smoothed  
1547 curve is fitted using Thoning's method (Thoning et al., 1989) after removing outliers.

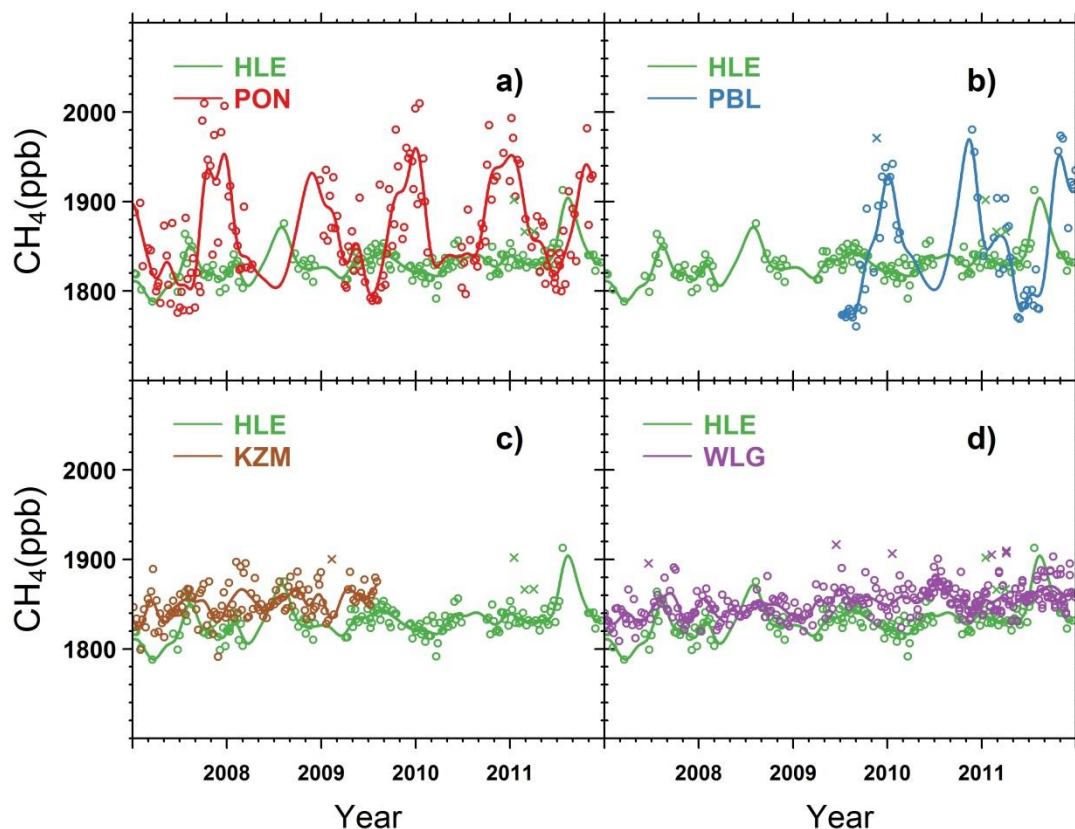




1549 **Figure 3 (a)** The mean CO<sub>2</sub> seasonal cycle at HLE, in comparison with the mean seasonal  
 1550 cycles derived from the in-situ CO<sub>2</sub> measurements over New Delhi at different altitude bands  
 1551 (3–4 km, 4–5 km, and 5–6 km) by the CONTRAIL project (2006–2010). **(b)** The mean CO<sub>2</sub>  
 1552 seasonal cycles at HLE, KZM and WLG. **(c)** The mean CO<sub>2</sub> seasonal cycles at HLE, PON  
 1553 and PBL. For each station, the mean seasonal cycle is derived from the harmonics of the  
 1554 smoothed fitting curve in Fig. 2. Shaded area indicates the uncertainty of the mean seasonal  
 1555 cycle calculated from 1 s.d. of 1000 bootstrap replicates. For the CONTRAIL datasets, CO<sub>2</sub>  
 1556 measurements over New Delhi were first averaged by altitude bands. A fitting procedure was  
 1557 then applied to the aggregated CO<sub>2</sub> measurements to generate the mean season cycle for  
 1558 different altitude bands.



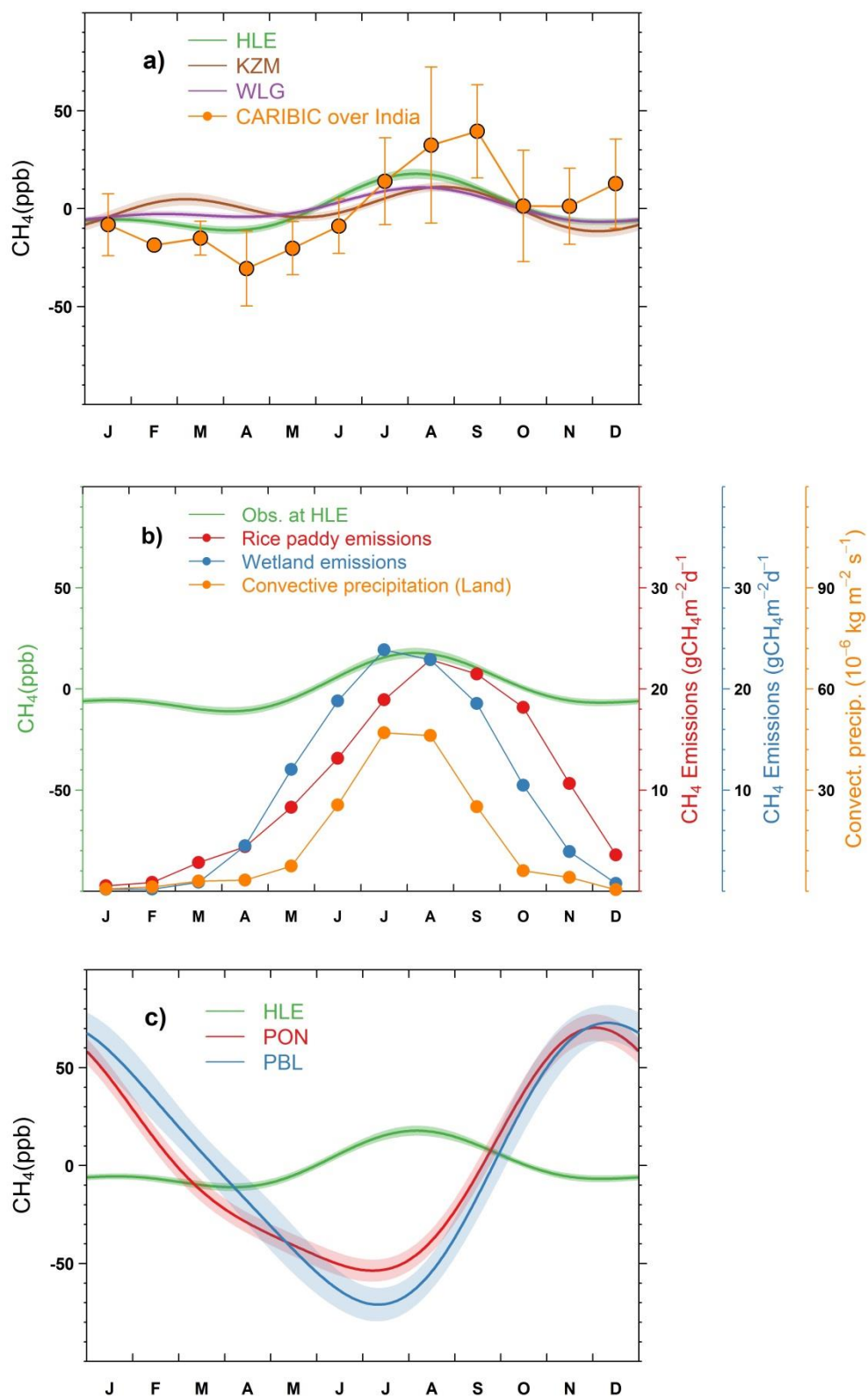
1559 **Figure 4** Time series of CH<sub>4</sub> flask measurements at (a) HLE and PON, (b) HLE and PBL, (c)  
1560 HLE and KZM, and (d) HLE and WLG. The open circles denote flask data used to fit the  
1561 smoothed curves, while the crosses denote discarded flask data lying outside 3 times the  
1562 residual standard deviations from the smoothed curve fits. For each station, the smoothed  
1563 curve is fitted using Thoning's method (Thoning et al., 1989) after removing outliers.



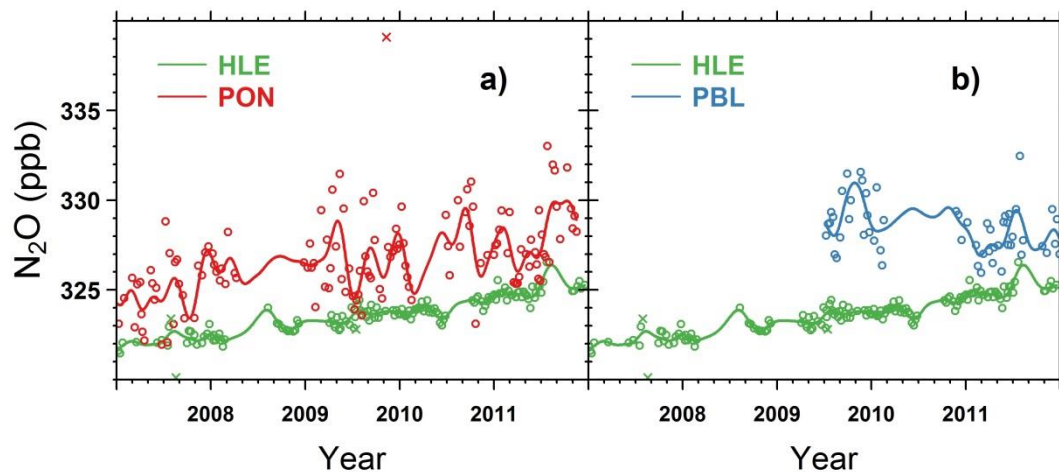
1564  
1565

1566 **Figure 5 (a)** The mean CH<sub>4</sub> seasonal cycles observed at HLE, KZM and WLG. The mean  
1567 CH<sub>4</sub> seasonal cycle derived from aircraft flask measurements by the CARIBIC project is also  
1568 presented. The CARIBIC flask measurements in the upper troposphere (200-300 hPa) during  
1569 2005–2012 are averaged over the Indian subcontinent (10°N-35°N, 60°E-100°E) by month to  
1570 generate the mean seasonal cycle. The error bars indicate 1 standard deviation of CH<sub>4</sub> flask  
1571 measurements within the month. **(b)** The seasonal variations of CH<sub>4</sub> emissions from rice  
1572 paddies and wetlands over the Indian subcontinent. The CH<sub>4</sub> emissions from rice paddies are  
1573 extracted from a global emission map for the year 2010 (EDGAR v4.2), imposed by the  
1574 seasonal variation on the basis of Matthews et al. (1991). The CH<sub>4</sub> emissions from wetlands  
1575 are extracted from outputs of a global vegetation model (BIOME4-TG, Kaplan et al., 2006).  
1576 The seasonal variation of deep convection over the Indian subcontinent is also presented,  
1577 indicated by convective precipitation obtained from an LMDz simulation nudged with  
1578 ECMWF reanalysis (Hauglustaine et al., 2004). The CH<sub>4</sub> emissions and convective  
1579 precipitation are averaged over the domain 10–35 °N, 70°–90°E to give a regional mean  
1580 estimate. **(c)** The mean CH<sub>4</sub> seasonal cycles observed at HLE, PON and PBL. For each  
1581 station, the mean seasonal cycle is derived from the harmonics of the smoothed fitting curve  
1582 in Fig. 4. Shaded area indicates the uncertainty of the mean seasonal cycle calculated from 1  
1583 s.d. of 1000 bootstrap replicates.

1584

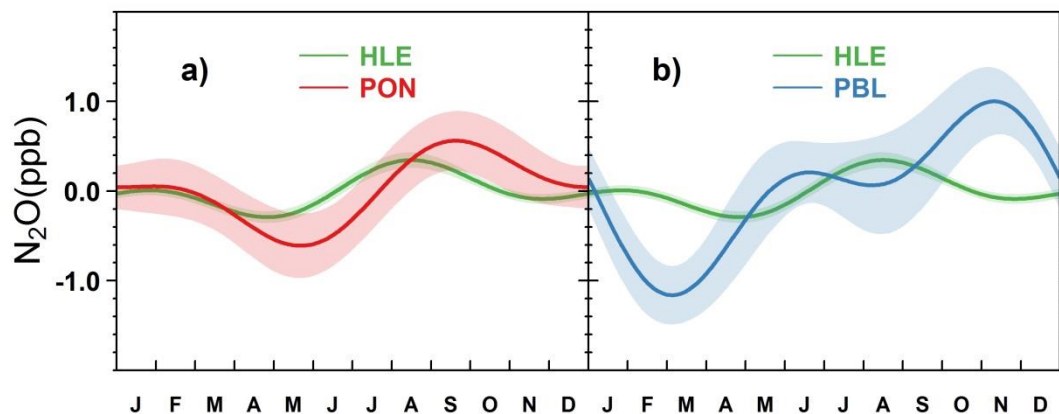


1586 **Figure 6** Time series of N<sub>2</sub>O flask measurements at (a) HLE and PON, (b) HLE and PBL.  
1587 The open circles denote flask data used to fit the smoothed curves, while crosses denote  
1588 discarded flask data lying outside 3 times the residual standard deviations from the smoothed  
1589 curve fits. For each station, the smoothed curve is fitted using Thoning's method (Thoning et  
1590 al., 1989) after removing outliers.



1591  
1592

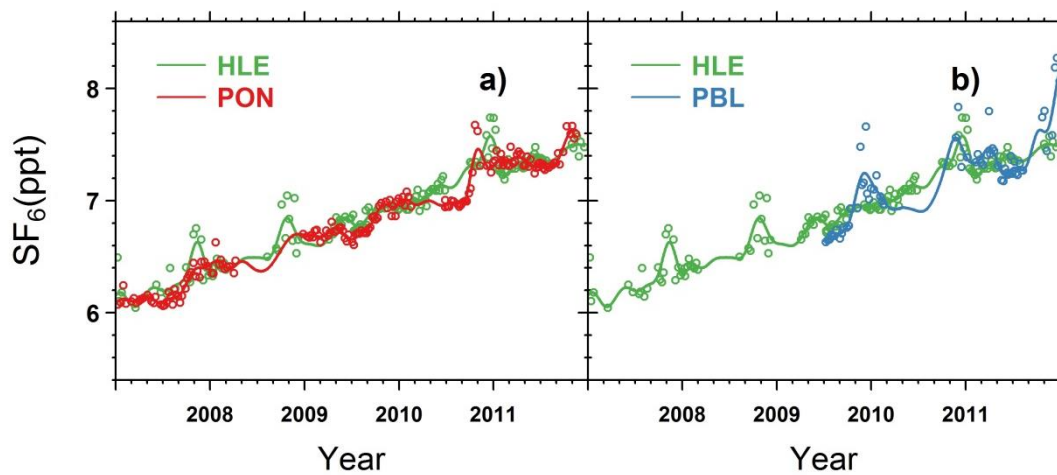
1593 **Figure 7** The mean N<sub>2</sub>O seasonal cycles observed at **(a)** HLE and PON, **(b)** HLE and PBL.  
1594 For each station, the mean seasonal cycle is derived from the harmonics of the smoothed  
1595 fitting curve in Fig. 6. Shaded area indicates the uncertainty of the mean seasonal cycle  
1596 calculated from 1 s.d. of 1000 bootstrap replicates.



1597

1598

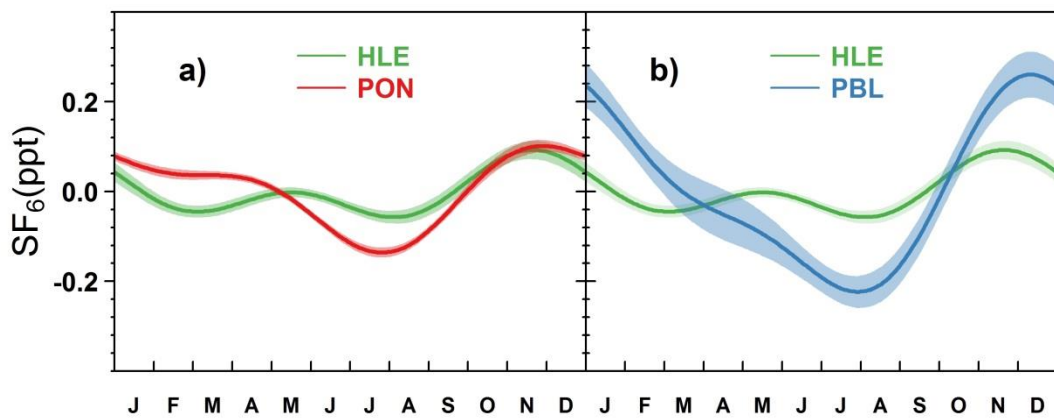
1599 **Figure 8** Time series of SF<sub>6</sub> flask measurements at (a) HLE and PON, (b) HLE and PBL, (c)  
1600 HLE and KZM, and (d) HLE and WLG. The open circles denote flask data used to fit the  
1601 smoothed curves. For each station, the smoothed curve is fitted using Thoning's method  
1602 (Thoning et al., 1989) after removing outliers.



1603

1604

1605 **Figure 9** The mean SF<sub>6</sub> seasonal cycles observed at (a) HLE and PON, (b) HLE and PBL.  
1606 For each station, the mean seasonal cycle is derived from the harmonics of the smoothed  
1607 fitting curve in Fig. 8. Shaded area indicates the uncertainty of the mean seasonal cycle  
1608 calculated from 1 s.d. of 1000 bootstrap replicates.

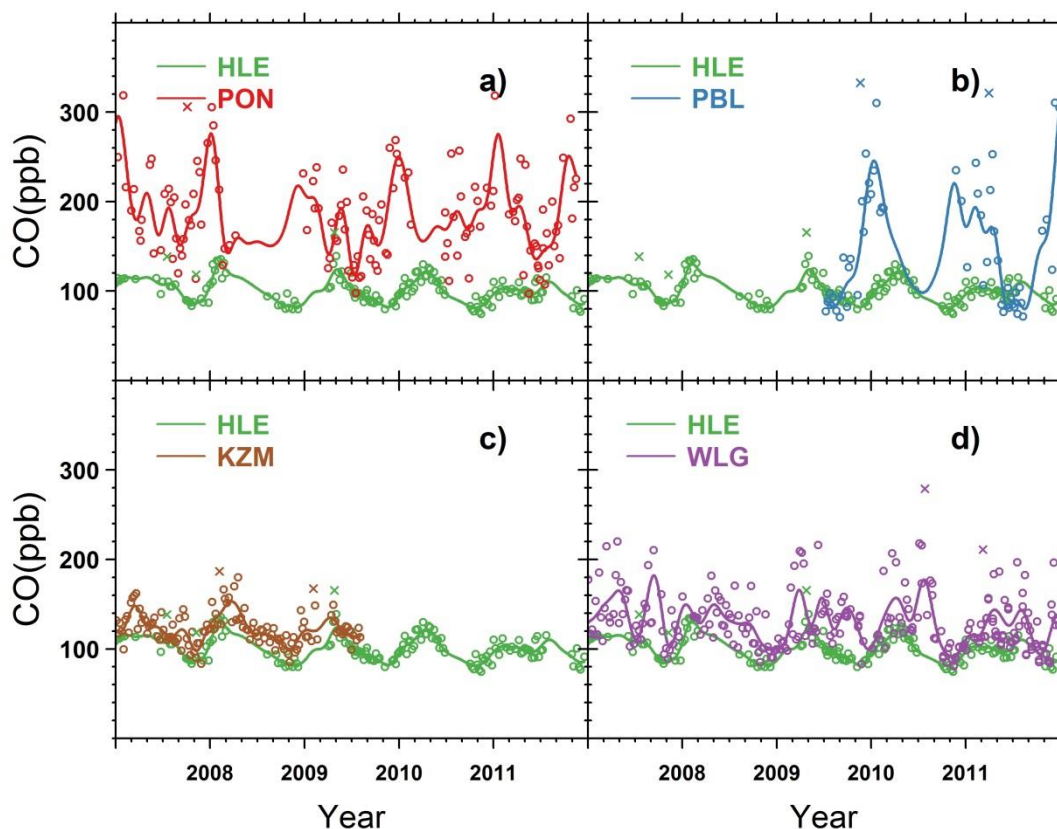


1609

1610



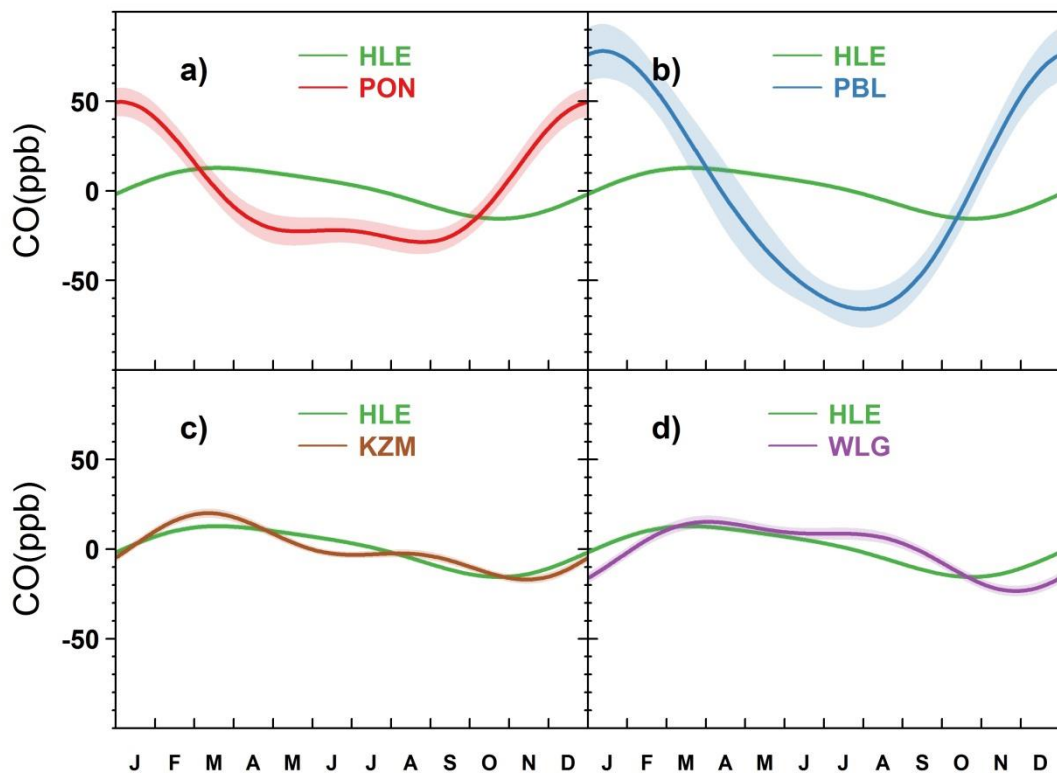
1611 **Figure 10** Time series of CO flask measurements at (a) HLE and PON, (b) HLE and PBL, (c)  
1612 HLE and KZM, and (d) HLE and WLG. The open circles denote flask data used to fit the  
1613 smoothed curves, while the crosses denote discarded flask data lying outside 3 times the  
1614 residual standard deviations from the smoothed curve fits. For each station, the smoothed  
1615 curve is fitted using Thoning's method (Thoning et al., 1989) after removing outliers.



1616

1617

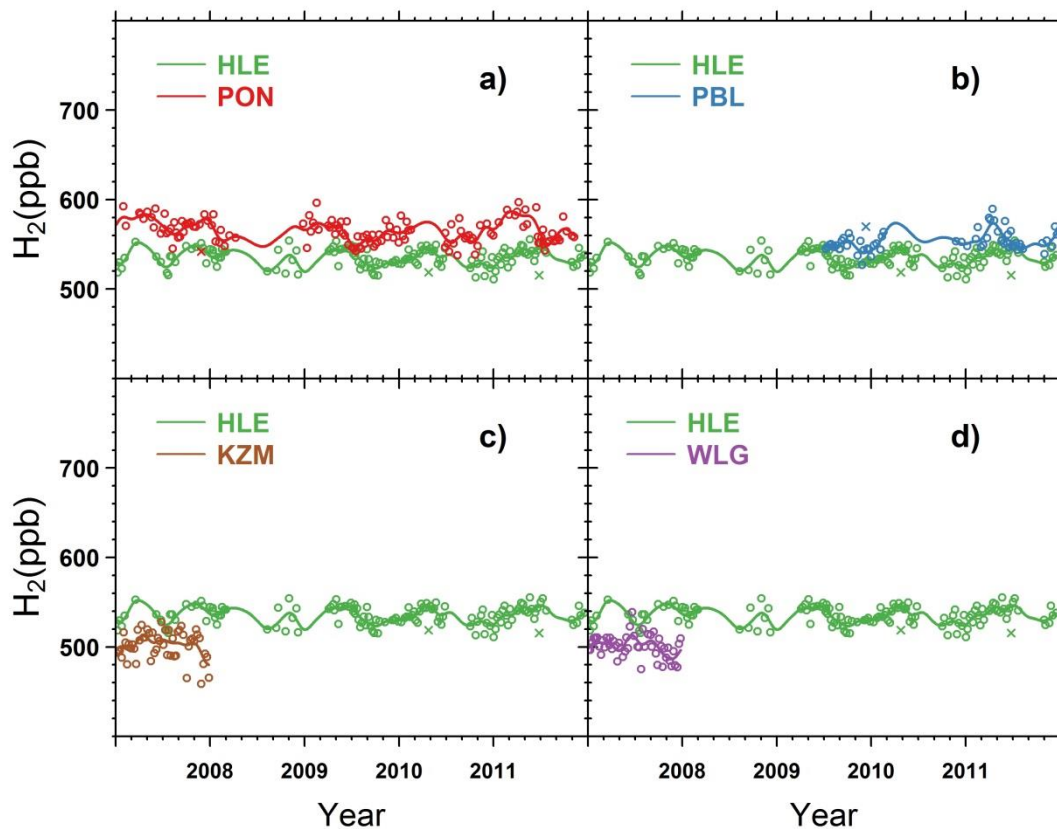
1618 **Figure 11** The mean CO seasonal cycles observed at (a) HLE and PON, (b) HLE and PBL,  
1619 (c) HLE and KZM, and (d) HLE and WLG. For each station, the mean seasonal cycle is  
1620 derived from the harmonics of the smoothed fitting curve in Fig. 10. Shaded area indicates  
1621 the uncertainty of the mean seasonal cycle calculated from 1 s.d. of 1000 bootstrap replicates.



1622

1623

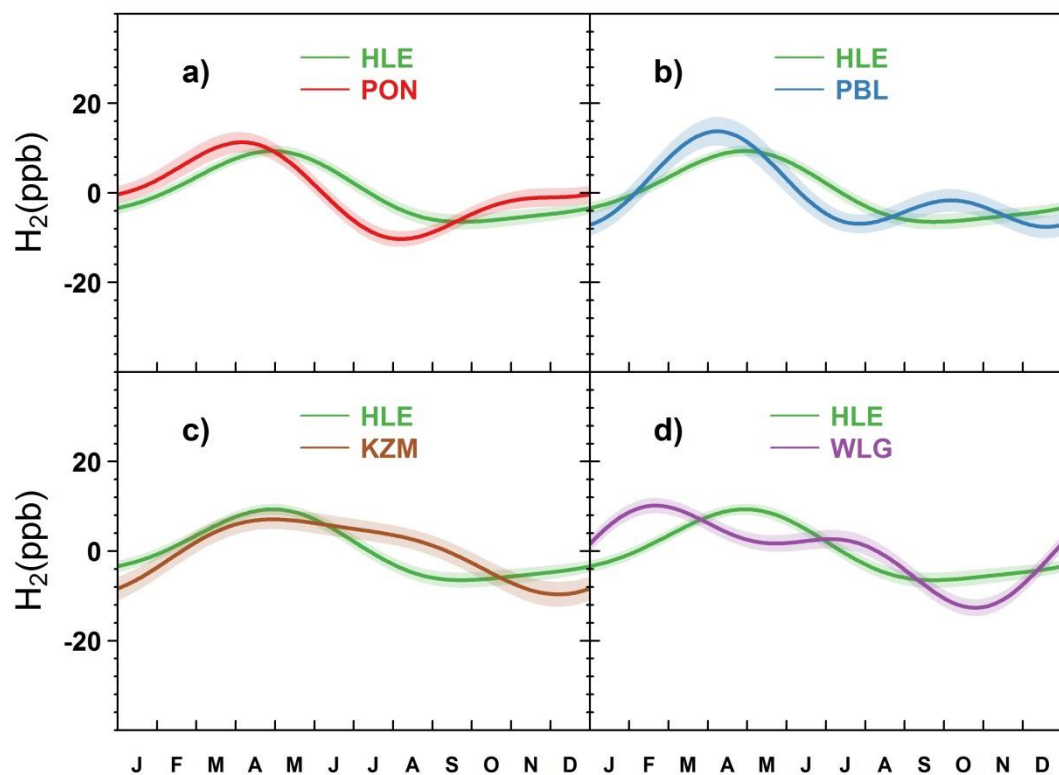
1624 **Figure 12** Time series of H<sub>2</sub> flask measurements at (a) HLE and PON, (b) HLE and PBL, (c)  
1625 HLE and KZM, and (d) HLE and WLG. The open circles denote flask data used to fit the  
1626 smoothed curves, while the crosses denote discarded flask data lying outside 3 times the  
1627 residual standard deviations from the smoothed curve fits. For each station, the smoothed  
1628 curve is fitted using Thoning's method (Thoning et al., 1989) after removing outliers.



1629

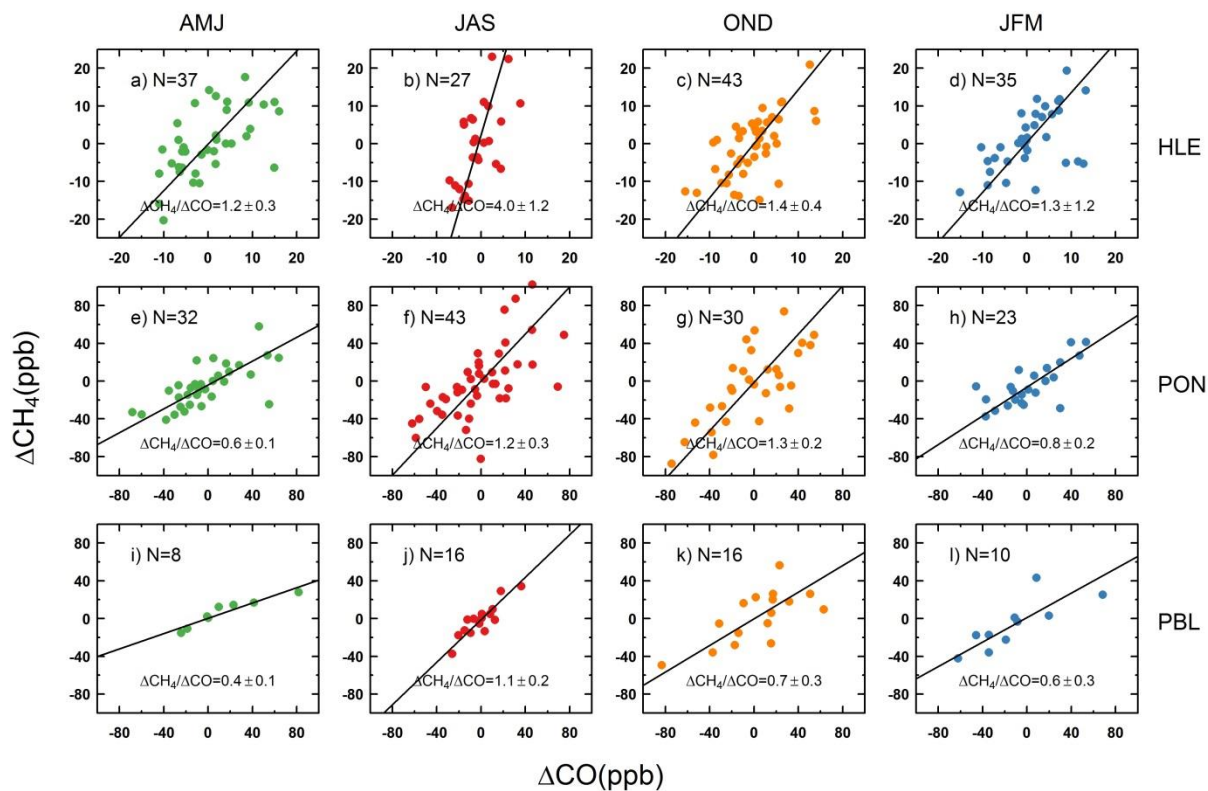
1630

1631 **Figure 13** The mean  $H_2$  seasonal cycles observed at (a) HLE and PON, (b) HLE and PBL, (c)  
1632 HLE and KZM, and (d) HLE and WLG. For each station, the mean seasonal cycle is derived  
1633 from the harmonics of the smoothed fitting curve in Fig. 12. Shaded area indicates the  
1634 uncertainty of the mean seasonal cycle calculated from 1 s.d. of 1000 bootstrap replicates.



1635

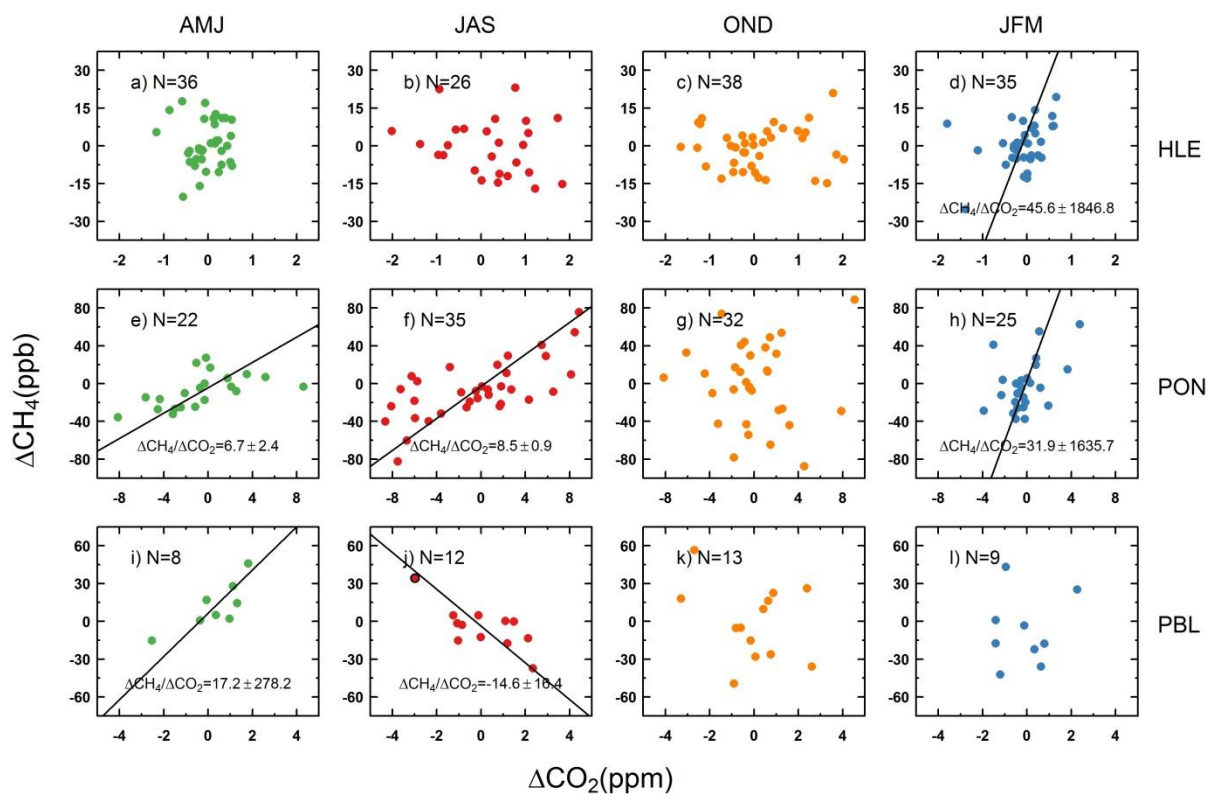
1636 **Figure 14** The relationships between  $\Delta\text{CH}_4$  and  $\Delta\text{CO}$  at HLE (a–d), PON (e–h), and PBL (i–  
 1637 l) for April–June (AMJ), July–September (JAS), October–December (OND), and January–  
 1638 March (JFM). For each panel,  $\Delta\text{CH}_4$  and  $\Delta\text{CO}$  are estimated as residuals from smoothed  
 1639 curves. The  $\Delta\text{CH}_4/\Delta\text{CO}$  ratio is the slope of the fitting line from the orthogonal distance  
 1640 regression, with the SD calculated from 1000 bootstrap replications.



1641

1642

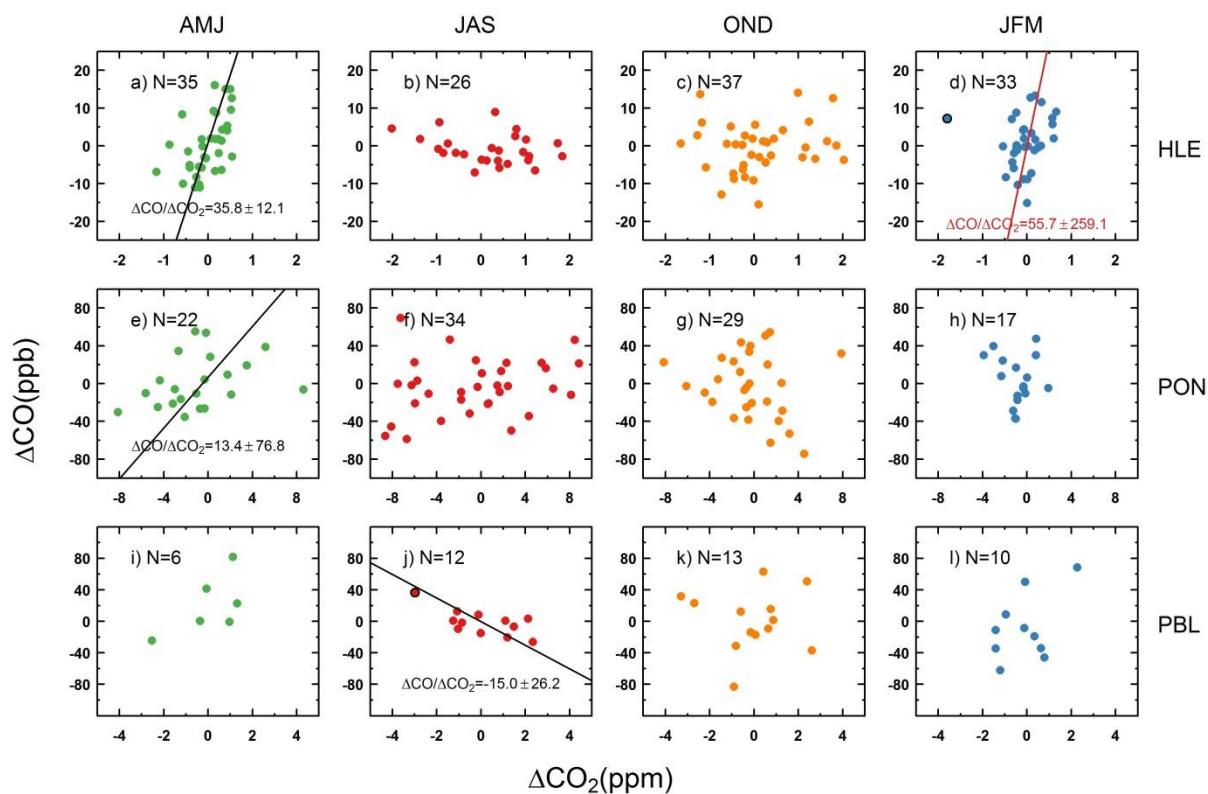
1643 **Figure 15** The relationships between  $\Delta\text{CH}_4$  and  $\Delta\text{CO}_2$  at HLE (a–d), PON (e–h), and PBL (i–l) for April–June (AMJ), July–September (JAS), October–December (OND), and January–  
 1644 (i–l) for April–June (AMJ), July–September (JAS), October–December (OND), and January–  
 1645 March (JFM). For each panel,  $\Delta\text{CH}_4$  and  $\Delta\text{CO}_2$  are estimated as residuals from smoothed  
 1646 curves. The  $\Delta\text{CH}_4/\Delta\text{CO}_2$  ratio is the slope of the fitting line from the orthogonal distance  
 1647 regression, with the SD calculated from 1000 bootstrap replications. For  $\Delta\text{CH}_4$  and  $\Delta\text{CO}_2$  that  
 1648 is not significantly correlated, the fitting line is not plotted.



1649

1650

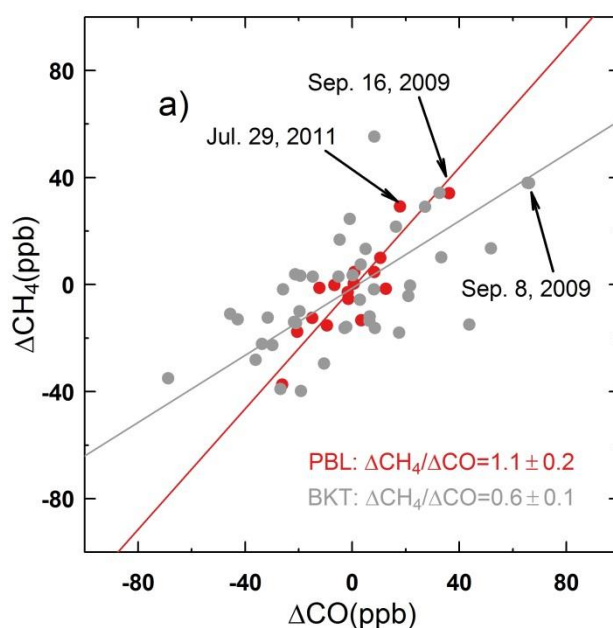
1651 **Figure 16** The relationships between  $\Delta\text{CO}$  and  $\Delta\text{CO}_2$  at HLE (a–d), PON (e–h), and PBL (i–  
 1652 l) for April–June (AMJ), July–September (JAS), October–December (OND), and January–  
 1653 March (JFM). For each panel,  $\Delta\text{CO}$  and  $\Delta\text{CO}_2$  are estimated as residuals from smoothed  
 1654 curves. The  $\Delta\text{CO}/\Delta\text{CO}_2$  ratio is the slope of the fitting line from the orthogonal distance  
 1655 regression, with the SD calculated from 1000 bootstrap replications. For  $\Delta\text{CO}$  and  $\Delta\text{CO}_2$  that  
 1656 is not significantly correlated, the fitting line is usually not plotted.



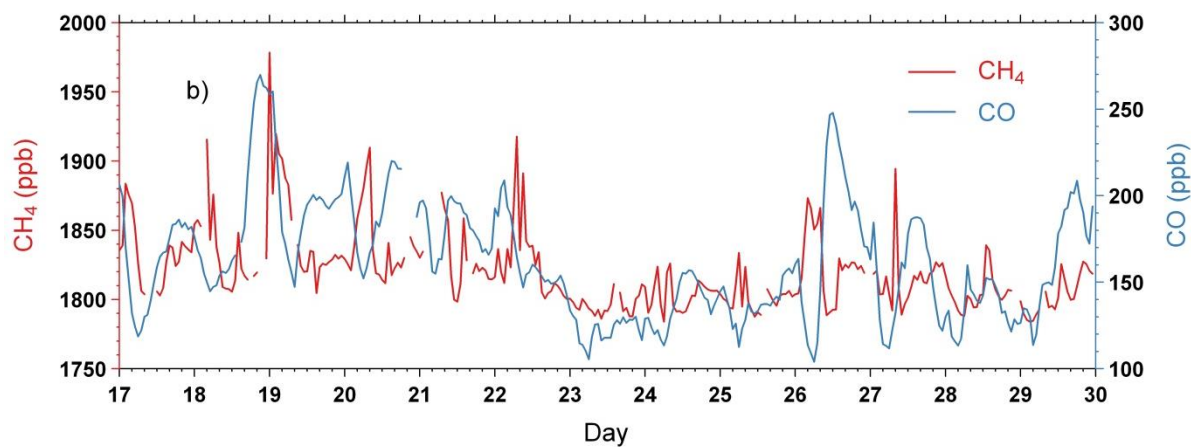
1657

1658

1659 **Figure 17 (a)** The relationship between  $\Delta\text{CH}_4$  and  $\Delta\text{CO}$  at PBL (colored by red) and BKT  
 1660 (colored by grey) during July–September (JAS) over the period of 2007–2011.  $\Delta\text{CH}_4$  and  
 1661  $\Delta\text{CO}$  are estimated as residuals from smoothed curves. The  $\Delta\text{CH}_4/\Delta\text{CO}$  ratio is the slope of  
 1662 the fitting line from orthogonal distance regression (ODR), with the SD calculated from 1000  
 1663 bootstrap replications. Two abnormal events at PBL are labeled, with enhancements of  $\text{CH}_4$   
 1664 and CO on September 16, 2009 and July 29, 2011, respectively. Enhancements of  $\text{CH}_4$  and  
 1665 CO are also observed at BKT on Sep. 8, 2009. Enhancements of  $\text{CH}_4$  and CO are observed during July 17-  
 1666 21, 2011.  
 1667 21, 2011.



1668



1669